Dynamic Optimization of Fractionation Schedules in Radiation Therapy

by

Jagdish Ramakrishnan

Submitted to the Department of Electrical Engineering and Computer Science
in partial fulfillment of the requirements for the degree of
Doctor of Philosophy
at the
MASSACHUSETTS INSTITUTE OF TECHNOLOGY
June 2013

Author .....
Department of Electrical Engineering and Computer Science
May 22, 2013

Certified by .....
Professor Thomas Bortfeld
Professor of Radiation Oncology, Harvard Medical School
Thesis Supervisor

Certified by .....
Professor David L. Craft
Assistant Professor of Radiation Oncology, Harvard Medical School
Thesis Supervisor

Certified by .....
Professor John N. Tsitsiklis
Clarence J Lebel Professor of Electrical Engineering
Thesis Supervisor

Accepted by .....
Professor Leslie A. Kolodziejski
Chairman, Department Committee on Graduate Students

Dynamic Optimization of Fractionation Schedules in Radiation Therapy

by

Jagdish Ramakrishnan

Submitted to the Department of Electrical Engineering and Computer Science
on May 22, 2013, in partial fulfillment of the
requirements for the degree of
Doctor of Philosophy

Abstract

In this thesis, we investigate the improvement in treatment effectiveness when dynamically optimizing the fractionation scheme in radiation therapy.

In the first part of the thesis, we consider delivering a different dose each day depending on the observed patient anatomy. Given that a fixed prescribed dose must be delivered to the tumor over the course of the treatment, such an approach results in a lower cumulative dose to a radio-sensitive organ-at-risk when compared to that resulting from standard fractionation. We use the dynamic programming algorithm to solve the problem exactly. Next, we suggest an approach which optimizes the fraction size and selects a treatment plan from a plan library. Computational results from patient datasets indicate this approach is beneficial.

In the second part of the thesis, we analyze the effect of repopulation on the optimal fractionation scheme. A dynamic programming framework is developed to determine an optimal fractionation scheme based on a model of cell kill due to radiation and tumor growth in between treatment days. We prove that the optimal dose fractions are increasing over time. We find that the presence of accelerated tumor repopulation suggests larger dose fractions later in the treatment to compensate for the increased tumor proliferation.

Thesis Supervisor: Professor Thomas Bortfeld
Title: Professor of Radiation Oncology, Harvard Medical School

Thesis Supervisor: Professor David L. Craft
Title: Assistant Professor of Radiation Oncology, Harvard Medical School

Thesis Supervisor: Professor John N. Tsitsiklis
Title: Clarence J Lebel Professor of Electrical Engineering

Acknowledgments

I am very thankful to my parents and sister, whose love, support, and encouragement helped me reach where I am today. I am also grateful to my entire family, both immediate and extended, who made it possible for me to have the opportunities I have today.

Without my advisors, Prof. Thomas Bortfeld, Prof. David Craft, and Prof. John Tsitsiklis, I could not have made it through this journey. I am forever indebted to John for constantly inspiring me and helping me through every part of the research process. I thank David for answering my seemingly endless list of questions and giving me invaluable suggestions. I thank Thomas for keeping my research grounded in reality and helping me see the big picture. I also thank Prof. Jan Unkelbach for practical advice and very fruitful collaboration, especially for the work in Chapters 4 and 5. I would like to thank Prof. Dimitri Bertsekas for being part of my thesis committee and providing me with constructive feedback. I am thankful for his books, which have influenced me tremendously.

My colleagues, friends, and collaborators at MGH have been very influential. I thank Yi Wang for providing contoured patient datasets and making it easy for me to test the methods in this report. I would like to thank the entire group at MGH, particularly those in the optimization group with whom I interacted often: Alex, Andrea, Christian, Chuan, David P., Dualta, Ehsan, Greg, Hamed, Jeremiah, and Wei; they played an important role in my learning process.

I would like to thank my officemates and the SYNDEG members for their friendship and help: Ali, Hoda, Jimmy, Kimon, Kuang, Mihalis, Spyros, Yuan, and Yunjian. Thanks to the administrative staff at LIDS, particularly Brian, Jennifer, and Lynne, for their help throughout my time at MIT. I enjoyed every minute working as a TA with Aliaa, Jimmy, Katie, Kuang, Shashank, and Uzoma, and also Prof. Alan Willsky. I would like to thank the LIDS, ORC, and RLE community; I made many friends and had interesting conversations. The weekly graduate mentoring seminar played an important

role in helping me transition into grad school at MIT. I am thankful to Prof. Alan V. Oppenheim for leading this seminar and am grateful for the friendship of those I met. Thanks to Anton, Diego, Florin, Jason, and Spyros for playing tennis over the last few years. I am also thankful to the members of the table tennis club and team, and Alex, Carlos, and Liang for their coaching and tips. My exciting experiences as part of the team will be etched in my memory forever. I am thankful to my friends in Atlanta, who kept in touch with me whenever I visited. I am also thankful to my friends at the SP Graduate Community for making my experiences unforgettable. Thanks to Matt for his thoughts when writing parts of this thesis. Thanks to Dan for being a mentor and teaching me invaluable lessons. Finally, I am grateful for the grace in my life because I have been given more than I could have hoped for.

For any mistakes in this report and/or naïveté, I am solely responsible.

The research in this thesis was partially supported by Siemens.

Contents

List of Figures

List of Tables

Chapter 1

Introduction

> Things alter for the worse spontaneously, if they be not altered for the better designedly.
>
> Sir Francis Bacon

1.1 Motivation

This thesis deals with dynamic optimization in radiation therapy. Conventional radiation therapy procedures deliver an equal dose to the tumor every day over the course of 30-40 days. The spatial and temporal dose distribution is optimized assuming the patient anatomy is static over the course of treatment. Yet, due to uncertainties in the daily patient setup as well as motion, among other reasons, radiation-sensitive organs near the tumor can get exposed to high radiation doses, which could result in acute or late side-effects. Furthermore, treatment planning procedures barely account for temporal effects, such as tumor growth and shrinkage, and radiation response. In this thesis, we seek to understand, both qualitatively and quantitatively, the improvement in treatment effectiveness that can result from dynamic adaptation of the fractionation scheme, i.e., the total number of treatment days and dose delivered per day.

One way to adapt doses and treatments is to make use of information acquired

between fractions (or treatment days). Such adaptation is becoming technologically feasible because of improved imaging and information acquisition technologies. This type of treatment modification, known as adaptive radiation therapy (ART), permits customized day-to-day dose delivery to mitigate uncertainty in organ motion and/or patient setup. The question arises as to whether adapting the fraction size based on an acquired image of the patient anatomy immediately before delivery can improve treatment outcome. If so, by how much? And under what circumstances? Although this thesis primarily deals with optimization of fractionation schemes, we are also interested to know whether spatial adaptation results in further improvement besides that due to simply changing the fractionation scheme. We seek to identify the types of scenarios in which adaptivity based on feedback information will be particularly fruitful.

Conventional radiation treatment plans mostly ignore the dynamic nature of the inherent biological processes in a patient. Over the last 50 years, our understanding of the biological effects of radiation has improved. With better models and imaging technologies such as magnetic resonance imaging (MRI) and positron emission tomography (PET), biologically-based treatment planning, aiming at optimal dose delivery over time, has tremendous potential. Yet, the complexities of how radiation affects the underlying biological processes make it difficult to determine how, if at all, treatment planning should be changed. We seek to understand the relationship between biological modeling assumptions and the resulting optimal fractionation schedules. We investigate the circumstances under which these optimal schedules result in significant improvement over current treatments. We hope that eventually through future research the best possible individualized treatment can be administered to the patient, taking into account both geometric and biological uncertainties.

We can dynamically optimize treatment in multiple ways. One way is to make use of feedback information obtained from computed tomography (CT) or cone beam computed tomography (CBCT) images throughout the course of treatment. If treatment plans can be optimized and quality assured fast enough, we can adapt treatment immediately before delivery, which is known as online ART; otherwise, we can use offline

ART, in which past CT images are used to adapt future treatment. Ideally, we would like to adapt in real time as geometrical information about the patient anatomy is obtained during the course of treatment. It is also possible to use functional imaging to observe biological information, e.g., on metabolism, and adapt treatment. If existing technology cannot be used to observe such biological information, models can still be used to dynamically adjust a treatment. In the first part of this thesis, we provide methods to adapt immediately before the delivery of a fraction by using geometrical information about the patient anatomy. In the second part, we use models of cell dynamics to obtain insights about the optimal way to fractionate treatments. In this thesis, we use dynamic programming as the primary solution method.

1.2 Outline and main contributions

In this section, we provide an overview of the topics covered in this thesis. We briefly discuss the high level insights of each chapter and the way we approached the problem. In doing so, we also briefly discuss the main contributions. A more detailed list of contributions is given in the chapters themselves.

In Chapter 2, we provide an analysis of the adaptive fractionation problem introduced in [48]. A tumor and one primary organ-at-risk (OAR) is considered. The main idea is to use a large dose to the tumor when observing a favorable patient anatomy and a small dose when observing an unfavorable anatomy. Given that a fixed prescribed dose is delivered by the end of treatment, this approach results in a decrease in the total OAR dose over the course of treatment. We develop and evaluate various solution methods, both exact and heuristic. We frame the problem in a dynamic programming framework and derive the structure of an optimal policy. We develop various heuristic approaches based on the structure of the optimal one. The cost of one of the heuristics converges to the optimal cost as we increase the number of days of treatment. The algorithm in [48] is shown to perform very well compared to the optimal even though it is an approximate DP approach. Though a dynamic programming approach has been

used for adaptive fractionation in the past [13], it was in the context of the biological effective dose (BED) model.

In Chapter 3, we investigate the benefit of adaptive fractionation methods for prostate cancer patients. We used three patient datasets, each consisting of daily CT images. We find that adaptive fractionation is beneficial when using the BED model but not so much when using the physical dose model. We develop an approach to update the probability distribution of the anatomy favorability over the course of treatment. Such an approach is found to be useful when historical data from other patients is not characteristic of the patient-specific anatomy variations from day to day. We also suggest adaptation by selection of treatment plan from a plan library. The primary advantage of the plan library is that the quality assurance (QA) procedure is avoided after the initial plan generation phase. We study a proof-of-principle example in which the library consists of two plans with different margins around the tumor. We find that there is significant benefit from adaptive plan selection compared to a conventional approach. While we mainly decoupled the problems of adaptive fractionation and plan selection in our work, there were large gains from combining the two approaches.

In Chapter 4, we analyze the effect of accelerated repopulation on optimal fractionation schemes based on extensions of the BED model. There are multiple ways to model accelerated repopulation. One approach is to increase the tumor proliferation rate with already delivered dose or BED. Alternatively, accelerated repopulation can be modeled implicitly by assuming a proliferation rate that is dependent on the number of tumor cells. Due to radiation treatment, fewer cells remain towards the end of treatment, thus resulting in faster tumor growth. We develop a solution approach based on dynamic programming to solve the optimal fractionation problem with repopulation for general tumor growth characteristics. The optimization problem consists of minimizing the expected number of tumor cells under a constraint on the BED in the OAR. We prove that the optimal dose fractions are increasing over time. We find that faster tumor growth suggests shorter overall treatment duration. In addition, the presence of accelerated repopulation suggests larger dose fractions later in the treatment to com-

pensate for the increased tumor proliferation. We characterize the special structure of the problem for the case of exponential and Gompertz tumor growth. More research is needed to determine tumor repopulation characteristics from clinical outcome data for specific disease sites.

In Chapter 5, we model the repair effect in addition to tumor repopulation and generalize the methods in the previous chapter to the case of a continuous dose rate treatment. We write the dynamics governing the number of tumor cells at any instant of time as an ordinary differential equation. We show that the proposed continuous-time model is consistent with the discrete-time one in the previous chapter. Yet, the work in this chapter is not completely developed and a similar setup is found in [87]. However, we hope that the derivations shed new perspective and provide a basis for future work.

The final chapter summarizes the thesis and provides directions for future research.

1.3 Background

According to the American Cancer Society, at least 50% of cancer patients undergo radiation therapy over the course of treatment. Radiation therapy plays an important role in curing early stage cancer, stopping cancer from spreading to other areas, and treating symptoms of advanced cancer. For many patients, external beam radiation therapy is one of the best options for cancer treatment. Another form of radiation therapy is brachytherapy, in which seeds continuously emitting radiation are placed inside a patient's body. In this thesis, we primarily focus on external beam radiation therapy; thus in this section we will limit our discussion to this form of therapy.

1.3.1 Delivery of radiation treatment

Once a patient is diagnosed with cancer, a simulation 3D CT image of the anatomy is taken prior to therapy. This CT is the basis for diagnosis and treatment planning. A

physician or resident under the supervision of a physician contours the revelant tumor volume and OARs, and specifies the set of constraints that need to be met in the treatment plan (e.g., tumor prescribed dose). The primary target for radiation is an expanded tumor volume. The visible tumor volume on the CT that is cancerous is known as the gross tumor volume (GTV). To account for uncertainty in microscopic spread not visible in the CT image, an expanded GTV, known as the clinical target volume (CTV), is delineated. This is the primary volume that physicians want to treat. Finally, to account for uncertainty in setup and organ motion from day to day, a margin is added around the CTV, resulting in the planning target volume (PTV). For example, for prostate cancer, it is reasonable to include a 5 mm margin uniformly around the CTV. In the treatment planning phase, the PTV is prescribed a uniform dose (anywhere between 40 Gy and 80 Gy). There are generally constraints such as a limit on the maximum or mean dose on critical structures.

The treatment procedure is broken up into many sessions or fractions (where a patient undergoes at most one session per day). A typical treatment, for example, is 5 sessions per week for 7 weeks. One of the reasons for the above margin expansions of the tumor volume is due to uncertainty in organ motion. Interfraction motion uncertainty happens *between* fractions; for example, motion where a patient is setup in a different position than in the previous session. This causes the target to have a displacement. Intrafraction motion occurs *during* treatment sessions. An example could be the breathing of the patient (inhaling and exhaling) which causes the target to move even as the treatment is ongoing.

Different types of beam modalities can be used for external beam radiation treatment. The two most common ones are photon beams and proton beams. Proton treatments are preferable to photon treatments due to the nature of the dose as a function of depth. Once the proton beam penetrates the skin, the dosage increases exponentially as a function of the depth until it falls sharply down to zero. This allows for more accurate dosage to the tumor cells but at the same time, is vulnerable to causing critical errors when uncertainty is present. For a photon beam, however, when the

beam penetrates the skin, the dosage increases rapidly until it peaks. After peaking, there is an exponential decrease in dose as a function of the depth. Although photons are not able to focus the dose as well as protons, they are more robust to uncertainties such as patient setup errors and organ motion.

After the imaging and contouring phases, the distribution of the radiation dose on the patient anatomy is optimized. External beams of radiation can be delivered in multiple ways. For photon beams, developments over the last few decades have enabled modulation of the intensity of incoming beams as opposed to uniform intensity using 3D conformal therapy. This modality is known as intensity-modulated radiation therapy (IMRT). One popular way to deliver IMRT is to use a dynamic multi-leaf collimator (MLC). The MLC leaves can move dynamically with time and block the incoming radiation to create intensity modulation of the beam. In this way, instead of a uniform dose of radiation, a modulated fluence profile is delivered from each beam angle. Generally, a two step procedure is used in this case. First, the fluence maps of the beams are optimized. Next, the fluence map is approximately sequenced into MLC leaf movements. Other approaches such as direct aperture optimization avoid these two steps altogether and directly optimize the MLC leaves. Intensity modulation can also be delivered for proton beams, except that an MLC is not used. One way to deliver the appropriate intensities would be to use beam scanning. This type of treatment is known as intensity-modulated proton therapy (IMPT). The advantage of this modality is that the optimized fluence map can be directly mapped with beam scanning and does not have to be sequenced into MLC leaf trajectories.

1.3.2 Treatment plan optimization

In this subsection, we discuss optimization of the fluence intensity map in the treatment plan. We omit discussion of MLC leaf sequencing; for references on possible approaches, see [35, 75].

The basic problem is to optimize beam intensities (or bixel weights) delivered from

various beams (generally coplanar) around the patient to capture the best tradeoff between delivering a high dose to the tumor and minimizing the dose to the healthy tissue. We let $x \in \mathbb{R}^n$ be the vector of bixel weights. For IMRT, the number of bixels, n, can range from 1,000 to 100,000. In order to determine the dose delivered to individual points on the patient (referred to as voxels), a dose deposition matrix $D : \mathbb{R}^n \to \mathbb{R}^m$ is calculated (generally using Monte Carlo simulations). This deposition matrix D describes a linear mapping from the vector of bixels x to a vector of doses delivered to the corresponding patient voxels. The number of patient voxels m ranges anywhere from 100,000 to 1,000,000 (all the points on a 3D scan of the patient) for a full-scale problem. There are a number of ways to formulate the problem, including linear/quadratic and other nonlinear formulations (see [69] for various approaches). Regardless of the exact details of the formulation, the basic idea is to tradeoff between dose to the tumor and healthy tissue. Usually, there are constraints on the minimum tumor dose and maximum or mean dose to healthy OARs.

There are many metrics used to quantify the quality of treatment plan such as mean or maximum dose to relevant organs of interest. But, often the dose-volume histogram (DVH) is used to graphically assess the quality of a treatment plan. The DVH curve for a volume plots the dose versus the percentage of the volume that receives at least that much dose. In this way, DVH curves are generated for all of the organs of interest and used for assessment.

1.3.3 Biological effective dose (BED) model

It is known that the effect of the same dose on different types of cancer varies. For example, prostate cancers are known to be very sensitive to radiation [51] while head and neck cancers are less so [74]. A common way to quantify this effect is to use the biological effective dose (BED) model. The BED is defined as

$$\text{BED} = d\left(1 + \frac{d}{[\alpha/\beta]},\right) \tag{1.1}$$

where d is the physical dose and the α-β ratio denoted $[\alpha/\beta]$ is a tissue specific parameter. Essentially, the α and β refer, respectively, to a linear and quadratic dose effect on tissue. For example, when the linear effect only matters, i.e., if $\beta = 0$, the BED equals the physical dose. We will make use of this model in Chapter 3 when adaptively varying the fraction size for prostate cancer. For a more detailed derivation of the BED from linear and quadratic dose effects, refer to Section 4.3 in Chapter 4.

1.4 Literature review

The first part of the thesis (Chapters 2 and 3) fits in the general area of ART. The second part (Chapters 4 and 5) deals with biological-based treatment planning. In this section, we begin by surveying the literature in these two broad categories. Then, we review literature that is more closely related to the work in this thesis. There is a vast amount of literature in each of these subsections. We do not by any means attempt to provide a comprehensive review, but rather strive to survey existing work particularly as they relate to this thesis.

1.4.1 Adaptive radiation therapy

In its broadest context, adaptive radiation therapy (ART) is a radiation treatment process that uses feedback information to modify and improve treatment plans [41, 96]. Feedback information could include patient anatomy information such as positions of tumor and organ-at-risk (OAR), and can be obtained from imaging modalities such as cone-beam computed tomography (CBCT), ultrasound imaging, or portal imaging [63]. Detailed coverage of ART can be found in books such as [47].

We can correct for inter-fractional variations in patient anatomy by adapting a treatment plan either offline or online. An offline adaptation uses imaging information available after the delivery of a fraction to modify the treatment plan for the next fraction. On the other hand, an online adaptation uses information acquired immediately

before the delivery of a fraction for a quick modification of the treatment plan for that fraction. The advantage of online ART is the availability of more data (inclusion of patient anatomy for the current fraction). However, due to patient wait time and treatment duration limitations, online ART requires (i) fast re-optimization of the treatment plan, and (ii) re-planning across a small number of degrees of freedom. Conversely, in offline ART, a re-optimized treatment plan can be determined on a slower time-scale.

Due to the immediate possibility of lower cumulative dose to healthy organs through treatment plan re-optimization between fractions, offline ART has received much attention in the research community. One of the early approaches used information about tumor variations (both systematic and random) during the first few fractions to determine a customized treatment plan for the remaining fractions [96, 97]. The customized treatment plan generally has a smaller planning target volume (PTV) suited to the particular patient. Such adaptation is shown to improve treatment efficacy and to allow for dose escalation to the tumor [26, 95]. Another approach focused on using a smaller PTV initially and re-optimizing treatment plans between fractions to compensate for the accumulated dose errors [16, 18, 66, 84, 85]. We do note that the practical applicability of this method relies on the ability to accurately determine the delivered dose at each voxel. However, determining the delivered dose accurately requires reliable deformable registration algorithms, which is still a major research topic.

In online ART, the focus has been on making adjustments to the existing treatment plan rather than on re-optimizing for an entirely new plan. This is primarily because the time between the acquisition of patient anatomy information and the delivery of a plan is on the order of minutes rather than hours. In this case, a full re-optimization and complete quality assurance of the treatment plan may not be possible. Several online ART approaches have been developed that make quick modifications to either the fluence map or multi-leaf collimator (MLC) leaves to match the planned dose [14, 53, 93]. Whereas these methods involve spatially varying the dose distribution, other methods, including the work in this thesis, consider temporally varying the fraction size from day to day [13, 48].

1.4.2 Biological based treatment planning

One can incorporate biological information into the treatment process by using appropriate models in the treatment planning optimization problem. While such models have uncertainties, they can provide insights on how to potentially improve treatment. In the future, biological imaging technologies may allow customized delivery to the patient based on biological processes observed during the course of treatment. Below, we briefly review some literature in biological based treatment planning.

We can incorporate biological aspects into treatment planning by using models of tumor and normal tissue response such as tumor control probability (TCP) and normal tissue complication probability (NTCP). There are many ways to model these probabilities; a short list of references is [33, 49, 86, 99]. Other biologically based models include the linear-quadratic (LQ) cell survival model [20], the BED model [20], complication-free tumor control probability [33], and the equivalent uniform dose (EUD) model [56]. Several studies have investigated the use of biological based models for optimizing a treatment plan [34, 71, 82]. However, due to lack of confidence in the parameters of these models, such biological-based treatment plans are not universally used in the clinic. Some studies have cautioned on the use of TCP and NTCP models in treatment planning due to parameter uncertainty [42, 55].

Using biological information obtained from imaging, it is also possible to adapt treatment. With technological advances such as functional and molecular imaging, there is potential to track previously unobservable biological processes such as metabolic activity [68], tumor hypoxia [11], and tumor proliferation rates [3]. One approach is "dose painting," where escalated dose is delivered to regions of the tumor exhibiting a different biological property such as increased radio-resistance. Many dose painting studies have been conducted using various imaging modalities such as dynamic contrast-enhanced MRI [80], ^{18}F-fluorocholine PET [62], and ^{11}C-choline PET [10]. Other sophisticated approaches such as dynamically changing the beam intensities from day-to-day based on the patient's biological condition have also been studied [23, 38, 40].

1.4.3 Overview of literature in relation to thesis

We primarily use the dynamic programming (DP) approach in this thesis. The DP approach is useful for sequential decision making problems, especially when there is a need for balancing the immediate and future costs associated with making a decision at any particular stage [4,64]. For offline ART, the DP approach can be used to compensate for past accumulated errors in dose to the tumor [18, 19, 70]. For online ART, an approach for adaptive fractionation based on biological models and imaging also makes use of DP [13,39]. A spatiotemporal DP approach that adapts to the patient's biological condition has also been recently been studied [40]. There is a significant amount of literature, especially from the mathematical biology community, on optimal control theory and DP for cancer treatment. Many of these works [44, 60, 100] have looked into optimization of chemotherapy. For radiation therapy fractionation without the use of imaging information, many studies [1, 28, 87] have used the DP approach and control theory based on deterministic biological models. The work in Chapter 4 follows this line of thought but is motivated by accelerated tumor repopulation.

Chapters 2 and 3 of this thesis deal with adaptive fractionation, which is a special case of online ART. Adaptive fractionation assuming a physical dose model was introduced in [48]. In Chapter 2, we solve the adaptive fractionation problem using a DP approach; the results are also published in [65]. For the BED model, a DP approach was used to solve the adaptive fractionation problem in [13]. In a similar spirit, the work in [39] selects a dose based on the patient's observed biological condition. In Chapter 3, a method that can adapt the belief about the patient's future condition into the DP approach is also introduced. Even with several works that have described possible adaptive fractionation approaches, such methods have not been substantiated by results from patient datasets. In Chapter 3, prostate patient data is used to show that adaptive fractionation (and also treatment plan selection from a plan library) can be beneficial.

Chapters 4 and 5 deal with the effect of tumor repopulation on optimal fractiona-

tion schemes. There is a large amount of literature on optimal fractionation; we mainly discuss papers that relate to our work. Previous works have considered the case of exponential tumor growth with a constant rate of repopulation [2,32,88]. Optimal fractionation schedules for other tumor growth models, e.g., Gompertz and logistic, have also been considered although mostly in the context of constant daily doses [50, 79]. Using the BED model, a recent paper [52] has mathematically analyzed the fractionation problem for the case of no repopulation. An extension of this result to the case where an inhomogeneous OAR dose is delivered has also been investigated [78]. The work in Chapter 4 extends the mathematical framework in [52] by incorporating tumor repopulation. There has been prior work [1, 76, 77, 94, 98] on the optimization of non-uniform fractionation schedules, even analyzing the effect of tumor repopulation as done in this thesis. However, they either have not used the BED model or have primarily considered other factors such as tumor re-oxygenation. Perhaps the closest work is [87], which considers both faster tumor proliferation and re-oxygenation during the course of treatment. However, while a dose intensification strategy is also suggested in [87], the rationale for dose escalation is different: it is concluded that due to the increase in tumor sensitivity from re-oxygenation, larger fraction sizes are more effective at the end of treatment. Our work, on the other hand, suggests dose escalation due to accelerated tumor repopulation during the course of treatment.

In Chapter 4, we are primarily motivated by accelerated repopulation, which is an important cause of treatment failure in radiation therapy, especially for head and neck tumors [91, 92]. In addition to modeling tumor growth, we use the standard linear-quadratic (LQ) model [15] to describe the effects of radiation dose on the survival fraction of cells. Since our primary interest is in the effect of tumor repopulation, we do not consider other biological aspects such as re-oxygenation, re-distribution, and sublethal damage due to incomplete repair. However, it has been shown that such effects can also result in non-uniform optimal fractionation schemes [5, 87, 98]. Our main result is that accelerated repopulation suggests larger dose fractions later in the treatment to compensate for increased tumor proliferation. The results are consistent

with medical-oriented studies for prostate and cervical cancers [29, 81].

The notion of dose intensification during the course of treatment has now been suggested by many studies, including our work. The Norton-Simon hypothesis [57, 58] suggests increasing the dose intensity over the course of chemotherapy due to a Gompertzian tumor growth assumption. Due to the increased sensitivity of the tumor to radiation from re-oxygenation, such a dose intensification strategy has also been suggested by several studies [1,28,87]. It has been noted in [61] that increased oxygenation and proliferation at the end of treatment could be one reason for the effectiveness of concomitant boost therapy, where increased radiation is delivered at the very end of treatment. Medical-oriented studies [29,81] also suggest larger fraction sizes to compensate for accelerated repopulation. This is consistent with our mathematical framework incorporating accelerated tumor repopulation. Further clinical studies that substantiate the dose intensification strategy would be useful.

Chapter 2

A dynamic programming approach to adaptive fractionation

2.1 Introduction

In this chapter, we consider delivering a different dose to the tumor each day depending on the observed patient anatomy. We study various solution methods for this adaptive fractionation problem. The two messages of this chapter are: (i) dynamic programming (DP) is a useful framework for adaptive radiation therapy, particularly adaptive fractionation, because it allows us to assess how close to optimal different methods are, and (ii) the proposed heuristic methods are near-optimal, and therefore, can be used to evaluate the best possible benefit of using an adaptive fraction size.

We now briefly motivate the adaptive fractionation problem introduced in [48]. We focus on a model of the variations of the tumor and one primary OAR, which is usually the limiting factor in escalating the dose to the tumor. Using an adaptive fraction size can allow us to take advantage of a "favorable" patient anatomy by increasing the fraction size. Similarly, we can decrease the fraction size for an "unfavorable" anatomy. One simple way to think about this problem is to consider variations of the distance between the tumor and the OAR from day to day (see Figure 2-1). If the distance is

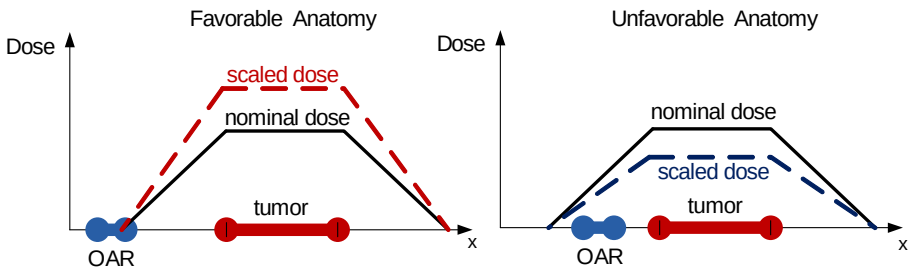

Figure 2-1: Adaptive fractionation capitalizes on tumor-OAR variations. Nominal dose corresponds to leaving the fraction size unchanged, while scaled dose corresponds to a changed fraction size. When we have a favorable anatomy (i.e., the tumor and OAR are far apart) as in the left panel, we can use a larger fraction size. Similarly, for an unfavorable anatomy (i.e., the tumor and OAR are close together) as in the right panel, we can use a smaller fraction size. Our model is more general than this 1-dimensional example and can be used for 3-dimensional realistic settings as well.

large, we can escalate the dose to the tumor (since the OAR dose per unit tumor dose is small) and vice versa, if the distance is small. Given that a fixed prescribed dose must be delivered to the tumor, adaptive fractionation results in a lower cumulative dose to the OAR over the course of the treatment. We emphasize that our model is more general than this 1-dimensional distance setting and can be applied to 3-dimensional realistic settings as well.

The purpose of this study is to develop and evaluate solution methods for the adaptive fractionation problem. We use the dynamic programming (DP) algorithm to solve the problem exactly and to assess how close to optimal various heuristic methods are. The dynamic programming approach has been used before for adaptive fractionation in [13], but this was in the context of the BED model. We focus on the fractionation problem using a physical dose model, which was introduced in [48]. The results of our study indicate that heuristic methods, both the ones proposed in this chapter and in [48], are near-optimal under most conditions. The consequence is that these methods can be used to evaluate in a simple manner the best possible benefit of using an adaptive fraction size. Furthermore, simple heuristics as proposed in this chapter provide a quick way to measure the gain that results from adaptively varying the fraction size.

We first discuss the main contributions of this chapter in Section 2.2. In the next

section, we discuss the model and formulate the adaptive fractionation problem. Sections 2.4 and 2.5 describe the dynamic programming (DP) approach and its theoretical properties, and Section 2.6 describes two heuristics. In Section 2.7, the algorithm in [48] is derived and shown to be a variant of the open-loop feedback control approximate DP approach. Results from numerical simulations are evaluated in Section 2.8. Some further theoretical properties of one of the heuristics are described in Section 2.9. Finally, Section 2.10 includes discussions about realistic implementations, model assumptions, and future directions.

2.2 Contributions

The idea of adaptive fractionation is not new; it was already introduced and an algorithm was developed in [48]. Our contributions include further developing solution methods and analyzing them on a theoretical level. In particular, we:

1. use the DP algorithm to establish a benchmark and to solve the problem exactly. Under this problem setting, this gives us a lower bound which no other algorithm can improve upon. We are able to show numerically that many of the heuristic algorithms, including the one in [48], perform close to optimal for most assumed probability distributions of the patient anatomy. However, when there is a high probability of large tumor-OAR distances, we see differences as large as 10% between an optimal policy and the algorithm in [48].

2. prove properties of an optimal policy and find that for most realistic cases, an optimal policy has a special threshold form.

3. develop two intuitive, numerically near-optimal heuristic policies, which could be used for more complex, high-dimensional problems. Furthermore, one of the heuristics requires only a simple statistic (e.g., the median) of the motion probability distribution, making it a reasonable method for realistic settings.

4. establish clearly the connection between this work and the one in [48] by rederiving the algorithm in [48] as a variant of the open-loop feedback control approximate DP approach (see [4] for a description of such an approach).

5. demonstrate through numerical simulations that we can expect a significant decrease in dose to the OAR when: (i) we have a high probability of large tumor-OAR distances, (ii) we use many fractions (as in a hyper-fractionated setting), and (iii) we allow large daily fraction size deviations.

6. prove that one of the proposed heuristics is asymptotically optimal as the number of treatments N is large. The rate of convergence is $O\left(\frac{\sqrt{\log N}}{\sqrt{N}}\right)$.

2.3 Model and formulation

We now describe the details of the model and formulate the adaptive fractionation problem. Let N be the number of fractions and P be the total prescribed dose to the tumor. The patient anatomy in the kth day is represented by a variable denoted by s_k, which is sampled, independent of everything else, from a known probability distribution $p(\cdot)$ estimated from historical data. We assume that the patient anatomy s_k is observed just before the delivery of the kth fraction and can be obtained, for example, from imaging modalities such as CBCT. We could also use this formulation for intra-fractional variations, where s_k would change during a fraction; in this case, it would be more appropriate to assume that patient anatomy instances are correlated rather than independent from one another. In general, the distribution $p(\cdot)$ can be either continuous or discrete but for simplicity, we assume a continuous distribution and denote by S the set of possible anatomy instances. We define r_k to be the remaining prescribed dose left to deliver to the tumor in the kth and future fractions. We must determine the fraction size u_k in the kth fraction based on the remaining dose r_k and patient anatomy s_k. Here, r_k and s_k together represent the state of the system because they are the only relevant pieces of information needed to determine the fraction size

u_k. It can be seen that the dynamics of the system are described by the equations $r_{k+1} = r_k - u_k$, $s_k \sim p(\cdot)$, for $k = 1, 2, \ldots, N$, with r_1 initialized to the prescribed dose P.

Given a patient anatomy s_k, the dose delivered to the OAR in the kth fraction can be written as $u_k h(s_k)$, where $h(s_k)$ is the OAR dose per unit Gy dose delivered to the tumor. For the 1-dimensional setting in Figure 2-1, the function $h(s_k)$ describes the dose falloff, as a function of the location of the OAR. We could use other choices for $h(s_k)$; what we need is a function that describes how favorable a particular patient anatomy s_k is. If current technology allows for a quick way to supply information about the favorability of a patient anatomy before the delivery of a fraction, this information can be captured in the $h(s_k)$ function. The main assumption here that a linear increase in the dose to the tumor results in a linear increase in the dose to the OAR, which is reasonable and is used in practice. For notational convenience, we also define the cumulative distribution function (CDF) for $h(s_k)$ as

$$F^{\mathrm{h}}(z) = \int_{\{s\,:\,h(s)\leq z\}} p(s)\,\mathrm{d}s. \tag{2.1}$$

In the model description, we have included the patient anatomy s_k as a state variable. However, this could result in a very high-dimensional state space if the entire 3D or 4D anatomy information is included. In the following remark, we suggest an alternative but equivalent state space description for this problem.

Remark 1. *We could use $h(s_k)$ as the state instead of the entire anatomical information given by s_k. This would reduce the state space to a 2D quantity $(r_k, h(s_k))$. In this case, instead of $p(\cdot)$, we would use the relevant probability distribution $p^h(\cdot)$ associated with the CDF $F^h(\cdot)$ defined in (2.1).*

The optimization problem of interest is to minimize the expected total dose to the OAR subject to constraints that ensure that: (i) the prescribed dose to the tumor is met with certainty, and (ii) the fraction size for each day is within a lower bound, $\underline{u}$, and an upper bound, $\overline{u}$. Although optimizing non-linear TCP/NTCP functions might

be a better choice here, it is simpler to use total dose, which is a reasonable surrogate for most situations. For convenience in analysis, we also incorporate constraint (i) into the objective cost function by adding a terminal cost $g(r_{N+1})$, which assigns an infinite penalty when the prescribed dose P is not met. Mathematically, we can formulate the adaptive fractionation problem as follows:

$$\begin{aligned}
\min_{\{\mu_k\}} \quad & \mathbb{E}\left[g(r_{N+1}) + \sum_{k=1}^{N} \mu_k(r_k, s_k) h(s_k)\right] \\
\text{s.t.} \quad & \underline{u} \leq \mu_k(r_k, s_k) \leq \overline{u}, \qquad k = 1, 2, \ldots, N, \quad \forall r_k, \forall s_k \\
& r_1 = P, \\
& r_{k+1} = r_k - \mu_k(r_k, s_k), \qquad k = 1, 2, \ldots, N, \\
& s_k \sim p(\cdot), \qquad k = 1, 2, \ldots, N,
\end{aligned} \tag{2.2}$$

where

$$g(r_{N+1}) = \begin{cases} 0, & \text{if } r_{N+1} = 0, \\ \infty, & \text{otherwise,} \end{cases}$$

and where the expectation $\mathbb{E}[\,\cdot\,]$ is taken with respect to the probability distribution $p(\cdot)$.

In the above optimization problem, we are searching for an *optimal policy* $\mu_k^*(r_k, s_k)$, which for any given time k, is a function of the remaining dose r_k and the patient anatomy s_k. Here, the solution is not simply a single value of the optimal fraction size for any particular day but rather, a policy or a strategy that can possibly choose different fraction sizes based on state information. This is characteristic of closed-loop control, which uses state (feedback) information to make decisions. Furthermore, a brute search over all possible functions $\mu(r_k, s_k)$ to solve this problem is not feasible. Notice that the first term in the objective function $g(r_{N+1})$ simply ensures that after N fractions, the prescribed dose to the tumor is met *exactly*. The second term is the total dose to the OAR resulting from using the policy μ_k.

2.4 A dynamic programming approach

We can solve the problem (2.2) exactly by using the DP algorithm (Bellman's backward recursion):

$$J_{N+1}(r_{N+1}, s_{N+1}) = g(r_{N+1}) = \begin{cases} 0, & \text{if } r_{N+1} = 0, \\ \infty, & \text{otherwise,} \end{cases}$$

$$J_k(r_k, s_k) = \min_{\underline{u} \le u_k \le \overline{u}} \Big(u_k h(s_k) + \mathbb{E}\left[J_{k+1}(r_k - u_k, s_{k+1}) \right] \Big), \tag{2.3}$$

for $k = N, N-1, \ldots, 1$, where the expectation is taken with respect to the distribution $p(\cdot)$ of s_{k+1}:

$$\mathbb{E}\left[J_{k+1}(r_k - u_k, s_{k+1}) \right] = \int_S p(s) J_{k+1}(r_k - u_k, s)\, \mathrm{d}s.$$

For numerical implementation, however, we need to discretize the variables r_k and s_k and solve a corresponding discrete problem. All of our subsequent numerical results refer to this discrete problem.

It is well known that the policy resulting from the above DP algorithm is optimal for the problem (2.2) — see [4]. Hence, the cost-to-go function $J_k(r_k, s_k)$ is the resulting cost from using an optimal policy starting with a given remaining dose r_k and patient anatomy s_k in the kth fraction. The basic idea of the DP algorithm is to start from the last fraction (when the optimal decision μ_N^* must be exactly equal to the remaining dose r_N for any possible s_N), determine the optimal decision μ_{N-1}^* given this new information, and proceed backwards in determining the present optimal policy with information about future optimal policies. We can see that $J_k(r_k, s_k)$ is computed by minimizing the sum of the present cost associated with delivering the fraction size u_k in the kth fraction (i.e., $u_k h(s_k)$) and the expected future cost resulting from delivering the fraction size u_k given that we use an optimal policy thereafter (i.e., $\mathbb{E}\left[J_{k+1}(r_k - u_k, s) \right]$). Essentially, the DP algorithm involves precomputing offline and storing the fraction size u_k, for every possible fraction k and value of the state (r_k, s_k). Therefore, choosing the fraction size online right before the delivery of the fraction simply involves a quick table lookup. A few observations about simplifying the DP algorithm in (2.3) are given in

the following remark.

Remark 2. *As suggested in Remark 1, we can simplify the DP algorithm by reducing the state space to a 2D quantity* $(r_k, h(s_k))$*. A second simplification involves removing the uncontrollable state* s_k *(or equivalently,* $h(s_k)$*) by "averaging it out" and keeping track only of expected cost-to-go functions. For completeness, the simplified algorithm is given below.*

$$\overline{J}_{N+1}(r_{N+1}) = g(r_{N+1}) = \begin{cases} 0, & \text{if } r_{N+1} = 0, \\ \infty, & \text{otherwise}, \end{cases}$$

$$\overline{J}_k(r_k) = \mathbb{E}\left[\min_{\underline{u} \le u_k \le \overline{u}} \Big(u_k h(s_k) + \overline{J}_{k+1}(r_k - u_k) \Big)\right], \tag{2.4}$$

for $k = N, N-1, \ldots, 1$*. For ease of exposition, we still use the original DP algorithm given in (2.3) for the analysis and discussions in this chapter.*

We now summarize interesting theoretical properties of an optimal policy resulting from the qualitative structure of the cost-to-function. The piecewise linear structure of the cost-to-go function (see next section for details) results in a special structure of an optimal policy. Essentially, if it is possible to deliver the treatment with a sequence of smallest fraction sizes $\underline{u}$ and largest ones $\overline{u}$, an optimal policy does *exactly* that, i.e., the resulting optimal policy has the threshold structure:

$$\mu_k^*(r_k, s_k) = \begin{cases} \underline{u}, & \text{if } h(s_k) \ge T_k(r_k), \\ \overline{u}, & \text{if } h(s_k) < T_k(r_k), \end{cases} \tag{2.5}$$

for $k = 1, 2, \ldots, N$, where the $T_k(r_k)$ are pre-computed thresholds (see next section for details). The optimal policy (2.5) makes sense because unfavorable or large values of $h(s_k)$ result in delivering a small fraction size $\underline{u}$ and vice versa. The policy is completely characterized by the thresholds $T_k(r_k)$, $k = 1, 2, \ldots, N$, which represent the points at which it is optimal to deliver $\underline{u}$ when above it and $\overline{u}$ when below it. We note that because the optimal policy has the structure (2.5), we can restrict the search for u_k in

(2.3) to the set $\{\underline{u}, \overline{u}\}$ rather than the entire range of values between them and still preserve optimality. Furthermore, as we will see in a future section, this structure of an optimal policy can serve as the basis for simpler heuristics that could perform very close to the optimal. To get further intuition about the optimal policy, let us consider the case where the sequence of patient anatomy instances or costs $h(s_k)$, $k = 1, 2, \ldots, N$, are known ahead of time for the entire treatment. Then, it is clear that the solution would be to deliver $\overline{u}$ for the fractions with the smaller costs and $\underline{u}$ otherwise. Now, we can view our original problem, where the information about the patient anatomy is only available before the delivery of the fraction, as one of deciding whether the anatomy of any particular day will be one of the fractions with the smaller costs. The threshold $T_k(r_k)$ helps us make this determination.

2.5 Theoretical properties of the optimal policy

We provide additional details on the theoretical properties of optimal policies, after first commenting on a generalization of our previously stated assumptions.

Remark 3. *Although we assumed s_k to be independent and identically distributed in the previous section, our methods apply more generally to the case where the sequence of patient anatomy instances satisfy the Markov property. That is, the patient anatomy s_{k+1} is only dependent on s_k and not on previous anatomies before the kth day. In this case, the dependencies would be summarized in a new probability distribution $p_k(s_{k+1}|s_k)$; the analysis and results in this section would still go through.*

To facilitate the discussion, we define

$$\mathcal{F}_k = \{r_k : (N-k+1)\underline{u} \leq r_k \leq (N-k+1)\overline{u}\}\,, \tag{2.6}$$

$$\underline{B}_k(r_k) = \max(\underline{u}, r_k - (N-k)\overline{u}),$$

and

$$\overline{B}_k(r_k) = \min(\overline{u}, r_k - (N-k)\underline{u})).$$

The set $\mathcal{F}_k$ represents the *feasible* set of remaining dose values in the kth fraction. We can verify this by noting that because the prescribed dose to the tumor must be met exactly, the remaining dose r_k must be between the smallest and the largest possible fraction size deliverable to the tumor for the remaining fractions (i.e., $(N-k+1)\underline{u}$ and $(N-k+1)\overline{u}$). As we will see below in Lemma 2.5.1, we can rewrite a simplified DP algorithm in which $\underline{B}_k(r_k)$ and $\overline{B}_k(r_k)$ can be interpreted as the minimum and maximum allowable dose in the kth fraction, respectively. We assume that the minimum of a function over an empty set is equal to infinity.

Lemma 2.5.1. *The DP algorithm given in (2.3) can be rewritten as follows*

$$J_k(r_k, s_k) = \min_{\underline{B}_k(r_k) \le u_k \le \overline{B}_k(r_k)} \Big(u_k h(s_k) + \overline{J}_{k+1}(r_k - u_k) \Big), \tag{2.7}$$

with the same terminal condition as before.

Proof. See Appendix 2.11.1. □

In the following theorem (see Figure 2-2), we describe the qualitative structure of the cost-to-go function and characterize the structure of an optimal policy.

Theorem 2.5.2. *The cost-to-go function $J_k(r_k, s_k)$, for $k = 1, 2, \ldots, N$, is continuous, non-decreasing, convex, and piecewise linear in r_k for $r_k \in \mathcal{F}_k$, with breakpoints at $(N-k+1-i)\underline{u} + i\overline{u}$, for $i = 0, 1, \ldots, N-k+1$. Furthermore, there exists an optimal policy, for $k = 1, 2, \ldots, N$, with the form:*

$$\mu_k(r_k, s_k) = \begin{cases} \overline{u}, & \text{if } r_k \ge \overline{u} + A_k(s_k) \\ r_k - A_k(s_k), & \text{if } \underline{u} + A_k(s_k) \le r_k < \overline{u} + A_k(s_k) \\ \underline{u}, & \text{if } r_k < \underline{u} + A_k(s_k), \end{cases} \tag{2.8}$$

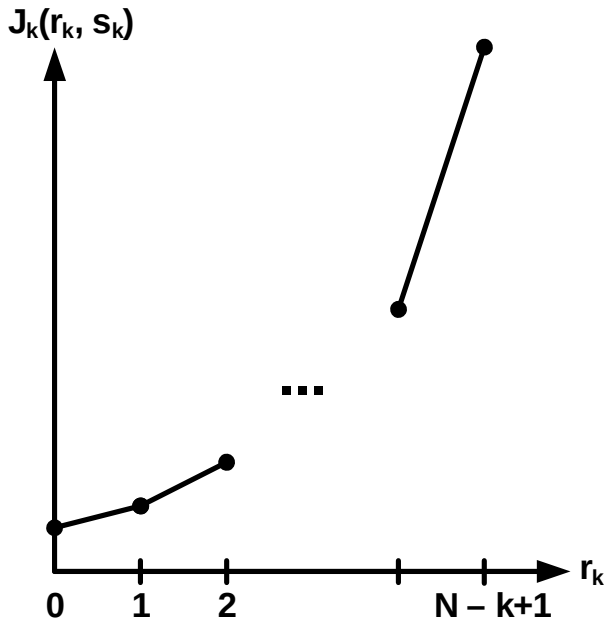

Figure 2-2: Special structure of the cost-to-go function $J_k(r_k, s_k)$. For simplicity, we use $\underline{u} = 0$ and $\overline{u} = 1$ for the plot and see that J_k has $N - k + 1$ line segments and breakpoints at all integer points in the range $[0, N - k + 1]$.

where $A_k(s_k) = \arg\min_{y \in \mathcal{F}_{k+1}} \left[-yh(s_k) + \overline{J}_{k+1}(y)\right]$.

Proof. See Appendix 2.11.2. □

The interpretation of the above optimal policy structure is that for a fixed patient anatomy s_k, provided that the dose stays within the lower bound $\underline{u}$ and upper bound $\overline{u}$, an optimal policy is to deliver a dose which linearly increases with the remaining dose r_k. If we fix the remaining dose r_k, we find an optimal policy stated in the corollary below.

Corollary 2.5.3. *There exists an optimal policy, for $k = 1, 2, \ldots, N$, which has the form:*

$$\mu_k(r_k, s_k) = \begin{cases} \underline{B}_k(r_k), & \text{if } h(s_k) \geq C_k(r_k) \\ r_k - ((N - k - i^*)\underline{u} + i^*\overline{u}), & \text{if } D_k(r_k) \leq h(s_k) < C_k(r_k) \\ \overline{B}_k(r_k), & \text{if } h(s_k) < D_k(r_k), \end{cases}$$

where i^* is an integer between 0 and $N-k$ such that $(r_k - ((N-k-i^*)\underline{u} + i^*\overline{u})) \in [\underline{B}_k(r_k), \overline{B}_k(r_k)]$.

Proof. See Appendix 2.11.3. □

For a fixed remaining dose r_k, the above corollary states that an optimal policy will take exactly one of three values: the minimum dose deliverable when the cost of the patient anatomy $h(s_k)$ is above a point $C_k(r_k)$, $r_k - ((N-k-i^*)\underline{u} + i^*\overline{u})$ when the cost $h(s_k)$ is between the points $D_k(r_k)$ and $C_k(r_k)$, and the maximum dose deliverable when the cost $h(s_k)$ is below $D_k(r_k)$. By running the discretized DP algorithm on Matlab using reasonable parameters, we plot the optimal policy decision region for the 15th day (midway through treatment) in Figure 2-3 and see that it has the properties described by the above two results.

An additional special consequence of the above theorem is that when it is possible to deliver the treatment with a sequence of smallest and largest fraction sizes (i.e., when r_k is a nonnegative integer combination of $\underline{u}$ and $\overline{u}$), an optimal policy does exactly that. Moreover, an optimal policy has a threshold form and is essentially unique when the probability distribution $p(\cdot)$ is continuous. This is stated mathematically in the following corollary.

Corollary 2.5.4. *If there exists an integer i between 0 and N such that the initial remaining dose (or the prescribed dose) can be written as $r_1 = (N-i)\underline{u} + i\overline{u}$, then there exists an optimal policy of the threshold form:*

$$\mu_k^*(r_k, s_k) = \begin{cases} \underline{u} & \text{if } h(s_k) \geq T_k(r_k), \\ \overline{u} & \text{if } h(s_k) < T_k(r_k), \end{cases} \tag{2.9}$$

for $k = 1, 2, \ldots, N$. Furthermore, this is the unique optimal policy (except possibly on a zero probability set) if the probability distribution $p(\cdot)$ is continuous.

Proof. We proceed by induction. Let $k = 1$ and assume, for the base case, that there exists an integer i_1 between 0 and N such that the initial remaining dose (or the prescribed dose) can be written as $r_1 = (N - i_1)\underline{u} + i_1\overline{u}$. We consider three cases:

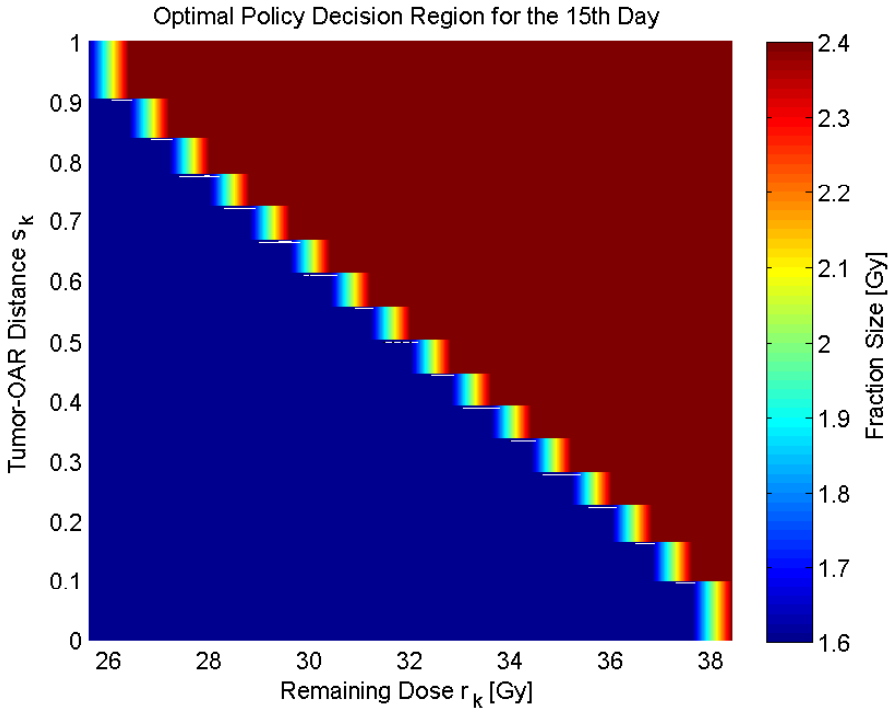

Figure 2-3: Decision region of an optimal policy. We use the following input parameters to the DP algorithm: $N = 30$, $P = 60$ Gy, $\underline{u} = 1.6$ Gy, $\overline{u} = 2.4$ Gy, $p(s_k) \sim U[0, 1]$, and $h(s_k) = 1 - s_k$. We see that the plotted optimal policy agrees with Corollary 2.5.3, and for a fixed remaining dose, takes on exactly three values. We also observe that for a fixed tumor-OAR distance, the optimal policy delivers a dose which linearly increases with the remaining dose (truncated at the limits so that the fraction size stays within the interval $[\underline{u}, \overline{u}]$), which is in agreement with Theorem 2.5.2. The white streaks in the plot are probably due to discretization errors.

1. When $i_1 = 0$, i.e. $r_1 = N\underline{u}$, the only possible solution is $u_1 = u_2 = \ldots = u_N = \underline{u}$, in which case we are done.

2. Similarly, when $i_1 = N$, $u_1 = u_2 = \ldots = u_N = \overline{u}$ is the only solution.

3. We consider the more interesting case when i_1 is an integer between 1 and $N-1$. First, we notice that for any choice of u_1 between $\underline{u}$ and $\overline{u}$, $r_2 = r_1 - u_1$ remains feasible, and hence, the cost-to-go function $J_2(r_1 - u_1, s)$ is finite for all anatomy instances s. Second, since $r_1 = (N - i_1)\underline{u} + i_1\overline{u}$, from Theorem 2.5.2, we have that $J_2(r_1 - u_1, s)$ is linear in u_1 for all values in between $\underline{u}$ and $\overline{u}$. Since taking an expectation preserves linearity, the function $\mathbb{E}\left[J_2(r_1 - u_1, s_2)\right]$ is also linear in u_1. Now, in the DP equation

$$J_1(r_1, s_1) = \min_{\underline{u} \le u_1 \le \overline{u}} \Big(u_1 h(s_1) + \mathbb{E}\left[J_2(r_1 - u_1, s_2)\right] \Big), \tag{2.10}$$

we are minimizing a linear function because adding a linear function $u_1 h(s_1)$ preserves linearity. So, for any feasible r_1, we can write

$$\mathbb{E}\left[J_2(r_1 - u_1, s_2)\right] = a(r_1)u_1 + b(r_1),$$

where $a(r_1)$ and $b(r_1)$ represent the slope and intercept, respectively. Let $T_1(r_1) = -a(r_1)$. Then, since we are minimizing a linear function over an interval in (2.10), $\mu_1^*(r_1, s_1)$ has the desired threshold form:

$$\mu_1^*(r_1, s_1) = \begin{cases} \underline{u}, & \text{if } h(s_1) \ge T_1(r_1), \\ \overline{u}, & \text{if } h(s_1) < T_1(r_1). \end{cases}$$

Now, it is clear that from the above form for $\mu_1^*(r_1, s_1)$, there exists an integer i_2 between 0 and $N-1$ such that the remaining dose in the next fraction can be written as $r_2 = (N - 1 - i_2)\underline{u} + i_2\overline{u}$. We can complete the induction by assuming the appropriate form for r_k in the induction hypothesis and following the same

line of argument as above.

Notice that if $h(s_k) = T_k(r_k)$, any choice of μ_k between $\underline{u}$ and $\overline{u}$ will be optimal. In fact, this is exactly the set of all optimal decisions. However, under the assumption that $p(\cdot)$ is continuous, the event $h(s_k) = T_k(r_k)$ happens with zero probability, and therefore, we need not specify the value of μ_k for this case. It follows that the policy (2.9) is essentially unique when $p(\cdot)$ is continuous. □

There is also a similar result to Corollary 2.5.4, in which the threshold condition is written in terms of r_k (as opposed to $h(s_k)$); it can be derived using similar arguments as in the above results. The assumption in Corollary 2.5.4 that the initial remaining dose can be written as $r_1 = (N-i)\underline{u} + i\overline{u}$ simply requires that it be possible to deliver the treatment with a sequence of smallest fraction sizes $\underline{u}$ and largest ones $\overline{u}$. Otherwise, it would not be possible for the cumulative sum of the fraction sizes to be equal to the prescribed dose when restricting to only the smallest or the largest fraction size. In that respect, the assumption here is reasonable and is generally satisfied in a realistic setting or at least satisfiable with a slight modification of the lower bound $\underline{u}$ and upper bound $\overline{u}$. For the case of continuous $p(\cdot)$, the uniqueness of the policies in Theorem 2.5.2 and Corollary 2.5.3 can be shown in a similar way as in the proof of Corollary 2.5.4.

2.6 Heuristic policies based on optimal policy structure

Although it is possible to solve the problem exactly using the DP algorithm, we develop two heuristics that make use of the structure of an optimal policy and approximate the threshold $T_k(r_k)$ in (2.5) by using: (i) the remaining dose r_k, which summarizes past information, and (ii) the distribution $p(\cdot)$, which summarizes information about the expected patient anatomy in the future. We believe that such heuristics can provide

simpler and intuitive solutions that can possibly be applied to more complex, high-dimensional problems, where using the DP algorithm is no longer computationally feasible.

Without loss of generality we assume $0 \leq h(s_k) \leq 1$, for all s_k. For simplicity we assume that $(\underline{u}+\overline{u})/2 = P/N$, so that $\underline{u}$ and $\overline{u}$ need each to be applied half of the time over the course of treatment. Our Heuristic 1 uses the following threshold:

$$T_k(r_k) = \begin{cases} 0, & \text{if } r_k = (N-k+1)\underline{u}, \\ 1, & \text{if } r_k = (N-k+1)\overline{u}, \\ M, & \text{otherwise,} \end{cases}$$

where M is the median of $h(s_k)$, which by definition satisfies $F^{\mathrm{h}}(M) = \frac{1}{2}$. Such a policy has a simple interpretation: If the remaining dose r_k in the kth fraction is such that we must deliver the smallest fraction size $\underline{u}$ for the remaining fractions (in which case $r_k = (N-k+1)\underline{u}$), we set the threshold to 0, ensuring that regardless of the anatomy s_k, we always deliver the smallest fraction size $\underline{u}$. And, similarly, if the remaining dose r_k is $(N-k+1)\overline{u}$, we set the threshold to 1 and as a result, deliver the largest fraction size $\overline{u}$ for the remaining fractions. Otherwise, for the interesting case when r_k is between $(N-k)\underline{u}$ and $(N-k)\overline{u}$, this policy simply delivers the smallest fraction size $\underline{u}$ when the cost $h(s_k)$ is above its median M (on average, this will happen half of the time) and the largest fraction size $\overline{u}$ when below it (on average, this will happen the other half of the time). Ignoring the possibility that the threshold $T_k(r_k)$, for $k = 1, 2, \ldots, N$, can take extreme values (either 0 or 1), this policy is stationary, in the sense that the thresholds do not change with the fraction k. This is a simplistic approximation to the true values of $T_k(r_k)$. The nice feature of this policy is that we do not need all of the information given in the probability distribution $p(\cdot)$; the only information required is the median M of $h(s_k)$. This could be useful in a realistic setting in which we do not actually have accurate information about the distribution $p(\cdot)$. Here, one could estimate the median M (perhaps by using statistical information from many patient datasets) and use the

above heuristic policy.

An even better heuristic policy might use the entire distribution $p(\cdot)$ (as opposed to just a statistic such as the median or mean) to determine the threshold $T_k(r_k)$. Consider Heuristic 2, which uses a threshold $T_k(r_k)$ that satisfies

$$F^{\mathrm{h}}(T_k(r_k)) = \frac{i_k}{N-k+1}, \tag{2.11}$$

where i_k is the number of largest fraction sizes $\overline{u}$ left to deliver in the remaining $N-k+1$ fractions. Given that $T_k(r_k)$ is fixed for the remaining $N-k+1$ fractions, the left hand side of (2.11) represents the percentage of the remaining fractions for which we *expect* to deliver the largest fraction size $\overline{u}$. And the right hand side represents the percentage of the remaining $N-k+1$ fractions for which we *must* deliver the largest fraction size $\overline{u}$. In some sense, this threshold represents the best balance between what we expect to deliver and what we must deliver. For the uniform distribution, i.e. $h(s_k) \sim U[0,1]$, the threshold $T_k(r_k)$ for Heuristic 2 has a simple closed form expression:

$$T_k(r_k) = \frac{i_k}{N-k+1}.$$

Of course, it may not be possible to write $T_k(r_k)$ as a closed form expression but it can be evaluated by looking at tabulated values of the function $F^{\mathrm{h}}(\cdot)$.[1]

2.7 Algorithm based on a variant of open-loop feedback control

In this section, we derive the algorithm in [48] as a variant of the approximate DP approach known as the open-loop feedback control (see [4] for a description of this

[1]For the case of a discrete probability distribution with a few possible patient anatomy instances, a naive implementation of Heuristic 2 can result in the threshold taking a value of 0 even though it is not necessary to deliver the smallest fraction size $\underline{u}$ for the remaining fractions. In such cases, in our numerical experiments, we forced the heuristic to deliver the largest fraction size $\overline{u}$ when $h(s_k) = 0$, and this resulted in better performance.

approach).

Recall from previous sections that, to solve the original optimization problem in (2.2), we use the DP Algorithm specified by (2.3). The expected cost-to-go function $\overline{J}_{k+1}(r_k - u_k)$ in (2.4) represents the expected future cost of delivering the control u_k given that we use an optimal policy in the future. We consider a suboptimal approach which approximates the cost-to-go function $\overline{J}_{k+1}$ by evaluating the cost incurred from using a heuristic policy in the future instead of an optimal one. Let us consider using a stationary policy (i.e., one that does not depend on time) which is independent of the future states, r_i for $i = k+1, k+2, \ldots, N$. This translates to replacing $\mu_i(r_i, s_i)$ with $\mu(s) = \mu(s_{k+1}) = \mu(s_{k+2}) = \ldots = \mu(s_N)$ in the optimization problem (2.2). Therefore, in the kth fraction (when the states r_k and s_k are known), we would be solving the following problem:

$$
\begin{aligned}
\min_{u_k,\,\mu} \quad & \mathbb{E}\left[g(r_{N+1}) + g_k(s_k, u_k) + \sum_{i=k+1}^{N} g_i(\mu(V_i), V_i) \right] \\
\text{subject to} \quad & \underline{u} \le u_k \le \overline{u}, \\
& \underline{u} \le \mu(s) \le \overline{u}, && \forall s \in S, \\
& r_{k+1} = r_k - u_k, \\
& r_{i+1} = r_i - \mu(V_i), && i = k+1, k+2, \ldots, N, \\
& V_{i+1} \sim p(\cdot), && i = k, k+1, \ldots, N,
\end{aligned}
$$

where we distinguish the random future anatomies by V_i and the observed (known) anatomy s_k. Since we assume V_i are independent and identically distributed, the expectation of the summation in the objective above simplifies to $(N-k)$ identical terms. Now we can remove the function $g(r_{N+1})$ by including the constraint $\underline{B}(r_k) \le u_k \le \overline{B}(r_k)$. Finally, we approximate the dynamics of the system $r_{k+1} = r_k - u_k$, $r_{i+1} = r_i - \mu(V_i)$, and $s_{i+1} \sim p(\cdot)$ by ensuring the expected delivered dose is equal to the prescription dose. This is captured by the equation $u_k + (N-k)E\left[\mu(V_k)\right] = r_k$. After these modifications, we obtain the following linear programming (LP) formulation to solve in the

kth fraction:

$$\begin{aligned} \min_{u_k,\,\mu} \quad & u_k h(s_k) + (N-k)\mathbb{E}\left[\mu(V_k)h(V_k)\right] \\ \text{subject to} \quad & \underline{B}(r_k) \le u_k \le \overline{B}(r_k), \\ & \underline{u} \le \mu(s) \le \overline{u}, \qquad\qquad \forall s \in S, \\ & u_k + (N-k)\mathbb{E}\left[\mu(V_k)\right] = r_k, \end{aligned}$$

where we take the expectation with respect to the distribution $p(\cdot)$. The LP algorithm above is the same algorithm as the one in [48]. We have derived this algorithm under our problem framework and clearly established the relationship between this work and the one in [48].

2.8 Numerical results

We discuss the results from implementing the adaptive algorithms (both exact and heuristic) in Matlab. For the problem parameters, we take the number of fractions N to be 30, the prescribed dose P to be 60 Gy, the smallest fraction size $\underline{u}$ to be 1.6 Gy, the largest fraction size $\overline{u}$ to be 2.4 Gy, the set of patient anatomy instances S to be 10 equally spaced values between 0 and 1 representing the distance between the tumor and OAR (see Figure 2-1), the distribution $p(\cdot)$ to be a discrete uniform, and the function $h(s_k)$ to be $1 - s_k$. Essentially, we are allowing for a 20% daily fraction size deviation from the standard 2 Gy per fraction.

We find that both Heuristic 1 and 2 do well in approximating the optimal threshold, and as a result, perform numerically close to optimal. In Figure 2-4, for one treatment simulation (i.e., one realization of the sequence $\{s_1, s_2, \ldots, s_N\}$), we show the thresholds of the optimal and heuristic policies. When the tumor-OAR distance s_k is large and above the threshold, which indicates a favorable anatomy, the policy delivers the largest fraction size $\overline{u}$, and vice versa. We note that, for this 1-dimensional setting, the threshold in Figure 2-4 is equal to $1 - T_k(r_k)$ because we are plotting the tumor-OAR

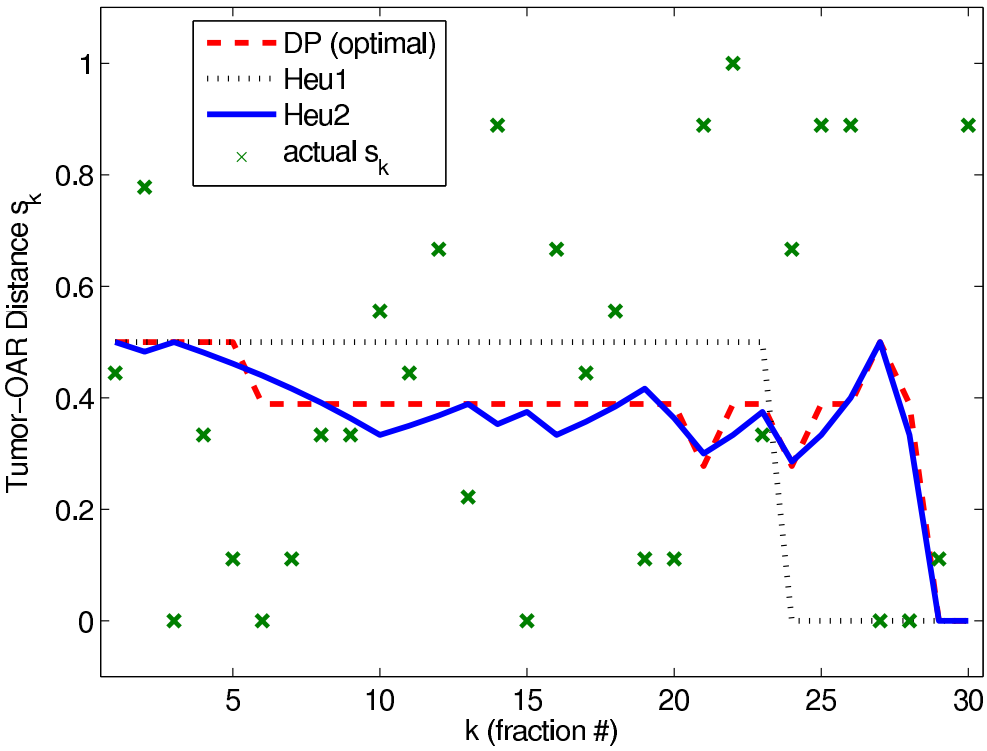

Figure 2-4: Thresholds of optimal and heuristic policies resulting from one treatment simulation run (i.e., one realization of the patient anatomy sequence $\{s_1, s_2, \ldots, s_N\}$). For this 1-dimensional example, the threshold lines plotted represent the point at which a policy delivers the smallest fraction size $\underline{u}$ when s_k is below it and the largest fraction size $\overline{u}$ when above it. These lines plotted are actually $1-T_k(r_k)$ because we are plotting s_k instead of $h(s_k) = 1 - s_k$. The 'x' markers correspond to the actual realization of the tumor-OAR distance s_k. Heuristic 1 (Heu1) makes a crude approximation to the optimal threshold while Heuristic 2 (Heu2) follows it closely. Since the 'x' markers are uniformly spread out and rarely take values near the thresholds, the heuristic algorithms perform well compared to the optimal DP approach.

distance s_k on the y-axis rather than $h(s_k)$. While Heuristic 2 closely approximates the optimal threshold, Heuristic 1 makes a crude approximation since it only uses the median M of $h(s_k)$. Since the realized tumor-OAR distances s_k (as shown by the 'x' markers) are uniformly spread out and rarely take values near the thresholds, we see that the heuristic algorithms perform well.

In Table 2.1, we see that when using a uniformly distributed motion model, the adaptive policies result in about a 10% decrease in dose to the OAR compared to that resulting from standard fractionation. Note that the DP approach represents the opti-

Table 2.1: Using a uniformly distributed motion model and a 20% daily fraction size deviation, we find about a 10% decrease in dose to the OAR when using adaptive policies. The dose to the OAR is averaged over 10,000 treatment runs in order to report results to two decimal places.

	Average Dose to OAR
Standard Fractionation	30.00
DP (Optimal)	27.00
Heuristic 1	27.13
Heuristic 2	27.00
Algorithm in [48]	27.07

mal policy, and hence, provides a baseline for comparison to the other heuristics. The difference in the dose to the OAR resulting from Heuristic 1 and the DP approach is very little, which means that using a statistic such as the median M of $h(s_k)$ is enough for achieving significant decrease in dose to the OAR. Such a policy could be advantageous in a realistic setting when it is not possible to have accurate information about the distribution $p(\cdot)$. As expected, Heuristic 2 performs even better than Heuristic 1 since it uses the entire distribution $p(\cdot)$ in the threshold computation. We can see that the numerical difference between the OAR dose resulting from Heuristic 2 and the DP approach is not even visible when using two decimal places. Finally, we also simulate the algorithm in [48] for comparison and notice that it is close to optimal as well, like the other heuristics.

In Figure 2-5, we vary both the number of fractions N and the daily fraction size deviations, and simulate the decrease in the OAR dose when using the optimal DP approach. We use 20%, 50%, and 100% daily fraction size deviations, and 5, 30, and 60 fractions for N. This allows us to understand the benefit of adaptive fractionation in hypo-, standard, and hyper-fractionation regimes. This, however, may not be entirely accurate because we simply normalize the dose per fraction so that the same prescribed dose P is met at the end of treatment, and we do not take into account the biological effect of varying N. The error bars in Figure 2-5 correspond to one standard deviation, as estimated from the simulation of 500 treatment runs. A larger number of fractions and daily fraction size deviation result in more chances to capitalize on favorable

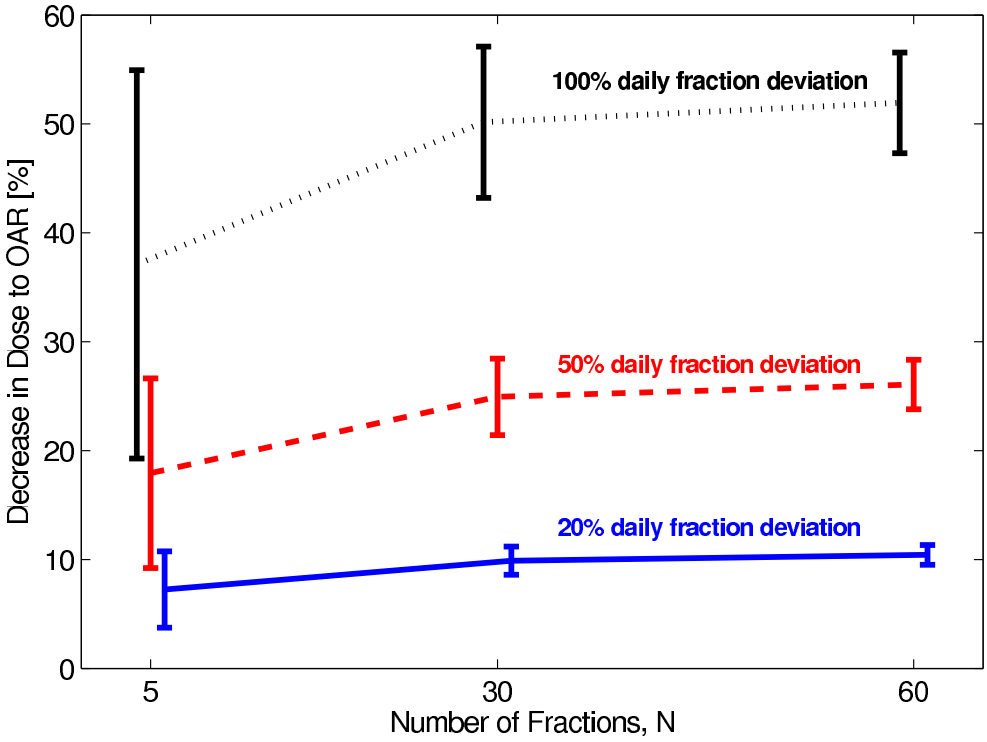

Figure 2-5: Comparing adaptive fractionation in hypo-, standard, and hyper-fractionated settings. We simulate the performance of just the optimal DP approach through 500 treatment runs. The fraction size is adjusted when varying the number of fractions N so that the same prescribed dose P is met at the end of treatment. The error bars correspond to one standard deviation, as estimated from the results of the 500 runs. We find a larger decrease in dose to the OAR when using more fractions and larger daily fraction size deviations.

anatomy, and therefore, result in more gain. We see bigger error bars when using larger daily fraction size deviations due to the increased variation in the ability to capitalize on favorable anatomy. On the other hand, we see smaller error bars when increasing the number of fractions, which means the treatment outcome is more predictable; this is because with a large number of fractions, laws of large numbers (from probability theory) take effect. In summary, Figure 2-5 shows that the percentage decrease in the dose to the OAR varies significantly (anywhere from 5 - 55%). But in general, we find more gain when using a larger number of fractions and daily fraction size deviations.

As we see in Figure 2-6, the decrease in dose to the OAR is more pronounced when we have a high probability of large tumor-OAR distances. We use three distributions,

each corresponding to parameters of the beta distribution ($p(s) = c \cdot s^{1-\alpha}(1-s)^{1-\beta}$, where c is a normalization constant), and plot them in the right panel. As before, we use 10 uniformly discretized values between 0 and 1 for the possible tumor-OAR distances. In the left panel, for the Unfavorable distribution, the percentage decrease in the OAR dose is minimal. On the other hand, there is a significant decrease in the OAR dose for the Uniform and Favorable distributions. We conclude that when the OAR tends to stay far away from the tumor, we see a larger decrease in dose to the OAR. In such cases, favorable anatomies are frequent enough so that the DP approach is able to make up for the small fraction sizes used for unfavorable anatomies. When allowing a 100% daily fraction size deviations and using the Favorable distribution, there is at least a 10% decrease in the OAR dose when comparing the optimal DP approach with the algorithm in [48]. Here, the algorithm in [48] "believes" favorable anatomies will be frequent enough over the course of treatment so that no matter what fraction size is delivered in the initial fractions, it will be able to make up for the much more infrequent unfavorable anatomies.

2.9 Convergence of Heuristic 1 to optimality as $N \to \infty$

We analyze the asymptotic properties of Heuristic 1 (as a function of the number of treatments, N). We find that the expected cost associated with Heuristic 1 converges to the expected cost associated with the optimal DP algorithm as $N \to \infty$, with the discrepancy being of order $O\left(\frac{\sqrt{\log N}}{\sqrt{N}}\right)$. The discussion in this section provides a theoretical justification for Heuristic 1 and in some sense, convinces us of its "soundness" as a solution approach. For our previous theoretical results, as mentioned in Remark 3, we only required the Markov property to hold true for the sequence of patient anatomy instances. The results in this section require however a stronger assumption, stated next.

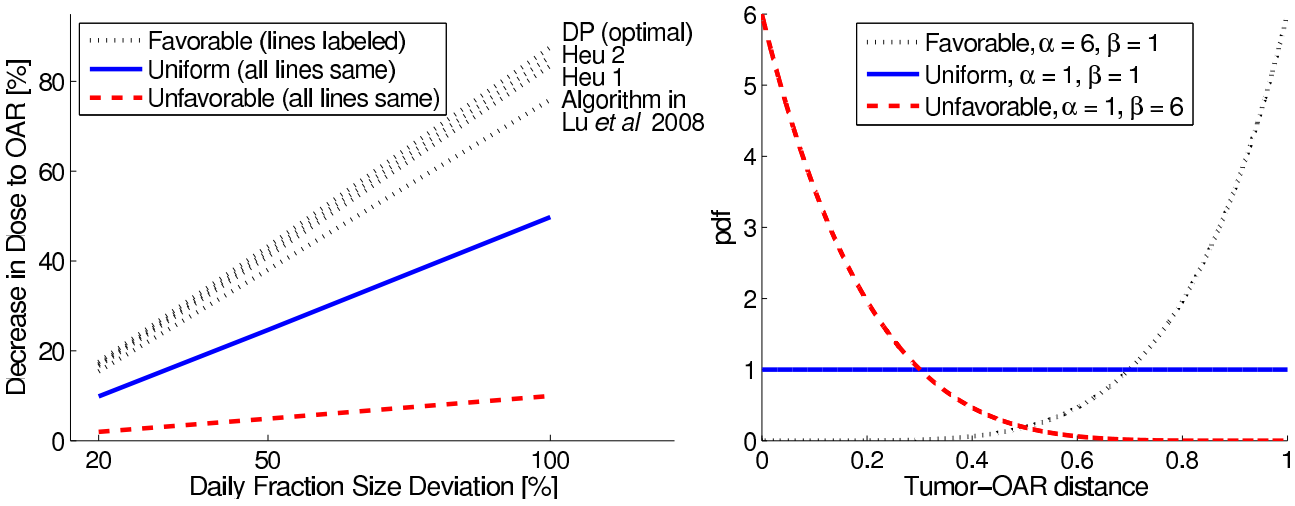

Figure 2-6: Results from varying the motion probability distribution. In the right panel, we show the three probability distributions used, each resulting from varying parameters of the beta distribution. In the left panel, we show the average percentage decrease (from 500 treatment runs) in dose to the OAR for each of these probability distributions. For probability distributions in which the OAR tends to stay far away from the tumor, there is a larger decrease in dose to the OAR, and the optimal DP approach is at least 10% better than the other heuristics.

Assumption 2.9.1. *The patient anatomy instances s_k, for $k = 1, 2, \ldots, N$, are independent.*

For our results to hold, we also need an additional assumption stated below to ensure that the probability distribution is well-behaved. For this section, we use the probability distribution $p^{\mathrm{h}}(\cdot)$ on $h(s_k)$ rather than $p(\cdot)$ on s_k.

Assumption 2.9.2. *The probability distribution of $h(s_k)$ is continuous, described by a density $p^h(\cdot)$, which is bounded above by a constant K (i.e., $|p^h(x)| \leq K$ for all x).*

We denote the expected cost associated with using the optimal DP approach and Heuristic 1 by $\mathcal{C}_{\mathrm{dp}}$ and $\mathcal{C}_{\mathrm{heu1}}$, respectively. We wish to show that $|\mathcal{C}_{\mathrm{heu1}} - \mathcal{C}_{\mathrm{dp}}| \to 0$ as $N \to \infty$. We will simplify the mathematical analysis by finding a lower bound for $\mathcal{C}_{\mathrm{dp}}$ instead of using the DP algorithm directly. To find such a lower bound, consider the fractionation problem when the sequence of costs $h(s_k)$, for $k = 1, 2, \ldots, N$, are known prior to treatment. The resulting expected cost, which we denote by $\mathcal{C}^*$, is definitely

smaller than $\mathcal{C}_{\text{dp}}$. Hence, we must have $\mathcal{C}^* \leq \mathcal{C}_{\text{dp}} \leq \mathcal{C}_{\text{heu1}}$, where the last bound is due to the optimality of the DP algorithm. The analysis below will involve showing $|\mathcal{C}_{\text{heu1}} - \mathcal{C}^*| \to 0$ as $N \to \infty$, which will also imply $|\mathcal{C}_{\text{heu1}} - \mathcal{C}_{\text{dp}}| \to 0$.

Even though it may be inconsistent with prior notation, in this section, s_k refers to a random variable, not an observed or known quantity. We will relate the cost $\mathcal{C}^*$ to the empirical median M_N, which we define below.

Definition 2.9.1. *The empirical median M_N satisfies $F_N(M_N) = 0.5$, where the empirical CDF F_N is defined as*

$$F_N(x) = \frac{1}{N} \sum_{k=1}^{N} \mathbb{I}_{\{h(s_k) \leq x\}}.$$

Here, $\mathbb{I}$ denotes the indicator random variable:

$$\mathbb{I}_A = \begin{cases} 1, & \textit{if event } A \textit{ occurs} \\ 0, & \textit{otherwise.} \end{cases}$$

In order to relate the empirical median M_N to $\mathcal{C}^*$, we note that the event $D_k = \{h(s_k) < M_N\}$ consists of $N/2$ patient anatomies with the lower costs (assuming, for simplicity, N is even). The event D_k^c then corresponds to those with the higher costs. Now, it is clear that

$$\mathcal{C}^* = \mathbb{E}\left[\sum_{k=1}^{N} h(s_k) \left(\overline{u}\mathbb{I}_{D_k} + \underline{u}\mathbb{I}_{D_k^c}\right)\right]. \tag{2.12}$$

We can similarly relate $\mathcal{C}_{\text{heu1}}$ to the true median M. We define the event $A_k = \{h(s_k) < M\}$, which consists of patient anatomies for which Heuristic 1 delivers $\overline{u}$. In order to incorporate the heuristic's boundary conditions, we define the events $B_k = \{r_k = (N-k)\overline{u}\}$ and $C_k = \{r_k = (N-k)\underline{u}\}$. Finally, we can write

$$\mathcal{C}_{\text{heu1}} = \mathbb{E}\left[\sum_{k=1}^{N} h(s_k) \left(\overline{u}\mathbb{I}_{A_k \cap B_k^c \cap C_k^c} + \underline{u}\mathbb{I}_{A_k^c \cap B_k^c \cap C_k^c} + \overline{u}\mathbb{I}_{B_k} + \underline{u}\mathbb{I}_{C_k}\right)\right].$$

The empirical CDF $F_N(\cdot)$ and empirical median M_N are estimates of the true underlying CDF $F^{\mathrm{h}}(\cdot)$ and true median M, respectively. Existing results in probability theory prove the uniform convergence of $F_N(\cdot)$ to $F^{\mathrm{h}}(\cdot)$ and also provide bounds on the rate of convergence. In order to show the convergence of $|\mathcal{C}_{\mathrm{heu1}} - \mathcal{C}^*| \to 0$, we will rely on the convergence of the empirical median M_N to the true median, M. The following two lemmas show convergence in probability and convergence in the r-th mean of M_N to M, respectively.

Lemma 2.9.1. *Assume a positive density in a small interval around the median M, i.e., $p^h(x) > 0$ for $x \in [M-\gamma, M+\gamma]$. Then,*

$$\mathbb{P}(|M_N - M| > \epsilon) \leq \begin{cases} 2e^{-2c^2 N\epsilon^2}, & \text{if } 0 < \epsilon \leq \gamma \\ 2e^{-2c^2 N\gamma^2}, & \text{if } \epsilon > \gamma, \end{cases}$$

where $c = \min_{x \in [M-\gamma, M+\gamma]} p^h(x)$.

Proof. See Appendix 2.11.4. □

Lemma 2.9.2. *Assume a positive density in a small interval around the median M, as in Lemma 2.9.1. Then, the empirical median M_N converges in the r-th mean to the true median M as $N \to \infty$. Furthermore, as a function N, we have for $r \geq 1$*

$$\mathbb{E}\big[|M_N - M|^r\big] = O\left(\left[\frac{\log N}{N}\right]^{\frac{r}{2}}\right).$$

Proof. See Appendix 2.11.5. □

The cost $\mathcal{C}^*$ uses the empirical median while $\mathcal{C}_{\mathrm{heu1}}$ uses the true median. Given the nice convergence properties of the empirical median to the true one, it is reasonable to relate the two costs and analyze convergence. The main difficulty lies in the boundary conditions corresponding to the sets B_k and C_k in the definition of $\mathcal{C}_{\mathrm{heu1}}$. In the next

lemma, we show that the probability of the sets B_k and C_k is small (exponentially decreasing with N) for all but the last $O\left(\sqrt{N \log N}\right)$ fractions.

Lemma 2.9.3. *For any $a > 0$, we have*

$$\max\left\{\mathbb{P}(B_k), \mathbb{P}(C_k)\right\} \leq \frac{1}{N^a},$$

if $k \leq N - \lfloor 2\sqrt{\frac{a}{2} N log N} \rfloor - 1$.

Proof. See Appendix 2.11.6. □

Finally, we state the main result in the following theorem.

Theorem 2.9.4. *Heuristic 1 is asymptotically optimal. That is, $|\mathcal{C}_{heu1} - \mathcal{C}_{dp}| \to 0$ as $N \to \infty$. The rate of convergence is $O\left(\frac{\sqrt{logN}}{\sqrt{N}}\right)$.*

Proof. See Appendix 2.11.7. □

We have shown that Heuristic 1 is "sound" in the sense that it is optimal in the limit as the number of treatments N is very large. Though the results in this section have little impact on the practical applicability of any particular method, it provides some theoretical insight.

2.10 Discussion and conclusions

Realistic implementation of the approaches described in this chapter require the following:

1. The motion probability distribution $p(\cdot)$ must be known. One could in principle collect and analyze population data, and assign probabilities corresponding to a few anatomy scenarios. However, this may not be an accurate representation of a patient-specific probability distribution. Updating the probability distribution as the sequence of patient anatomy instances are observed could be a topic of future research.

2. Immediately before the delivery of a fraction, imaging information about the patient anatomy must be available as well as reliable automatic contouring and/or contour registration algorithms to process this information. This would be needed in order to determine the favorability of the patient anatomy in any particular day. We can be optimistic that such technology will be available in the near future.

3. The OAR dose per unit dose to the tumor, $h(s_k)$, must be computable before the delivery of each fraction. In order to speed up the computation, one may use the same dose deposition matrix from the initial CT scan as an approximation and determine the dose projected on the OAR in the new CT. We emphasize that this model does not depend on using the OAR dose per unit tumor dose for $h(s_k)$; we simply need a function $h(s_k)$ which tells us how favorable a particular anatomy s_k is.

Other assumptions of our model include the following:

1. One primary OAR is the basis for making decisions about the fraction size. Multiple OARs can be used, for example, by using for $h(s_k)$ a weighted combination of the dose to each OAR per unit dose to the tumor. However, this does not capture the true tradeoff between the various OARs because there is also generally an upper limit to the dose of each OAR. The model would better represent the radiation therapy problem if, for example, the non-linear NTCP curves were incorporated into the cost function. There is potential for further research work here.

2. The prescribed dose to the tumor must be met exactly and is penalized with an infinite cost. One may also consider using a penalty (e.g., quadratic) on the deviation from the prescribed dose, which would possibly result in a "smoother" optimal policy that does not pick the extreme fraction sizes.

3. Variations in the patient anatomy are dose-independent and random. In order

to incorporate systematic time varying trends (e.g., tumor shrinkage), we can re-optimize the treatment plan (the dose profile) midway through treatment. Then, we can use one of the adaptive fractionation methods in this chapter for the first half of treatment assuming no systematic changes. For the latter half of treatment, we would re-optimize the treatment plan, update the motion probability distribution and/or escalate the prescribed dose if necessary, and restart the adaptive fractionation method. For other systematic offsets (e.g, patient setup errors), we assume daily imaging modalities are accurate enough for correction.

4. When the daily fraction size deviations are not too large, the biological impact of a varied fractionation scheme is negligible. It is likely that deviating 20% from standard fractionation does not result in a major difference between physical dose and biological dose [6]. Dose deviations of 50% and 100%, however, need further study. Using large deviations and varied fractionation may require additional considerations such as changes in the onset of early and late reactions. A biologically based adaptive fractionation approach is given in [13].

Under our framework, it is possible to derive the algorithm in [48] and see that it is a variant of the approximate DP approach known as open-loop feedback control (refer to [4] for a description of such an approach). From the numerical results, we conclude that the algorithm in [48] performs very close to optimal for almost all cases. However, we do see that the DP approach performs about 10% better when allowing 100% daily fraction size deviations and using a probability distribution that favors large tumor-OAR distances. One difference in the way these algorithms would be used in practice is that the DP approach involves an online table lookup, while the algorithm in [48] requires solving a linear programming (LP) problem right before the delivery of every fraction. Though a table lookup is quicker, solving a LP for this problem, where we are simply searching for a scalar variable u_k, is also very fast and can be done before each fraction without much time overhead.

Based on the linear-quadratic model of radiation effects, varying the fraction size during the course of treatment while ensuring a fixed total prescribed dose leads to a higher TCP [6]. One might argue that this benefit is neutralized by an increase in the NTCP for the OAR. However, assuming that the OAR has an underlying motion, even standard fractionation results in a different dose to the OAR from fraction to fraction. Adaptive fractionation will lead to a more uniform dose to the OAR because a small fraction size is delivered when the OAR-to-tumor dose ratio $h(s_k)$ is large (i.e., when the tumor and OAR are close together), and vice versa. Further research can be done to evaluate the biological benefit of varying the fraction size.

We have posed the adaptive fractionation problem in a theoretical framework and have provided several solution methods. First, we used the DP algorithm to establish a benchmark and to solve the problem exactly. This allowed us to show that the simple heuristics proposed in this chapter were numerically near-optimal. One of these heuristics only uses a statistic, such as the median or mean, rather than the entire probability distribution. Such a policy can provide a quick way to estimate the best possible benefit of using an adaptive fraction size in a realistic setting. We have demonstrated through numerical simulations that we can expect a significant decrease in dose to the OAR when: (i) we have a high probability of large tumor-OAR distances, (ii) we use many fractions (as in a hyper-fractionated setting), and (iii) we allow large daily fraction size deviations. We expect adaptive fractionation to be beneficial for disease sites in which the OAR exhibits significant motion from day to day. Some examples include pelvic cases such as rectal [59], prostate [83], and cervical [25] cancers.

2.11 Appendix: proofs

2.11.1 Proof of Lemma 2.5.1

Proof. From equation (2.3), we can see that $J_k(r_k, s_k) = \infty$ if $(r_k - u_k) \notin \mathcal{F}_{k+1}$ (since $\int_S p(s) J_{k+1}(r_k - u_k, s)\,\mathrm{d}s = \infty$ if $(r_k - u_k) \notin \mathcal{F}_{k+1}$). Therefore, we can rewrite Equation

(2.3) as

$$J_k(r_k, s_k) = \min_{u_k \in U_k(r_k)} \Big(u_k h(s_k) + \overline{J}_{k+1}(r_k - u_k) \Big),$$

where $U_k(r_k) = \{u_k : \underline{u} \leq u_k \leq \overline{u}, (r_k - u_k) \in \mathcal{F}_{k+1}\}$. Using the definition of $\mathcal{F}_{k+1}$ from Equation (2.6), we see that

$$\begin{aligned} U_k(r_k) &= \{u_k : \underline{u} \leq u_k \leq \overline{u}, (N-k)\underline{u} \leq r_k - u_k \leq (N-k)\overline{u}\} \\ &= \{u_k : \max(\underline{u}, r_k - (N-k)\overline{u}) \leq u_k \leq \min(\overline{u}, r_k - (N-k)\underline{u}))\} \\ &= \{u_k : \underline{B}_k(r_k) \leq u_k \leq \overline{B}_k(r_k)\}, \end{aligned}$$

from which we can write Equation (2.7). □

2.11.2 Proof of Theorem 2.5.2

Proof. We proceed by induction. For the base case, let $k = N$. It is clear that the optimal decision in this last fraction, $\mu_N^*(r_N, s_N)$, is equal to the remaining dose r_N. (Otherwise, we would incur an infinite penalty for not meeting the prescribed dose exactly.) In this case, for any $r_N \in \mathcal{F}_N$, $J_N(r_N, s_N) = r_N h(s_N)$, which has the desired continuous, non-decreasing, convex, and piecewise linear form. Now, assume that J_{k+1}, for $r_{k+1} \in \mathcal{F}_{k+1}$, also has this form as stated in the theorem. First, we prove convexity of J_k in r_k. Then, we prove the remaining properties of J_k along with the structure of an optimal policy.

Step 1: Proof of convexity For any $r_k^1, r_k^2 \in \mathcal{F}_k$, we have

$$\begin{aligned} J_k\left(\frac{r_k^1 + r_k^2}{2}, s_k\right) &= \min_{\underline{u} \leq u_k \leq \overline{u}} \left(u_k h(s_k) + \overline{J}_{k+1}\left(\frac{r_k^1 + r_k^2}{2} - u_k\right)\right) \\ &\leq u_k h(s_k) + \overline{J}_{k+1}\left(\frac{r_k^1 + r_k^2}{2} - u_k\right)\Big|_{u_k = \frac{\mu_k(r_k^1, s_k) + \mu_k(r_k^2, s_k)}{2}}, \end{aligned}$$

where $\mu_k(r_k, s_k) = \arg\min_{\underline{u} \leq u_k \leq \overline{u}} \big[u_k h(s_k) + \overline{J}_{k+1}(r_k - u_k)\big]$. Notice that the choice $\frac{\mu_k(r_k^1, s_k) + \mu_k(r_k^2, s_k)}{2}$ for u_k above is feasible (i.e., between $\underline{u}$ and $\overline{u}$) because the condition $\underline{u} \leq \mu_k(r_k, s_k) \leq \overline{u}$

is always true. We also claim that $(r_k^1 - \mu_k(r_k^1, s_k)), (r_k^2 - \mu_k(r_k^2, s_k)) \in \mathcal{F}_{k+1}$. To see this is true, suppose $(r_k^1 - \mu_k(r_k^1, s_k)) \notin \mathcal{F}_{k+1}$. Then,

$$\begin{aligned} J_k(r_k, s_k) &= \mu_k(r_k^1, s_k)h(s_k) + \overline{J}_{k+1}(r_k^1 - \mu_k(r_k^1, s_k)) \\ &= \mu_k(r_k^1, s_k)h(s_k) + \infty \\ &= \infty, \end{aligned}$$

which contradicts the optimality of μ_k. Hence, $(r_k^1 - \mu_k(r_k^1, s_k)), (r_k^2 - \mu_k(r_k^2, s_k)) \in \mathcal{F}_{k+1}$ must be true. Using this fact and the convexity of $\overline{J}_{k+1}(r_{k+1})$ in r_{k+1} (taking expectation preserves convexity), we have

$$\begin{aligned} J_k\left(\frac{r_k^1 + r_k^2}{2}, s_k\right) &\leq \left(\frac{\mu_k(r_k^1, s_k) + \mu_k(r_k^2, s_k)}{2}\right) h(s_k) \\ &\quad + \overline{J}_{k+1}\left(\frac{r_k^1 - \mu_k(r_k^1, s_k)}{2} + \frac{r_k^2 - \mu_k(r_k^2, s_k)}{2}\right) \\ &\leq \left(\frac{\mu_k(r_k^1, s_k) + \mu_k(r_k^2, s_k)}{2}\right) h(s_k) \\ &\quad + \frac{1}{2}\overline{J}_{k+1}\left(r_k^1 - \mu_k(r_k^1, s_k), w\right) + \frac{1}{2}\overline{J}_{k+1}\left(r_k^2 - \mu_k(r_k^2, s_k)\right) \\ &= \frac{1}{2}J_k\left(r_k^1, s_k\right) + \frac{1}{2}J_k\left(r_k^2, s_k\right). \end{aligned}$$

Therefore, $J_k(r_k, s_k)$ is convex in r_k (midpoint convexity implies convexity), and the result follows.

Step 2: Proof of remaining properties We assume $\underline{u} = 0$ and $\overline{u} = 1$ for simplicity. For the general case, the same arguments below can be used, with more bookkeeping and algebra. The proof below uses similar types of arguments as the proof for the inventory control problem in [4]. From the DP Algorithm, we have

$$J_k(r_k, s_k) = \min_{0 \leq u_k \leq 1} \left[u_k h(s_k) + \overline{J}_{k+1}(r_k - u_k)\right]. \tag{2.13}$$

By introducing the variable $y = r_k - u_k$, we can rewrite (2.13) as

$$J_k(r_k, s_k) = \min_{r_k - 1 \le y \le r_k} [G_k(y, s_k)] + r_k h(s_k), \tag{2.14}$$

where $G_k(y, s_k) = -yh(s_k) + \overline{J}_{k+1}(y)$. From the previous step, we have that $\overline{J}_{k+1}(y)$ is convex in y (taking expectation preserves convexity). Thus, the function G_k is convex in y because it is a sum of two convex functions in y: $-yh(s_k)$ and $\overline{J}_{k+1}(y)$. Let us suppose that the unconstrained minimum over y of $G_k(y, s_k)$ exists and denote it as $A_k(s_k)$:

$$A_k(s_k) = \arg\min_{y \in \mathbb{R}} G_k(y, s_k).$$

Since $\overline{J}_{k+1}(y)$ is infinite for $y \notin \mathcal{F}_{k+1}$, we can simplify the minimization by restricting y to be in $\mathcal{F}_{k+1}$:

$$A_k(s_k) = \arg\min_{y \in \mathbb{F}_{k+1}} G_k(y, s_k).$$

Now, in the induction, we assume J_{k+1}, for $r_{k+1} \in \mathcal{F}_{k+1}$, is continuous and piecewise linear with breakpoints at integers between 0 and $N - k$. Therefore, $G_k(y, s_k)$ also has the same form in y. Because we are minimizing a continuous, convex function in y over $\mathcal{F}_{k+1}$ (a compact, convex set), it follows that the minimizer $A_k(s_k)$ exists. Furthermore, due to the particular piecewise linear form of G_k in y, $A_k(s_k)$ can be restricted to be an integer between 0 and $N - k$ without loss of optimality. Finally, incorporating the constraint $r - 1 \le y \le r$, we have an optimal solution for (2.14):

$$y = \begin{cases} r_k - 1, & \text{if } r_k \ge 1 + A_k(s_k) \\ A_k(s_k), & \text{if } A_k(s_k) \le r_k < 1 + A_k(s_k) \\ r_k, & \text{if } r_k < A_k(s_k). \end{cases}$$

Using the reverse transformation $u_k = r_k - y$, we have

$$\mu_k(r_k, s_k) = \begin{cases} 1, & \text{if } r_k \geq 1 + A_k(s_k) \\ r_k - A_k(s_k), & \text{if } A_k(s_k) \leq r_k < 1 + A_k(s_k) \\ 0, & \text{if } r_k < A_k(s_k), \end{cases}$$

which has the desired form in (2.8). Substituting this policy into the DP equation, we have

$$J_k(r_k, s_k) = \begin{cases} h(s_k) + \overline{J}_{k+1}(r_k - 1), & \text{if } r_k \geq 1 + A_k(s_k) \\ (r_k - A_k(s_k))h(s_k) + \overline{J}_{k+1}(A_k(s_k)), & \text{if } A_k(s_k) \leq r_k < 1 + A_k(s_k) \\ \overline{J}_{k+1}(r_k), & \text{if } r_k < A_k(s_k). \end{cases} \tag{2.15}$$

Using the properties of piecewise linearity of J_{k+1} in r_{k+1} and integer $A_k(s_k)$, it is clear from (2.15) that J_k in r_k is piecewise linear with breakpoints between 0 and $N-k+1$. Furthermore, assuming J_{k+1} is continuous and non-decreasing in r_{k+1}, we can see from (2.15) that J_k is also continuous and non-decreasing in r_k. We have completed the induction. □

2.11.3 Proof of Corollary 2.5.3

Proof. We assume $\underline{u} = 0$ and $\overline{u} = 1$ for ease in exposition. We use the DP algorithm from Lemma 2.7:

$$J_k(r_k, s_k) = \min_{\underline{B}_k(r_k) \leq u_k \leq \overline{B}_k(r_k)} \Big(u_k h(s_k) + \overline{J}_{k+1}(r_k - u_k) \Big). \tag{2.16}$$

From Theorem (2.5.2), it follows that $\overline{J}_{k+1}(r_k - u_k)$ continuous, non-increasing, convex, and piecewise linear in u_k with breakpoints at $r_k - i$, where i is an integer between 0 and $N - k$. Note that there is at most a single breakpoint in between $\underline{B}_k(r_k)$ and $\overline{B}_k(r_k)$. We will assume that $u_k = r_k - i^*$ is this breakpoint, where i^* is between 0 and

$N-k$. The derivative of the objective in (2.16) is $h(s_k)$ plus a non-decreasing piecewise constant function. It follows that if $h(s_k)$ is very large, the optimum would be the smallest deliverable dose $\underline{B}_k(r_k)$. Similarly, if $h(s_k)$ is very small, the optimum would be the largest deliverable dose $\overline{B}_k(r_k)$. In between these two cases, the optimum would be $r_k - i^*$, which allows the subderivative of the objective in (2.16) to be zero. This results in the desired form of an optimal policy. We can also use the above argument for a general $\underline{u}$ and $\overline{u}$. □

2.11.4 Proof of Lemma 2.9.1

Proof. Since c is the minimum slope of $F(x)$ in the interval $[M-\gamma, M+\gamma]$, for $0 < \epsilon \leq \gamma$, we have

$$F(M-\epsilon) \leq F(M) - c\epsilon$$

and

$$F(M+\epsilon) \geq F(M) + c\epsilon. \tag{2.17}$$

Note that since we have a continuous distribution, $F(M) = 1/2$. Also, $F_N(M_N) = 1/2$, by definition. Now we will show that if $|M_N - M| > \epsilon$, then $|F(M_N) - F_N(M_N)| > c\epsilon$. If $M_N - M > \epsilon$, then

$$\begin{aligned} F(M_N) &> F(M+\epsilon) && (2.18)\\ &\geq F(M) + c\epsilon && (2.19)\\ &= F_N(M_N) + c\epsilon, \end{aligned}$$

which implies $F(M_N) - F_N(M_N) > c\epsilon$ as desired. In (2.18), we use the monotonicity property of the distribution $F(\cdot)$, and in (2.19), we use Equation (2.17). Similarly, if

$M_N - M < -\epsilon$, then:

$$\begin{aligned} F(M_N) &< F(M - \epsilon) \\ &\leq F(M) - c\epsilon \\ &= F_N(M_N) - c\epsilon, \end{aligned}$$

and therefore, $F(M_N) - F_N(M_N) < -c\epsilon$. We have shown that if $|M_N - M| > \epsilon$, then $|F(M_N) - F_N(M_N)| > c\epsilon$. The first inequality below makes use of this property. We have

$$\begin{aligned} \mathbb{P}(|M_N - M| > \epsilon) &\leq \mathbb{P}(|F(M_N) - F_N(M_N)| > c\epsilon) \\ &\leq \mathbb{P}(\sup_x |F_N(x) - F(x)| > c\epsilon) \\ &\leq 2\mathrm{e}^{-2c^2 N\epsilon^2}, \end{aligned} \tag{2.20}$$

where in (2.20), we use the Dvoretzky-Kiefer-Wolfowitz inequality.

For $\epsilon > \gamma$,

$$\begin{aligned} \mathbb{P}(|M_N - M| > \epsilon) &\leq \mathbb{P}(|M_N - M| > \gamma) \\ &\leq 2\mathrm{e}^{-2c^2 N\gamma^2}, \end{aligned}$$

where the last inequality follows from the result for the case $\epsilon \leq \gamma$. □

2.11.5 Proof of Lemma 2.9.2

Proof. We use the definition of the expected value that makes use of the cumulative distribution and write for $0 < \epsilon \leq \gamma$ (where γ is the distance from the median M within

which $p^{\mathrm{h}}(\cdot)$ has positive density as defined in Lemma 2.9.1) and $r \geq 1$:

$$\begin{aligned}
\mathbb{E}\big[|M_N - M|^r\big] &= r\int_0^1 x^{r-1}\,\mathbb{P}(|M_N - M| > x)\,\mathrm{d}x \\
&= r\int_0^\epsilon x^{r-1}\,\mathbb{P}(|M_N - M| > x)\,\mathrm{d}x + r\int_\epsilon^1 x^{r-1}\,\mathbb{P}(|M_N - M| > x)\,\mathrm{d}x \\
&\leq \epsilon^r + r\int_\epsilon^1 x^{r-1}\,\mathbb{P}(|M_N - M| > x)\,\mathrm{d}x \\
&\leq \epsilon^r + 2r\mathrm{e}^{-2c^2N\epsilon^2}\int_\epsilon^1 x^{r-1}\,\mathrm{d}x \qquad (2.21) \\
&= \epsilon^r\left(1 - 2\mathrm{e}^{-2c^2N\epsilon^2}\right) + 2\mathrm{e}^{-2c^2N\epsilon^2},
\end{aligned}$$

where in (2.21), we use Lemma 2.9.1 and the fact that the exponential function is monotonically decreasing in x. Since the above bound holds for $0 < \epsilon \leq \gamma$, we can take the minimum of the right-hand side over this range. Now, since we are interested in the limiting behavior as $N \to \infty$, we can choose to analyze the case for large N so that $\left[\frac{m\log N}{N}\right]^{\frac{1}{2}} \leq \gamma$, where m is some positive constant. In this case, we have

$$\begin{aligned}
0 \leq \mathbb{E}\big[|M_N - M|^r\big] &\leq \min_{0<\epsilon\leq\gamma}\left[\epsilon^r\left(1 - 2\mathrm{e}^{-2c^2N\epsilon^2}\right) + 2\mathrm{e}^{-2c^2N\epsilon^2}\right] \\
&\leq \left[\epsilon^r\left(1 - 2\mathrm{e}^{-2c^2N\epsilon^2}\right) + 2\mathrm{e}^{-2c^2N\epsilon^2}\right]_{\epsilon=\left[\frac{m\log N}{N}\right]^{\frac{1}{2}}} \\
&= m^{\frac{r}{2}}\left[\frac{\log N}{N}\right]^{\frac{r}{2}}\left(1 - \frac{2}{N^{2c^2m}}\right) + \frac{2}{N^{2c^2m}}
\end{aligned}$$

Since we can take m to be any positive constant in the above bound, we select large m such that the right-hand side is $O\left(\left[\frac{\log N}{N}\right]^{\frac{r}{2}}\right)$. Thus, we have

$$\mathbb{E}\big[|M_N - M|^r\big] = O\left(\left[\frac{\log N}{N}\right]^{\frac{r}{2}}\right),$$

as desired. □

2.11.6 Proof of Lemma 2.9.3

Proof. Below, we use Hoeffding's inequality:

$$\begin{aligned}
\mathbb{P}(B_k) &= \mathbb{P}(\text{that of the first } k \text{ fractions, at least } N/2 \text{ were delivered } \underline{u}) \\
&= \mathbb{P}\left(\sum_{i=1}^{k} I_{A_k^c} \geq \frac{N}{2}\right) \\
&= \mathbb{P}\left(\sum_{i=1}^{k} \left(I_{A_k^c} - \frac{1}{2}\right) \geq \frac{N}{2} - \frac{k}{2}\right) \\
&\leq \exp\left[\frac{-2\left(N/2 - k/2\right)^2}{k}\right].
\end{aligned}$$

By similar argument, we can show

$$\mathbb{P}(C_k) \leq \exp\left[\frac{-2\left(N/2 - k/2\right)^2}{k}\right].$$

Now, for $k \leq N - \lfloor 2\sqrt{\frac{a}{2}N\log N}\rfloor - 1$, we have

$$\begin{aligned}
\max\left\{\mathbb{P}(B_k), \mathbb{P}(C_k)\right\} &\leq \exp\left[\frac{-2\left(N/2 - k/2\right)^2}{k}\right] \\
&\leq \exp\left[\frac{-2\left(N/2 - (N - \lfloor 2\sqrt{\frac{a}{2}N\log N}\rfloor - 1)/2\right)^2}{N - \lfloor 2\sqrt{\frac{a}{2}N\log N}\rfloor - 1}\right] \\
&\leq \exp\left[\frac{-2\left((\lfloor 2\sqrt{\frac{a}{2}N\log N}\rfloor + 1)/2\right)^2}{N}\right] \\
&\leq \exp\left[\frac{-2\left(\sqrt{\frac{a}{2}N\log N}\right)^2}{N}\right] \\
&= \frac{1}{N^a}.
\end{aligned}$$

□

2.11.7 Proof of Theorem 2.9.4

Proof. For convenience, we define $\underline{u}_p$ and $\overline{u}_p$ to represent the percentage deviation for the upper limit and the lower limit of the tumor dose, respectively. These can be related

to the already defined quantities by the equations $\underline{u} = \underline{u}_p(P/N)$ and $\overline{u} = \overline{u}_p(P/N)$. We first bound $\mathcal{C}_{\text{heu1}}$:

$$\begin{aligned}\mathcal{C}_{\text{heu1}} &= \mathbb{E}\left[\sum_{k=1}^{N} h(s_k)\left(\overline{u}\mathbb{I}_{A_k\cap B_k^c\cap C_k^c} + \underline{u}\mathbb{I}_{A_k^c\cap B_k^c\cap C_k^c} + \overline{u}\mathbb{I}_{B_k} + \underline{u}\mathbb{I}_{C_k}\right)\right] \\ &\leq \mathbb{E}\left[\sum_{k=1}^{N} h(s_k)\left(\overline{u}\mathbb{I}_{A_k} + \underline{u}\mathbb{I}_{A_k^c} + \overline{u}\mathbb{I}_{B_k} + \underline{u}\mathbb{I}_{C_k}\right)\right].\end{aligned}$$

Now, using Equation (2.12) for $\mathcal{C}^*$ and the above bound for $\mathcal{C}_{\text{heu1}}$, we see that $\mathcal{C}_{\text{heu1}} - \mathcal{C}^* \leq \mathcal{V}_1 + \mathcal{V}_2$, where

$$\mathcal{V}_1 = \sum_{k=1}^{N} \mathbb{E}\left[h(s_k)\left(\overline{u}\left(I_{A_k} - I_{D_k}\right) + \underline{u}\left(I_{A_k^c} - I_{D_k^c}\right)\right)\right]$$

and

$$\mathcal{V}_2 = \sum_{k=1}^{N} \mathbb{E}\left[h(s_k)\left(\overline{u}I_{B_k} + \underline{u}I_{C_k}\right)\right].$$

We can bound these quantities:

$$\begin{aligned}\mathcal{V}_1 &= \sum_{k=1}^{N} \mathbb{E}\left[h(s_k)\left(\overline{u}\left(I_{A_k} - I_{D_k}\right) + \underline{u}\left(I_{A_k^c} - I_{D_k^c}\right)\right)\right] \\ &= \sum_{k=1}^{N} \mathbb{E}\left[\mathbb{E}\left[h(s_k)\left(\overline{u}\left(I_{A_k} - I_{(A_k^N)^c}\right) + \underline{u}\left(I_{A_k^c} - I_{(A_k^N)^c}\right)\right)|M_N\right]\right] \qquad (2.22) \\ &= \sum_{k=1}^{N} \mathbb{E}\left[\overline{u}\int_{M_N}^{M} xp^{\text{h}}(x)\,\mathrm{d}x + \underline{u}\int_{M}^{M_N} xp^{\text{h}}(x)\,\mathrm{d}x\right] \\ &= P\,\mathbb{E}\left[\overline{u}_p\int_{M_N}^{M} xp^{\text{h}}(x)\,\mathrm{d}x + \underline{u}_p\int_{M}^{M_N} xp^{\text{h}}(x)\,\mathrm{d}x\right] \\ &\leq P\left(\overline{u}_p - \underline{u}_p\right)\mathbb{E}\left[\left|\int_{M_N}^{M} xp^{\text{h}}(x)\,\mathrm{d}x\right|\right] \\ &\leq P\left(\overline{u}_p - \underline{u}_p\right)K\,\mathbb{E}\left[|M_N - M|\right] \qquad (2.23) \\ &= O\left(\frac{\sqrt{\log N}}{\sqrt{N}}\right), \qquad (2.24)\end{aligned}$$

where we use the law of iterated expectations in (2.22), Assumption 2.9.2 in (2.23), and Lemma 2.9.2 in (2.24). We also have

$$
\begin{aligned}
\mathcal{V}_2 &= \sum_{k=1}^{N} \mathbb{E}\left[h(s_k)\left(\overline{u} I_{B_k} + \underline{u} I_{C_k}\right)\right] \\
&= \mathbb{E}\left[h(s_k)\right] \sum_{k=1}^{N} \mathbb{E}\left[\overline{u} I_{B_k} + \underline{u} I_{C_k}\right] \qquad (2.25) \\
&= \mathbb{E}\left[h(s_k)\right] \sum_{k=1}^{N} \left[\overline{u}\mathbb{P}(B_k) + \underline{u}\mathbb{P}(C_k)\right] \\
&\leq \frac{P\,\mathbb{E}\left[h(s_k)\right]\left(\overline{u}_p + \underline{u}_p\right)}{N} \sum_{k=1}^{N} \max\left\{\mathbb{P}(B_k), \mathbb{P}(C_k)\right\} \\
&\leq \frac{P\,\mathbb{E}\left[h(s_k)\right]\left(\overline{u}_p + \underline{u}_p\right)}{N} \left[\sum_{k=1}^{N-\lfloor 2\sqrt{\frac{a}{2}N\log N}\rfloor - 1} \frac{1}{N^a} + O\left(\sqrt{N\log N}\right)\right] \qquad (2.26) \\
&\leq \frac{P\,\mathbb{E}\left[h(s_k)\right]\left(\overline{u}_p + \underline{u}_p\right)}{N} \left[\frac{1}{N^{a-1}} + O\left(\sqrt{N\log N}\right)\right] \\
&= O\left(\frac{\sqrt{\log N}}{\sqrt{N}}\right),
\end{aligned}
$$

where we use independence (Assumption 2.9.1) in (2.25) and Lemma 2.9.3 in (2.26). Now,

$$
\begin{aligned}
0 &\leq \mathcal{C}_{\text{heu1}} - \mathcal{C}_{\text{dp}} \\
&\leq \mathcal{C}_{\text{heu1}} - \mathcal{C}^* \\
&\leq \mathcal{V}_1 + \mathcal{V}_2 \\
&= O\left(\frac{\sqrt{\log N}}{\sqrt{N}}\right).
\end{aligned}
$$

Since $\lim_{N\to\infty} \frac{\sqrt{\log N}}{\sqrt{N}} = 0$, it is clear $|\mathcal{C}_{\text{heu1}} - \mathcal{C}_{\text{dp}}| \to 0$ as $N \to \infty$. □

Chapter 3

Adaptive fractionation and treatment plan selection from a plan library

3.1 Introduction

In this chapter, we investigate the benefit of both adaptive fractionation and treatment plan selection from a plan library. The presented methods are tested on three prostate datasets, each consisting of a simulation CT and CTs for 38 fractions. We find that the spatial adaptation offered by selection from a plan library and the temporal adaptation from varying the fraction size can result in significant improvement in dose distribution quality metrics.

Adaptive fractionation therapy was first introduced in [13, 48]. The main idea is to deliver a larger fraction size when the dose ratio (dose to OAR per unit dose to tumor) is small and vice versa. We use the dose to the anterior rectum as the primary metric for comparison; this is because it is the main dose-limiting organ in prostate cancer. We investigate the benefit of the dynamic programming (DP) approaches presented in [13,65] using patient datasets, which has not been studied before. We are particularly

interested in prostate cancer because of its low α-β ratio [51] and hence sensitivity to fractionation. We believe this property of prostate cancer particularly makes adaptive fractionation beneficial.

The purpose of this work is to develop novel adaptive treatment methods that avoid or at least alleviate the required quality assurance (QA) procedures when a treatment plan is adapted. The approach we take is to build and select from a library of physician pre-approved treatment plans, and make quick modifications by changing the fraction size based on the patient anatomy-of-the-day. We assume imaging information is obtained before the delivery of each fraction; with recent technological developments such as the CBCT, this assumption is reasonable. We assume that it is possible to automatically propagate contours [12] from the simulation CT. In some sense, a plan library is a hybrid approach, using both offline and online ART. The offline component is the generation of the set of treatment plans, and the online component is the selection based on imaging information before the delivery of a fraction. The benefit of a hybrid offline and online approach has been previously illustrated [45]. The concept of a plan pool for prostate cancer has also been discussed before in [46]. Still, the dosimetric benefits of such approaches need further investigation. In this chapter, we propose both adaptively choosing the fraction size and selecting from a plan library.

In Section 3.2, we discuss in detail the contributions of this chapter. In Section 3.3, the model, formulation, and solution approach are presented. Further discussion about the estimation of the dose ratio probability distribution and generation of a plan library is also provided. In Section 3.4, we present results from using adaptive fractionation and treatment plan selection on prostate datasets.

3.2 Contributions

We quantify the benefit of temporal adaptation by varying the fraction size and spatial adaptation by selecting a plan from a pre-approved plan library. Specifically, we:

1. suggest an approach for both adapting the fraction size and selecting a treatment

plan from a plan library. For adaptive fractionation, we refer to the DP approaches described in [13,65] and also in Chapter 2. For treatment plan selection, we choose a plan which results in the smallest dose ratio (also smallest dose in the OAR) as long as it provides sufficient tumor coverage.

2. provide an approach to estimate the dose ratio probability distribution from historical datasets. An approximate DP approach is suggested to incorporate an updated probability distribution over the course of treatment.

3. use three prostate datasets and find that adaptive fractionation is beneficial when using the BED model and not so much when using a physical dose model. This is especially the case because prostate cancer has a small α-β ratio and is very sensitive to fractionation.

4. propose a new type of fractionation scheme, which we name adaptive hypofractionation. The idea is to wait for the appropriate opportunity to deliver a large fraction size. Computational experiments suggest that such an approach can be advantageous because it results in reduced dose to the OAR and shortens the number of days of treatment in comparison to conventional fractionation. Although the standard hypofractionation does better for the three patient datasets we used, it is potentially beneficial and requires further investigation.

5. find that in some cases, when the assumed dose ratio probability distribution is different from the true one, the benefit of adaptive fractionation is reduced. However, the described approach of updating the probability distribution and using an approximate DP approach results in almost the same gain as if the true distribution were known.

6. find that selection from a plan library together with adaptive fractionation has significant benefit.

3.3 Formulation and methods

In Subsection 3.3.1, we formulate the adaptive fractionation and treatment plan selection problem. The proposed solution method decouples the problem by first choosing the fraction size based on a fixed treatment plan and second, selecting the best plan for the observed patient anatomy. In Subsection 3.3.2, we use the notion of equivalent uniform dose (EUD) as a metric for measuring the dose to the OAR and tumor. In Subsection 3.3.3, we describe an approach to estimate the probability distribution of the dose ratio from historical data. An approximate DP approach is described to handle the case when the dose ratio probability distribution is updated over the course of treatment. In Subsection 3.3.4, we discuss the generation of treatment plans and a plan library.

3.3.1 Model, formulation, and solution approach

In principle, given bounds on the fraction size each day and a library of treatment plans, we would like to simultaneously optimize the fraction size and select a treatment plan. We are interested in using the dose ratio (dose to the OAR per unit dose to the tumor) as such a measure of the favorability of a patient anatomy. Yet, estimation of the probability distribution of these dose ratios is not straightforward, especially because the ratios will differ based on the choice of the treatment plan. We, therefore, choose to decouple the two problems: first, select the fraction size assuming a fixed nominal plan, using an estimated probability distribution for the dose ratios, and second, select the treatment plan assuming a standard dose fraction.

We now introduce the necessary notation. Let N be the number of fractions and P be the total prescribed dose to the tumor. We denote by h_k the dose ratio in the kth day as observed from the patient anatomy of the day. The probability distribution $p(\cdot)$ of the dose ratio h_k can be estimated from patient datasets. We assume that h_k is observed just before the delivery of the kth fraction; this can be obtained from imaging modalities such as CBCT together with automatic contouring tools. We denote by

S the set of possible values of h_k. We define r_k to be the remaining prescribed dose or biological effective dose (BED) left to deliver to the tumor in the kth and future fractions. We can determine the fraction size u_k in the kth fraction based on the remaining dose r_k and dose ratio h_k. Thus, r_k and h_k represent the state of the system. The dynamics of the system are described by the equations $r_{k+1} = f(r_k, u_k)$, where the form of $f(r_k, u_k)$ depends on whether we are using physical dose or BED, with r_1 initialized to the prescribed dose P, and $h_k \sim p(\cdot)$, for $k = 1, 2, \ldots, N$. For a physical dose model, we would have $f(r_k, u_k) = r_k - u_k$, and for a BED model, we would have $f(r_k, u_k) = r_k - u_k \left(1 + \frac{u_k}{[\alpha/\beta]_T}\right)$, where $[\alpha/\beta]_T$ is the α-β ratio, a tissue specific parameter of the tumor.

For the fractionation problem, we are interested in minimizing the expected total dose or BED in the OAR. We would like to ensure that the prescribed dose to the tumor is met with certainty, and that the fraction size for each day is within a lower bound, $\underline{u}$, and an upper bound, $\overline{u}$. To solve the fractionation problem, we use the dynamic programming approaches presented in [13, 65]. The DP algorithm is given below:

$$J_{N+1}(r_{N+1}, h_{N+1}) = \begin{cases} 0, & \text{if } r_{N+1} = 0, \\ \infty, & \text{otherwise,} \end{cases}$$

$$J_k(r_k, s_k) = \min_{\underline{u} \le u_k \le \overline{u}} \Big(g(u_k, h_k) + \int_S p(h) J_{k+1}(r_k - u_k, h)\, \mathrm{d}h \Big), \tag{3.1}$$

for $k = N, N-1, \ldots, 1$, where $p(\cdot)$ is the distribution of h_{k+1}. In the above equations, a cost of $g(u_k, h_k)$ is incurred in each fraction. This could represent for example the dose to the OAR, in which case $g(u_k, h_k) = u_k h_k$. Or, it could represent the BED in the OAR, for which $g(u_k, h_k) = u_k h_k \left(1 + \frac{u_k h_k}{[\alpha/\beta]_O}\right)$, where $[\alpha/\beta]_O$ is the α-β ratio of the OAR. Further details about this dynamic programming approach can be found in Chapter 2 and in references [13, 65].

For the treatment plan selection problem, in the kth fraction, we choose the plan that results in the smallest dose ratio h_k for the observed patient anatomy assuming the target coverage is satisfied. This type of selection is myopic in that it does not

consider the future cost of selecting a treatment plan. This is in direct contrast with the discussed fractionation problem, where we choose a fraction size based on both the current cost and the resulting expected future cost. Yet, we think this approximation of selecting a treatment plan based only on the observed anatomy of the day is a good one. Let the control l_k be the plan we choose to deliver in the kth fraction. The control l_k is selected from the set $\{1, 2, \ldots, L_k\}$, which represents our plan library (either pre-selected or continually updated). Let the cost vector $h_k(l)$ represent the dose per unit Gy delivered to the OAR when using the lth treatment plan for the patient geometry in the kth day. Mathematically in the kth fraction then, we solve

$$\begin{aligned} &\underset{l_k \in \{1,2,\ldots,L_k\}}{\text{minimize}} \quad h_k(l_k) \\ &\text{subject to} \quad \text{dose to tumor voxels} \geq \frac{P}{N}. \end{aligned} \tag{3.2}$$

In summary, we choose to solve the fractionation and plan selection problems by decoupling them. We propose to solve the fractionation problem by using a dynamic programming method previously introduced in [13, 65]. For the treatment plan selection problem, we choose the plan that results in the smallest dose ratio h_k for the observed patient anatomy assuming that the target coverage is satisfied.

3.3.2 Equivalent uniform dose and biological effective dose

In the above formulations, it was assumed that a homogeneous dose is delivered to both the tumor and the OAR. In practice, however, the OAR actually receives a non-uniform dose distribution. Thus, the question of interest is how we can convert a non-uniform dose in the OAR to the dose ratio h_k for a given patient anatomy. Here, we use the concept of EUD [56], which allows us to convert a non-uniform dose to an equivalent uniform one. Given a dose distribution d_i, for which i indexes the set of voxels in the

OAR denoted $\mathcal{O}$, the EUD is defined as

$$\text{EUD}(a) = \left(\frac{1}{|\mathcal{O}|} \sum_{i \in \mathcal{O}} d_i^a \right)^{1/a},$$

where $|\mathcal{O}|$ is the number of voxels in the OAR and a is an exponent dependent on the OAR considered. For example, $a = 1$ represents the mean dose and would be a good choice for a parallel organ like the lung. For a serial organ, the max dose in the dose distribution becomes more important, and thus, a large value of a would be appropriate. For some organs, as in the prostate case, the organs are neither parallel nor serial, in which case an appropriate choice would be somewhere in between the two extremes. The EUD could also be a good measure of target coverage when a non-uniform dose is delivered to the tumor. In such cases, choosing a large enough negative value, such as $a = -20$, provides a good measure of dose to the tumor.

For the fractionation problem formulation, the cost incurred each day is $g(u_k, h_k)$, which represents either the physical dose or the BED in the OAR. Due to the non-uniform dose in the OAR, we calculate the dose ratio h_k as the EUD in the OAR divided by the dose per fraction to the tumor, which is typically 2 Gy. Thus, given that we are using the physical dose model, $g(u_k, h_k)$ actually represents the EUD in the OAR in the kth fraction. In this case, we are minimizing the sum of the EUD in the OAR over all fractions, which is not the same as the total EUD in the OAR at the end of treatment. Even though the total EUD in the OAR may be a more meaningful quantity, it also requires that we know exactly how much dose is delivered to each voxel at the end of treatment. Measuring this total dose requires deformable registration tools. We choose, however, not to use this approach because such methods are not always reliable. We also approximate the BED in each fraction by using the EUD and summing the BED over all fractions. These are the metrics we choose to use later in this chapter to judge the effectiveness of adaptive treatments.

3.3.3 Estimation of dose ratio probability distribution

For the fractionation problem, we would like to estimate the probability distribution of the dose ratio h_k using historical datasets. Since the dose ratios are highly dependent on the treatment plan, it is only reasonable to use data obtained from the same disease site and under similar treatment plans. We choose to assign probability mass to a fixed number of possible dose ratios. Suppose we would like to estimate the probability of m possible choices of dose ratios within some bounds $\underline{h}$ and $\overline{h}$. We split the interval $[\underline{h}, \overline{h}]$ into m intervals of equal size and denote by h^i the dose ratio corresponding to the midpoint of those intervals. Thus, the value under this ith scenario is $h^i = \underline{h} + \frac{\overline{h}-\underline{h}}{m}(i - 1/2)$. To each of these dose ratios, we associate a corresponding probability p^i. A simple way to determine p^i from historical datasets is to count the number of occurrences of the dose ratio h in the interval

$$\left[\underline{h} + \frac{\overline{h} - \underline{h}}{m}(i-1), \underline{h} + \frac{\overline{h} - \underline{h}}{m} i,\right],$$

and divide by the total number of measurements m. In summary, we can determine the probability of the dose ratios from historical datasets by using the formula

$$p^i = \frac{\text{number of occurrences of } i\text{th dose ratio in } m \text{ measurements}}{m}.$$

Even with a reasonable estimate of the probability distribution based on historical data, it is still likely that population data will not be an accurate representation of the patient-specific distribution. It is more appropriate, therefore, to update the probability distribution over the course of treatment. In the kth fraction, we would like to use an updated version of the probability distribution using the history of past dose ratios, $h_1, h_2, \ldots, h_k$. In this case, our state must include not only the current dose ratio, h_k, in the kth fraction but also the history of past dose ratios. We define the history state vector, $\mathbf{I_k} = (q_k^1, q_k^2, \ldots, q_k^m)$, where q_k^i is the number of occurrences of the ith dose ratio in k treatment fractions. We denote the associated conditional probabilities

$p(h_k|\mathbf{I_k})$ by $\mathbf{p_k} = (p_k^1, p_k^2, \ldots, p_k^m)$ for each of the possible dose ratios $\{h_k^1, h_k^2, \ldots, h_k^m\}$ in the kth fraction. We would like to update our prior knowledge from historical data, which is captured by the estimated distribution p^i, using the additional information from k patient anatomy instances. One way to update to the conditional distribution is through the formula:

$$p_k^i = \frac{c_r p^i + q_k^i}{c_r + k},$$

where c_r is a concentration parameter. The parameter c_r weighs our prior beliefs about the probability of each scenario. A larger value of c_r would put a higher weight on our estimated probability distribution from historical data.

We now discuss a DP approach when updating the probability distribution over the course of treatment. With the terminal condition ensuring that the prescribed dose is met, ideally we would like to run the DP algorithm with an augmented state vector:

$$J_k(r_k, \mathbf{I_k}) = \min_{\underline{u} \le u_k \le \overline{u}} \Big(g(u_k, h_k) + \sum_{i=1}^{m} p_k^i J_{k+1}(r_k - u_k, \mathbf{I_{k+1}}) \Big)$$

for $k = N, N-1, \ldots, 1$, where $\mathbf{I_{k+1}}$ is updated by incrementing the appropriate dose ratio scenario in $\mathbf{I_k}$. The above cost-to-go function J_k is defined on a state space of dimension $m+1$, which could still be computationally expensive if the number of possible dose ratios is large. A simplification which can result in a faster but effective algorithm is approximating J_{k+1} by re-running the DP algorithm assuming the updated probability distribution $\mathbf{p_{k+1}}$ for the remaining treatment days. We denote this cost-to-go function with an updated probability distribution as $\widetilde{J}_{k+1}$. Thus, we have an approximate DP algorithm

$$J_k(r_k, \mathbf{I_k}) \approx \min_{\underline{u} \le u_k \le \overline{u}} \Big(g(u_k, h_k) + \sum_{i=1}^{m} p_k^i \widetilde{J}_{k+1}(r_k - u_k, h^i) \Big)$$

where the function $\widetilde{J}_{k+1}$ above is the cost-to-go function resulting from using the original DP algorithm (3.1) assuming the updated probability distribution $\mathbf{p_{k+1}}$. To use this

approximate algorithm, the DP algorithm with time horizon $N-k-1$ needs to be run in real time before the delivery of the kth fraction.

3.3.4 Generation of a plan library

We would like to solve an IMRT problem that provides a tradeoff between target coverage and healthy organ sparing. There are a number of ways to formulate the problem, including linear/quadratic and other nonlinear formulations (see [69] for various approaches). Here, we choose to minimize the weighted sum of mean doses to the relevant OARs and ensure a prescribed dose P/N to the tumor. We define m_i, for $i = 1, 2, \ldots, 6$, to be the mean dose to the relevant OARs (see Table 3.1). Let d_i be the dose to the ith voxel (i.e., individual points on the patient anatomy), and let $\mathcal{T}$ be the set of target voxels (including margin expansion of the tumor volume). Mathematically, we solve the following problem in order to determine the treatment plan from the simulation CT:

$$\begin{aligned}
\underset{\{d_i \geq 0\}}{\text{minimize}} \quad & \frac{1}{6}\sum_{i=1}^{6} m_i \\
\text{subject to} \quad & \frac{P}{N} \leq d_i \leq 1.12\frac{P}{N}, \quad i \in \mathcal{T}, \\
& d_i \leq 1.12\frac{P}{N}, \qquad\quad i \notin \mathcal{T}, \\
& m_1 \leq \frac{P}{N}, \\
& m_j \leq 0.8\frac{P}{N}, \qquad\quad j = 2, 3, \ldots, 6.
\end{aligned} \tag{3.3}$$

Though it is not included in the above formulation, we actually optimize the beam intensities (beamlets) delivered from various angles rather than the dose distribution denoted by d_i. We can convert the optimization problem by simply adding the constraints $d = Dx$ and $x \geq 0$, where D is the dose deposition matrix, d is a vector of doses to voxels, and x is a vector of beamlets.

In order to adapt the treatment from day to day, we choose to create a library of plans. Depending on the anatomy observed before treatment, a plan is selected from

Table 3.1: Summary of notation for treatment plan optimization.

Notation	Definition
m_1	mean dose to anterior rectum
m_2	mean dose to posterior rectum
m_3	mean dose to bladder
m_4	mean dose to left femoral head
m_5	mean dose to right femoral head
m_6	mean dose to skin
d_i	dose to ith voxel
$\mathcal{T}$	set of tumor voxels including margin
P	prescription dose over entire treatment
N	number of treatment fractions

this library. Our purpose is to illustrate the benefit of using such a plan library. In this chapter, we generate 2 plans by changing the volume consisting of target voxels: CTV+2mm and CTV+5mm. These plans have different size margins (2mm and 5mm, respectively) that are uniformly expanded around the clinical target volume (CTV), which is the tumor volume visible in the CT. It is reasonable to assume that a conventional plan for prostate cancer uses a 5mm margin, i.e. the second plan CTV+5mm in our plan library.

3.4 Results from prostate cancer datasets

In Subsection 3.4.1, we provide details of how the plan library is generated and the dose ratio probability distribution estimated. We discuss results from using adaptive fractionation on prostate datasets using a physical dose model and the BED model in Subsections 3.4.2 and 3.4.3, respectively. We discuss the benefit of updating the probability distribution over the course of treatment in Subsection 3.4.4. Finally, in Subsection 3.4.5, we discuss results from using a plan library.

3.4.1 Treatment plan optimization and probability distribution estimation

We study three prostate cancer patient datasets, each consisting of a simulation CT image for optimizing a treatment plan and 38 CT images for each of the fractions. The target and the relevant organs in all of the CT images were contoured by either a physician or a resident under the supervision of a physician [83]. The target was the tumor volume plus the margin expansion for addressing uncertainties.

For each patient, we generate two plans; one consisting of a 2 mm margin expansion and the other a 5 mm expansion. We use seven 6 MV equispaced and coplanar photon beams. The dose deposition matrix is computed by the quadratic infinite beam (QIB) pencil-beam dose calculation algorithm in CERR 3.0 beta 3 (refer to [17]). The voxel resolution grid is 1.96 x 1.96 x 5 mm^3 for all three simulation CTs. The total number of beamlets for patient 1, 2, and 3 are 280, 325, and 251, respectively. These only include beamlets that contribute to the dose in the target. The total number of voxels per structure for each patient is given in Table 3.2. The number of voxels in the bladder, femoral heads, and skin were downsampled by a factor of 4, 8, and 16, respectively. We solve the formulation (3.3) with $P = 76$ Gy and $N = 38$ using Matlab's built-in linprog function (large-scale interior point algorithm). The average solution time for each treatment plan was about 5 minutes. For patient 3, the constraints in the formulation (3.3) were too stringent; thus, we relaxed the upper bound on all voxels from $1.12P/N$ to $1.2P/N$, and solved this relaxed problem instead.

For patient 1, we generated the DVH curves for the CTV and anterior rectum in the 2 mm and the 5 mm margin plan (Figure 3-1). We see that the dose to the primary OAR, the anterior rectum, is significantly lower in the 2 mm margin plan when compared to the 5 mm one; this makes sense because a smaller target volume means fewer constraints for the optimization solver. Thus, we can conjecture that for the 2 mm and 5 mm plans, the solution to (3.2) simply results in choosing the plan with the smallest margin as long as target coverage is ensured.

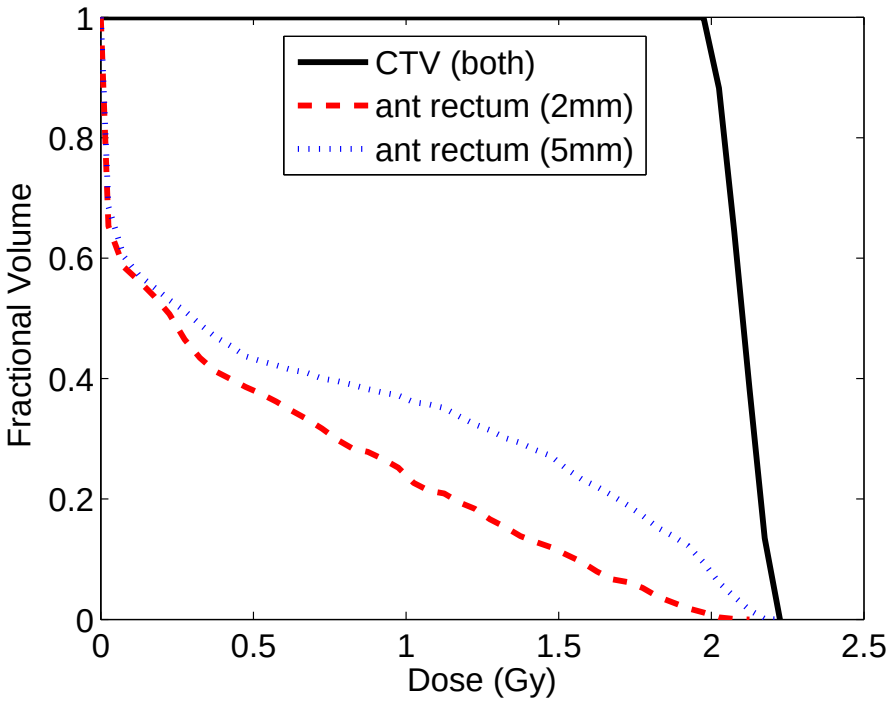

Figure 3-1: Dose volume histogram (DVH) for generated treatment plans. The CTV DVH curves for both the 2 mm and 5 mm margin plans are very close and indistinguishable on the above plot. Note that the anterior rectum DVH curve for the 2 mm margin plan is entirely below the one for the 5 mm plan.

Table 3.2: Number of voxels for each patient. The bladder, femoral heads, and skin voxels were downsampled by a factor of 4, 8, and 16, respectively. Any voxels not influenced by beamlets were removed.

	Number of voxels		
Structure	Patient 1	Patient 2	Patient 3
2 mm PTV	2,101	2,603	2,913
5 mm PTV	3,102	3,562	4,202
anterior rectum	1,142	751	668
posterior rectum	1,121	971	695
bladder	668	491	231
left femoral head	67	69	67
right femoral head	73	61	72
skin	2,487	2,729	1,807
total	10,761	11,237	10,655

For solving the fractionation problem, we need an estimate of the probability distribution of the dose ratio. We only use a single treatment plan, in our case the 5 mm plan, to estimate such a distribution. For the CT image of every fraction, we re-calculate the dose deposition matrix using CERR's QIB pencil beam algorithm as before. With the new dose deposition matrix for each fraction, the optimized beamlets from the simulation CT were used to compute the dose distribution on the patient anatomy. The patient setup was assumed to be perfect and the isocenter of the target, given by the center of mass of the target volume, was aligned exactly for every fraction. To compute the dose ratio (dose to the primary OAR of interest divided by dose to tumor), we use the formula $h = \mathrm{EUD}(a)/2$, where $\mathrm{EUD}(a)$ is the EUD with an exponent a and the two in the denominator comes from 2 Gy per fraction dose to the target. Possible choices for the exponent here could be 1, which is the mean dose, or larger values for a more serial organ. The primary OAR of interest in the prostate case is the anterior rectum, which is not completely parallel or serial; we choose $a = 3$ for this OAR. We assume that the dose ratio lies somewhere between 0.5 and 1 (i.e., $\underline{h} = 0.5$ and $\overline{h} = 1$). We set the number of possibilities m to be 10. For each patient, we count the fraction of dose ratios falling within the corresponding intervals of even length, and determine the true,

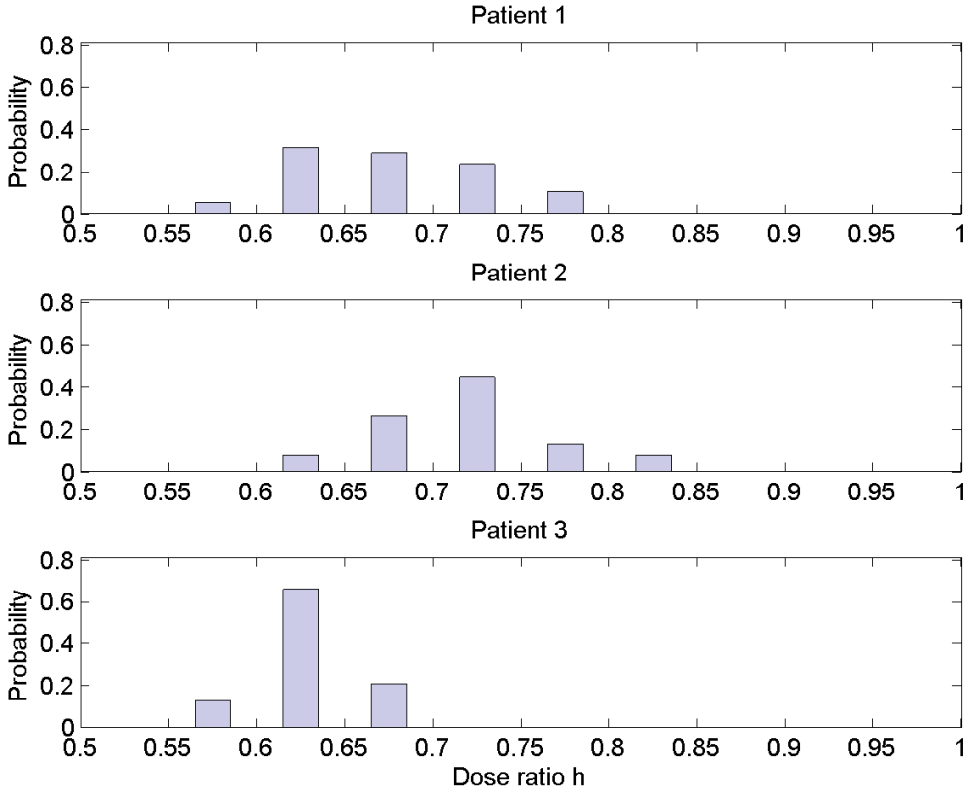

Figure 3-2: Estimation of true dose ratio probability distribution for each of the three patients. We discretized the possible dose ratios into 10 intervals in the range 0.5-1. Note that patient 3 has less variation than the other two patients due to less day to day organ motion.

discretized probability distribution of the dose ratios (Figure 3-2). When solving the fractionation problem, if we use this true distribution for each of the patients, we will be able to quantify the best possible benefit of using an adaptive fraction size.

3.4.2 Fractionation using physical dose model

We consider solving the adaptive fractionation problem using a physical dose model. That is, the state r_k represents the physical remaining dose and the dynamics equation satisfies $r_{k+1} = f(r_k, u_k) = r_k - u_k$. The cost per day is the dose resulting from delivering a fraction size u_k, i.e. $g(u_k, h_k) = u_k h_k$. For structural properties of an optimal policy,

refer to Chapter 2 or the paper [65]. As mentioned before, we will use only a single plan, in our case the 5 mm margin one, to determine the fraction size. The metric for comparison will be the sum of the EUD in the anterior rectum, our primary OAR, over all fractions. In this subsection, we will use the true, discretized probability distribution for each of the patients, shown in Figure 3-2, to measure the best possible gain of using an adaptive fraction size.

We run two simulations for each of the patients: 20% dose deviations from standard fractionation and 50% dose deviations. For the 20% deviations, the range of possible fraction sizes will lie within 20% of the standard 2 Gy per fraction, i.e. $\underline{u} = 1.6$ Gy and $\overline{u} = 2.4$ Gy. For 50 % deviations, we have $\underline{u} = 1$ Gy and $\overline{u} = 3$ Gy. We use $P = 76$ Gy, which results in 2 Gy per fraction for $N = 38$ days. We use the sum of the EUD (with exponent $a = 3$) in the OAR over all fractions as a metric for comparison. Let $D_{\text{conv}}^{\text{OAR}}$ be this EUD sum quantity when using the conventional 2 Gy per fraction and $D_{\text{adap}}^{\text{OAR}}$ when using an adaptive fraction size. Using the true discretized probability distributions in Figure 3-2, we find the resulting gain in total dose in the OAR when using an adaptive fraction size (Table 3.3). Note that reduction in dose to the OAR is not more than 3% for the three patients when using 50% deviations and around 1% or below when using 20% deviations. Note that patient 3 has the smallest gain which can be explained by the little motion observed in the estimated dose ratio probability distribution in Figure 3-2. These results indicate that using an adaptive fraction size is not much more beneficial than standard fractionation, especially since we are measuring the best possible gain assuming knowledge of the true probability distribution. Of course, larger deviations in the fraction size would result in bigger gain, but ignoring biological effects by using a physical dose model is not realistic. Indeed, it has been shown in [6] that biological effects are insignificant only when dose variations are less than 10%.

Table 3.3: Adaptive fractionation for prostate cancer using physical dose model. In this case, we note little gain when using adaptive fractionation. The dose to the OAR for conventional and adaptive fractionation are denoted $D_{\text{conv}}^{\text{OAR}}$ and $D_{\text{adap}}^{\text{OAR}}$, respectively.

	20% deviations			50% deviations		
Patient	$D_{\text{conv}}^{\text{OAR}}$ [Gy]	$D_{\text{adap}}^{\text{OAR}}$ [Gy]	Gain [%]	$D_{\text{conv}}^{\text{OAR}}$ [Gy]	$D_{\text{adap}}^{\text{OAR}}$ [Gy]	Gain [%]
1	51.52	50.96	1.09	51.52	50.11	2.74
2	54.53	54.02	0.92	54.53	53.26	2.33
3	47.65	47.46	0.40	47.65	47.16	1.03

3.4.3 Fractionation using BED model

We use the BED model and take into account the biological effect of varying the fraction size. There can be considerable potential for significant gain especially because we can allow for larger fraction size deviations. Now, we use $r_{k+1} = f(r_k, u_k) = r_k - u_k h_k \left(1 + u_k h_k/[\alpha/\beta]_T\right)$ for the dynamics equation and $g(u_k, h_k) = u_k h_k \left(1 + u_k h_k/[\alpha/\beta]_O\right)$ for the cost per fraction. We use typical α-β values for the tumor and OAR to compute the BED. Prostate tumors are known to have a very small α-β ratio compared to other disease sites [51]. This means that the tumor is sensitive to fractionation effects, and thus, there is potential for significant gain when compared to standard fractionation schemes. We use $[\alpha/\beta]_T = 1.5$ Gy and $[\alpha/\beta]_O = 3$ Gy. For standard fractionation, using 2 Gy per fraction for 38 fractions, we deliver a total BED of $38 \cdot 2\,(1 + 2/1.5) = 177.33$ Gy to the tumor. Thus, we use this as the total prescription dose in BED to be delivered to the tumor. The metric used for comparison to the standard fractionation scheme is the sum of the BED in each fraction, estimated by the EUD in the OAR (with exponent $a = 3$ as before). We denote this quantity $\widetilde{D}_{\text{conv}}^{\text{OAR}}$ when using conventional fractionation and $\widetilde{D}_{\text{adap}}^{\text{OAR}}$ when using adaptive fractionation. In comparison to the physical dose model used in the previous subsection, we find a significant gain using the BED model, especially when using 50% deviations from conventional fractionation (Table 3.4). We note as much as 9% reduction in the BED in the OAR, which would be significant enough to justify using adaptive fractionation. This type of improvement is probably

Table 3.4: Adaptive fractionation for prostate cancer using BED model. We note significant gain when using 50% deviations from standard fractionation. The BED in the OAR are denoted $\widetilde{D}^{\text{OAR}}_{\text{conv}}$ and $\widetilde{D}^{\text{OAR}}_{\text{adap}}$ for conventional and adaptive fractionation, respectively.

	20% deviations			50% deviations		
Patient	$\widetilde{D}^{\text{OAR}}_{\text{conv}}$ [Gy]	$\widetilde{D}^{\text{OAR}}_{\text{adap}}$ [Gy]	Gain [%]	$\widetilde{D}^{\text{OAR}}_{\text{conv}}$ [Gy]	$\widetilde{D}^{\text{OAR}}_{\text{adap}}$ [Gy]	Gain [%]
1	74.93	72.85	2.78	74.93	68.08	9.14
2	80.72	78.73	2.47	80.72	74.01	8.31
3	67.61	66.73	1.30	67.61	63.71	5.77

only going to arise for tumors with small α-β ratios like prostate cancer. Of course, here we are using the true probability distribution to measure the best possible gain. In a later subsection, we will investigate the result when using a probability distribution different from the true one.

The linear-quadratic (LQ) model, from which it is possible to derive the BED model, is an appropriate model for doses larger than 1 Gy [30] and doses smaller than 10 Gy [7]. It is thus possible for us to vary the dose more significantly than 20%. Clearly, this would increase the benefit of adaptive fractionation, especially for tumors with small α-β ratios like prostate cancer. We instead focus on an even more interesting type of schedule, which we name *adaptive hypofractionation*. For tumors such as prostate that have small α-β ratios, it is typical to hypofractionate (or deliver fewer number of large fractions). In our case, given that we would like to deliver 5 fractions with a total BED of 177.33 Gy as before, this results in delivering 6.58 Gy per fraction. In principle, we could set the $\underline{u} = 1$ Gy and $\overline{u} = 6.58$ Gy and run our previous result. However, we would like to address a more interesting question: can we deliver a few large fractions adaptively over the course of treatment so that we can end the treatment course earlier? We could use a principle similar to hypo-fractionation except that we wait for the right opportunity to deliver the treatment. We propose an approximate approach to solve this problem based on the previous algorithms. First, we solve the fractionation problem with $\underline{u} = 0$ Gy and $\overline{u} = 6.58$ Gy. If the optimal dose is less than

Table 3.5: Adaptive hypofractionation and standard hypofractionation in comparison to conventional treatment. We show that there is a significant gain in BED_O for both types of hypofractionated treatments. Adaptive hypofractionation does worse than hypofractionation because the first five fractions were not unfavorable. If the first five fractions were in fact unfavorable, adaptive hypofractionation may fair better than simply hypofractionation.

Patient	Adaptive hypofractionation [% gain]	Hypofractionation [% gain]
1	14.63	24.51
2	13.31	25.99
3	21.26	26.54

2 Gy (e.g., 0 Gy), then deliver a 2 Gy fraction if possible or whatever remaining dose is left to deliver. On the other hand, if the optimal dose is greater than 2 Gy (e.g., 6.58 Gy), then deliver the dose as is. Finally, if the remaining dose is 0 Gy midway during the treatment course, the entire BED has been delivered and the patients treatment is complete. We run this algorithm for the three prostate patient datasets and find that adaptive hypofractionation does better than conventional fractionation (Table 3.5) and takes advantage of the days in which the dose ratio is particularly small (Figure 3-3). We also note in Figure 3-3 that the treatments are completed in 25 days for patients 1 and 2, and 18 days for patient 3, which are significantly fewer than the 38 fractions. In Table 3.5, we have also simulated hypofractionated treatment by delivering 6.58 Gy for the first 5 fractions. While we note that hypofractionation does better than adaptive hypofractionation, the gain can fluctuate significantly depending on the dose ratios in the first 5 days. Thus, adaptive hypofractionation provides a balance between conventional therapy and hypofractionated therapy; on the one hand, it addresses the uncertainty of organ motion by waiting for the right opportunity and on the other, provides a shorter, more effective treatment than conventional fractionation.

3.4.4 Updating probability distribution over treatment course

In this subsection, we analyze what happens when the prior probability distribution estimated through historical data is very different from the true probability distribution.

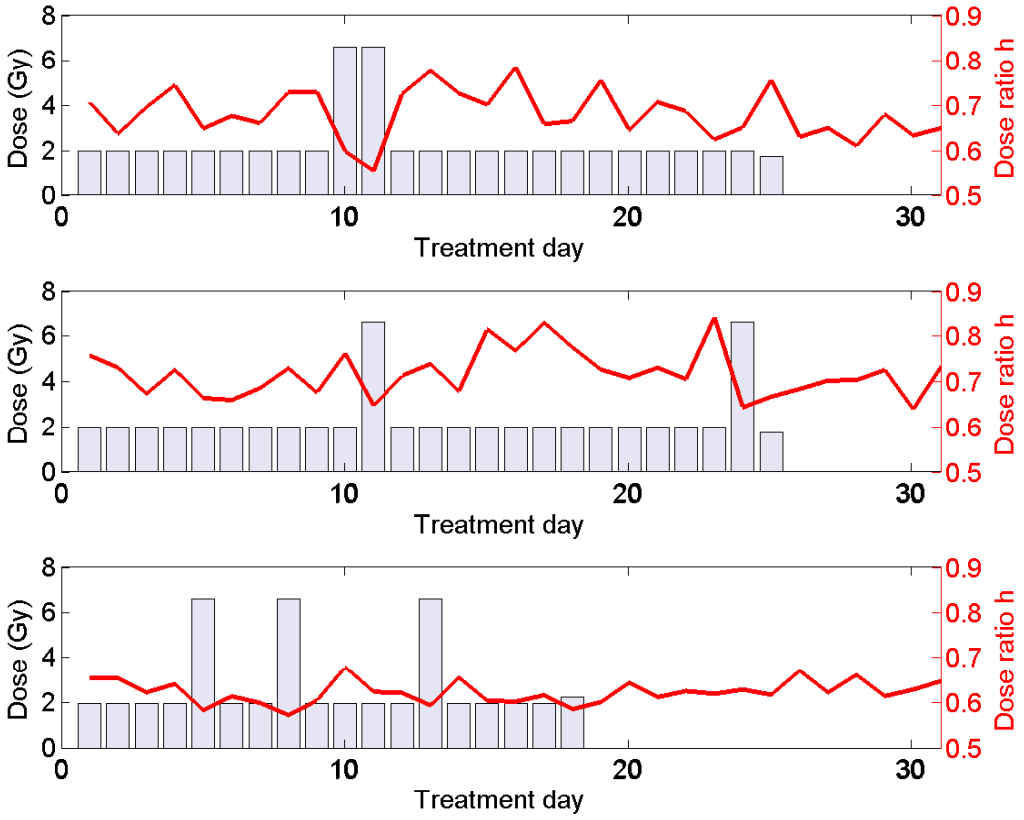

Figure 3-3: Illustration of adaptive hypofractionation for prostate patients. Note that large fractions are delivered when the dose ratio is particularly small. We also note fewer days of treatment delivery are required compared to conventional treatment.

To investigate this, we construct a probability distribution that is different from the ones in Figure 3-2. Consider a distribution which assigns 0.5 probability to the first two buckets of the ten possible dose ratios in the interval $[0.5, 1]$ (Figure 3-4). Using 50% deviations from standard fractionation and the BED model with the same parameters as in the previous subsection, we find that the gain reduces significantly (Table 3.6). To address this problem, we use the algorithm suggested in Subsection 3.3.3. We update the probability distribution over the course of treatment and re-run the DP algorithm before the delivery of each fraction. We use a small concentration parameter $c_r = 2$ to put little weight on our prior distribution and a large weight on the observations from the patient anatomy when updating the distribution. Figure 3-4 shows that about midway through treatment (fraction 19), the probability distribution looks much closer to the true one, and at the end of treatment, the probability distribution looks almost identical to the true one. As treatment progresses, the time horizon over which the DP algorithm is run gets smaller. In our simulation, we find the DP algorithm takes less than 1.5 minutes for the first fraction and less than that for later fractions. We find that this approach of updating the probability distribution achieves almost the entire gain as when using the true distribution (Table 3.6). For patient 3, we find that this algorithm does even better than when the true distribution is known. However, this is only a single run; on average, the gain will be smaller when the true distribution is known, regardless of whether it is being updated or not.

3.4.5 Treatment plan selection from a plan library

In this subsection, we quantify the benefit of adapting a plan both spatially (by selecting from a plan library) and temporally (by adaptively varying the fraction size). For the treatment plan selection, we choose the plan that results in the smallest dose ratio as long as the target coverage is satisfied. In our example, we only have two plans: CTV+2mm and CTV+5mm. The CTV+2mm plan has fewer target coverage constraints, and thus, will have a smaller dose ratio than the CTV+5mm plan (assum-

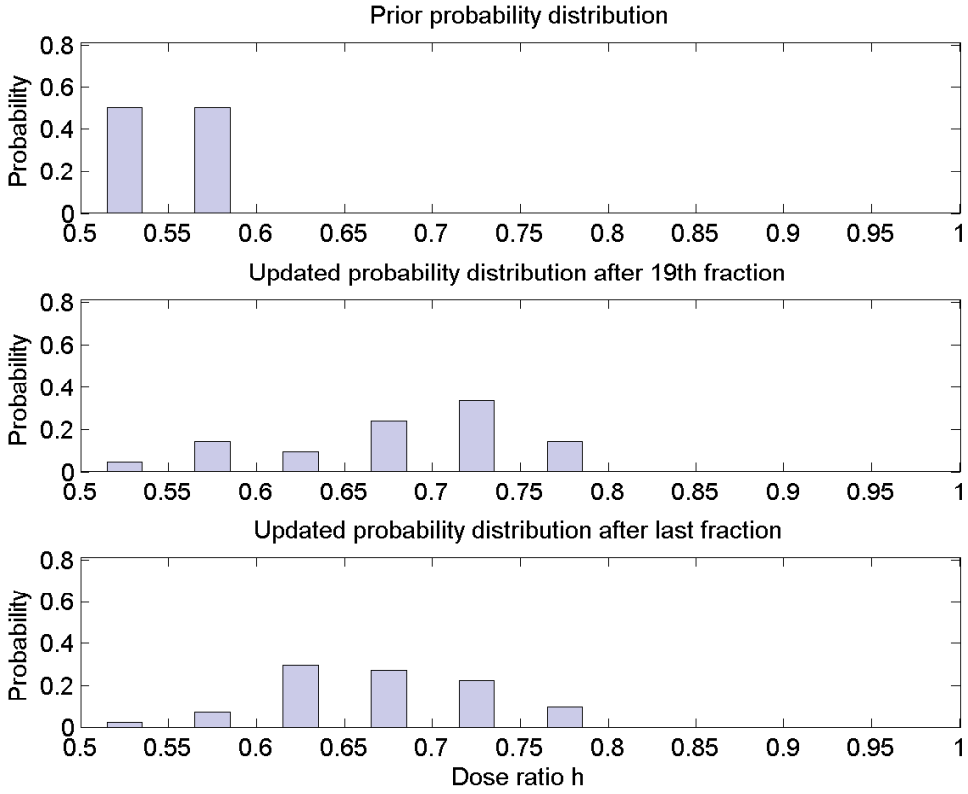

Figure 3-4: Illustration of probability distribution adapted over the course of treatment. The top plot displays the prior probability distribution. The middle and bottom plots show the updated distribution after the 19th and the last fraction. The concentration parameter c_r is chosen to be 2.

Table 3.6: Improvement in gain when updating dose ratio probability distribution over course of treatment. The BED model with 50% deviations is used. We quantify the gain resulting from using the true probability distribution, resulting from using a prior distribution significantly different from the true one, and resulting from using an updated distribution. The gains are denoted G_{true}, G_{prior}, and G_{updated} respectively. The prior distribution assigns 0.5 probability to the first two buckets of the ten possible dose ratios.

Patient	G_{true} [%]	G_{prior} [%]	G_{updated} [%]
1	9.14	5.95	8.94
2	8.31	4.92	7.76
3	5.77	2.95	6.39

ing we compute the dose ratio by dividing the EUD in the OAR by the target dose of 2 Gy). Our plan selection then reduces to whether or not the CTV+2mm plan provides sufficient target coverage. If target coverage is ensured, the CTV+2mm is chosen, and if not, the CTV+5mm is chosen. In order to determine target coverage, we compute the EUD with exponent $a = -20$ in the CTV and make sure it is at least the required dose of 2 Gy. If so, the CTV+2mm plan is delivered and otherwise the CTV+5mm plan is delivered. We find significant reduction in the physical dose in the OAR resulting from adaptively selecting these two types of plans (Table 3.7). We note that the reduction in dose for patient 3 is much greater than the other two patients; this is because the CTV+2mm plan was used for most (92.1%) of the fractions. This is quite interesting because patient 3 received the least benefit compared to the others when adaptively varying the fraction size. Indeed, the dose ratio probability distribution in Figure 3-2 tells us that patient 3 had little organ motion. This leads us to conclude that more organ motion is better for adaptive fractionation and little motion is better for spatial adaptation. This is part of the reason why a combination of both spatial adaptation and temporal dose variations can together result in significant improvement in treatment effectiveness (Table 3.8).

Table 3.7: Results from treatment plan selection. We compute the gain in the physical dose to the OAR as a result of selecting between two plans. The conventional treatment is to deliver the CTV+5mm plan throughout the treatment. The physical dose in the OAR using conventional and adaptive selection are D^{OAR}_{conv} and D^{OAR}_{plan}, respectively. The fraction of the days that the CTV+2mm plan was used is given by Frac_{2mm}.

Patient	D^{OAR}_{conv} [Gy]	D^{OAR}_{plan} [Gy]	Gain [%]	Frac_{2mm} [%]
1	51.52	45.90	10.90	55.3
2	54.53	53.99	0.99	18.4
3	47.65	38.48	19.24	92.1

Table 3.8: Results from using both adaptive fractionation and plan selection. The BED model with 50% deviations was used. We note significant gain for all three patients. The gain from using plan selection, from adaptive fractionation, and both are denoted G_{plan}, G_{adap}, and G_{both} respectively.

Patient	$\widetilde{D}^{OAR}_{\text{conv}}$ [Gy]	G_{plan}	G_{adap} [%]	G_{both} [%]
1	74.93	13.43	9.15	22.46
2	80.72	1.25	8.32	10.30
3	67.61	23.72	5.78	28.41

3.5 Discussion and conclusions

We have presented an adaptive spatio-temporal approach, which involves varying the fraction size and selecting from a plan library. For the three prostate patients, we find that adaptive fractionation based on a physical dose model does not result in significant benefit. However, using the BED model, we find that there is significant gain, especially because of the low α-β ratio of prostate cancer. We present an interesting concept called adaptive hypofractionation, which is potentially beneficial. Further investigation of the benefit of this approach would be useful. We show that an inaccurate estimate of the dose ratio probability distribution can reduce the benefit considerably. But, updating the distribution based on observations of the patient anatomy during the course of treatment and using an approximate DP approach overcomes this problem. We find that adaptive fractionation is beneficial when there is significant organ motion. On the other hand, selection from a library of plans, which consist of differing margins around

the tumor volume, is more beneficial when there is less motion. Thus, the combination of both adaptive fractionation and treatment plan selection has a significant potential for improving treatments.

We point out limitations and further remarks about our assumptions:

1. For the methods in this chapter, we required an image of the patient anatomy before the delivery of every fraction. We hope that this information together with reliable automatic contouring and/or contour registration algorithms [12] will be available in the future.

2. We assumed that the dose ratio is computed fast enough before delivery of each fraction. In this chapter, we re-computed the dose deposition matrix to determine the OAR dose ratio. However, it is possible to approximate this by using the same dose deposition matrix from the simulation CT for every fraction; this could be reasonable for a photon beam modality. If possible, fast dose computation on a CBCT image could also be used.

3. The patient setup in this chapter was assumed to be perfect. That is, for every fraction, we aligned the center of mass of the target volume to be the isocenter. It may be necessary to consider a margin of error here even with image guidance. We do not consider other intangibles such as contouring error when ensuring target coverage for the CTV. It may be necessary to add a slight margin to the CTV to determine target coverage.

4. We used the dose to one primary OAR, the anterior rectum in the prostate case, as a metric for treatment effectiveness. It is possible to use other appropriate cost functions here. Using multiple OARs and tracking them separately could be a useful direction for future research. This would, however, involve additional states and would increase the computation time for the DP.

5. We did not compute DVH type metrics to determine treatment effectiveness. For such metrics, it is necessary to use deformable registration tools to determine the

total dose in each voxel. Perhaps such metrics can be used in the future given these registration tools are more reliable.

Future work could include determining other disease sites that could benefit from adaptive fractionation and/or plan selection from a library of plans. It is possible to re-optimize a treatment plan before every fraction perhaps, but many treatment centers require QA procedures. The pre-approved library of plans approach has the advantage of not having to go through these extra QA procedures. In this chapter, we selected a plan with a small margin and another with a large margin to be part of the plan pool. However, this approach was heuristically determined from intuition. A question of interest could be how one can generate such a plan library. It may be possible to mathematically optimize, for example, two treatment plans to be part of the library so that treatment effectiveness is maximized and target coverage is ensured. At first glance, this problem appears to be combinatorial in nature and possibly difficult to solve. This could be an interesting problem for future research.

Chapter 4

Effect of tumor repopulation on optimal fractionation

4.1 Introduction

Radiation therapy treatments are typically fractionated (i.e., spaced out in time) so that normal tissue has time to recover. However, such time in between treatments allows cancer cells to proliferate and can result in treatment failure [37]. The problem of interest then is the determination of an optimal fractionation schedule to counter the effects of tumor repopulation. In this chapter, we develop a framework for optimizing *non-uniform* (in time) dose schedules for general tumor growth curves, motivated primarily by the phenomenon of accelerated repopulation, i.e., a faster repopulation of surviving tumor cells towards the end of radiation treatment. Accelerated repopulation is considered to be an important cause of treatment failure in radiation therapy, especially for head and neck tumors [91, 92]. We choose to model this behavior by using decelerating tumor growth curves, where a larger number of tumor cells results in slower growth. Thus, faster growth is exhibited towards the end of radiation treatment, when there are fewer cells.

To determine an optimal fractionation schedule, we formulate an optimization prob-

lem. Consider a tumor and one dose-limiting organ-at-risk (OAR). We assume that a dose d_i to the tumor in the ith day results in a homogeneous dose of γd_i to the OAR, where γ is the normal tissue sparing factor that satisfies $0 < \gamma < 1$. We would like to maximize the tumor control probability (TCP) subject to an upper limit on the normal tissue complication probability (NTCP). A convenient way to model TCP is to use Poisson statistics [54], under which

$$\text{TCP} = \exp(-X_{N-1}^{+}),$$

where X_{N-1}^{+} is the expected number of tumor cells surviving after the last dose of radiation. In this case, maximizing the TCP is equivalent to minimizing the expected number of cells remaining at the end of treatment. For the rest of the chapter, we focus on minimizing X_{N-1}^{+} subject to a given level of probability of normal tissue complication.

In Section 4.2, we list the main contributions. In Section 4.3, we provide background and existing results on optimal fractionation without tumor repopulation. In Section 4.4, we formulate the fractionation problem including general repopulation characteristics. We propose a dynamic programming (DP) approach to solve the problem and state the main result that optimal dose fractions are non-decreasing over time. In Section 4.4.4, we analyze the special structure of the problem for the case of Gompertz tumor growth. In Section 4.5, we discuss numerical results under exponential or Gompertz growth models. The results indicate that accelerated repopulation suggests larger dose fractions toward the end of treatment to compensate for the increased tumor proliferation.

4.2 Contributions

In this chapter, we provide an insightful analysis of the effect of tumor repopulation on optimal fractionation schemes. Specifically, we:

1. formulate a problem that includes general tumor repopulation characteristics and

develop a DP approach to solve it.

2. prove that the optimal doses are non-decreasing over time, due to the decelerating nature of tumor growth curves.

3. analyze the special structure of the problem for the case of Gompertz tumor growth and show that it is equivalent to maximizing a discounted version of the biological effective dose in the tumor.

4. show that when there is repopulation, the optimal number of dose fractions is finite.

5. find through numerical simulations that faster tumor growth suggests shorter overall treatment duration. In addition, the presence of accelerated repopulation suggests larger dose fractions later in the treatment to compensate for the increased tumor proliferation.

4.3 Optimal fractionation without tumor repopulation

We provide some background relevant to optimal fractionation in the absence of repopulation. This will be basis for the new results presented in Section 4.4. We first describe the LQ model of radiation effects and the biological effective dose (BED) model. In the second subsection, we state the optimal fractionation scheme when repopulation is not considered [52].

4.3.1 LQ model

The relationship between radiation dose and the fraction of surviving cells is described by the LQ model of radiation effects. Observations from irradiating cells *in vitro* support this model [21]. The LQ model relates the expected survival fraction S after a single

delivered dose d, in terms of two tissue parameters α and β, through the equation

$$S = \exp(-(\alpha d + \beta d^2)).$$

Thus, the logarithm of the survival fraction consists of a linear component with coefficient α and a quadratic component β (Figure 4-1). For N treatment days with radiation doses $d_0, d_1, \ldots, d_{N-1}$, the resulting survival fractions from each individual dose can be multiplied, assuming independence between dose effects. The resulting equation is

$$S = \exp\left(-\sum_{k=0}^{N-1}\left(\alpha d_k + \beta d_k^2\right)\right). \tag{4.1}$$

The effect of the quadratic factor β, in the above equation, is that the survival fraction is larger when splitting the total dose into individual dose fractions (Figure 4-1). Thus, there is an inherent trade-off between delivering large single doses to maximize cell kill in the tumor and fractionating doses to spare normal tissue. It is now clear that the physical dose d by itself does not entirely capture the biological effect on tissue. A common quantity that is used instead to quantify the effect of the radiation treatment is the *biological effective dose* (BED). It is defined by

$$\mathrm{BED}(d) = \frac{1}{\alpha}\left(\alpha d + \beta d^2\right) = d\left(1 + \frac{d}{[\alpha/\beta]}\right), \tag{4.2}$$

where $[\alpha/\beta]$ is the ratio of the respective tissue parameters. Thus, the BED in the above equation captures the effective biological dose in the same units as physical dose. A small value $[\alpha/\beta]$ means that the tissue is sensitive to large doses; the BED in this case grows rapidly with increasing dose. Note that BED, which is practically used to quantify fractionation effects in a clinical setting, is related to the LQ model used *in vitro* by setting $\mathrm{BED} = -\ln(S)/\alpha$. With the relation given in Equation (4.2), we define $\mathrm{BED}_T(d)$ as the BED in a tumor with parameter $[\alpha/\beta]_T$, and $\mathrm{BED}_O(d)$ as the BED in an OAR with parameter $[\alpha/\beta]_O$. We assume throughout the chapter that $[\alpha/\beta]_T$ and

$[\alpha/\beta]_O$ are positive. Finally, we also define (for convenience in notation) the total BED in the tumor, BED_T, and the total BED in the OAR, BED_O, from delivering the doses $d_0, d_1, \ldots, d_{N-1}$:

$$\text{BED}_T = \sum_{k=0}^{N-1} \text{BED}_T(d_k) = \sum_{k=0}^{N-1} d_k \left(1 + \frac{d_k}{[\alpha/\beta]_T}\right)$$

and

$$\text{BED}_O = \sum_{k=0}^{N-1} \text{BED}_O(d_k) = \sum_{k=0}^{N-1} \gamma d_k \left(1 + \frac{\gamma d_k}{[\alpha/\beta]_O}\right),$$

where γ is the sparing factor and $[\alpha/\beta]_T$ and $[\alpha/\beta]_O$ are the α/β-ratios in the tumor and OAR, respectively. A common way to model normal tissue complication (NTCP) is a sigmoidal function of the BED in the OAR, BED_O. Thus, since a sigmoidal function is monotonic in its argument, it suffices to impose an upper limit on BED_O. From here on, our optimization problem of interest is to minimize the expected number of tumor cells subject to an upper limit on BED_O. The problem is stated mathematically as

$$\underset{\{d_i \geq 0\}}{\text{minimize}} \quad X_{N-1}^{+} \quad \text{s.t.} \quad \text{BED}_O \leq c, \tag{4.3}$$

where X_{N-1}^{+} is the expected number of tumor cells after radiation treatment and c is an appropriate constant.

4.3.2 Optimal BED based fractionation

In the absence of repopulation, the expected number of cells at the end of treatment, X_{N-1}^{+}, is $X_0 S$, where X_0 is the initial number of tumor cells and S is the expected survival fraction given in (4.1) resulting from delivering doses $d_0, d_1, \ldots, d_{N-1}$. Taking natural logarithms and dividing by $-\alpha_T$, where α_T is a tumor tissue parameter, minimizing the expected number of tumor cells is equivalent to maximizing the BED in the tumor, BED_T. The next lemma states that the constraint on BED_O is always binding.

Lemma 4.3.1. *In the absence of repopulation, the constraint in (4.3) will be satisfied*

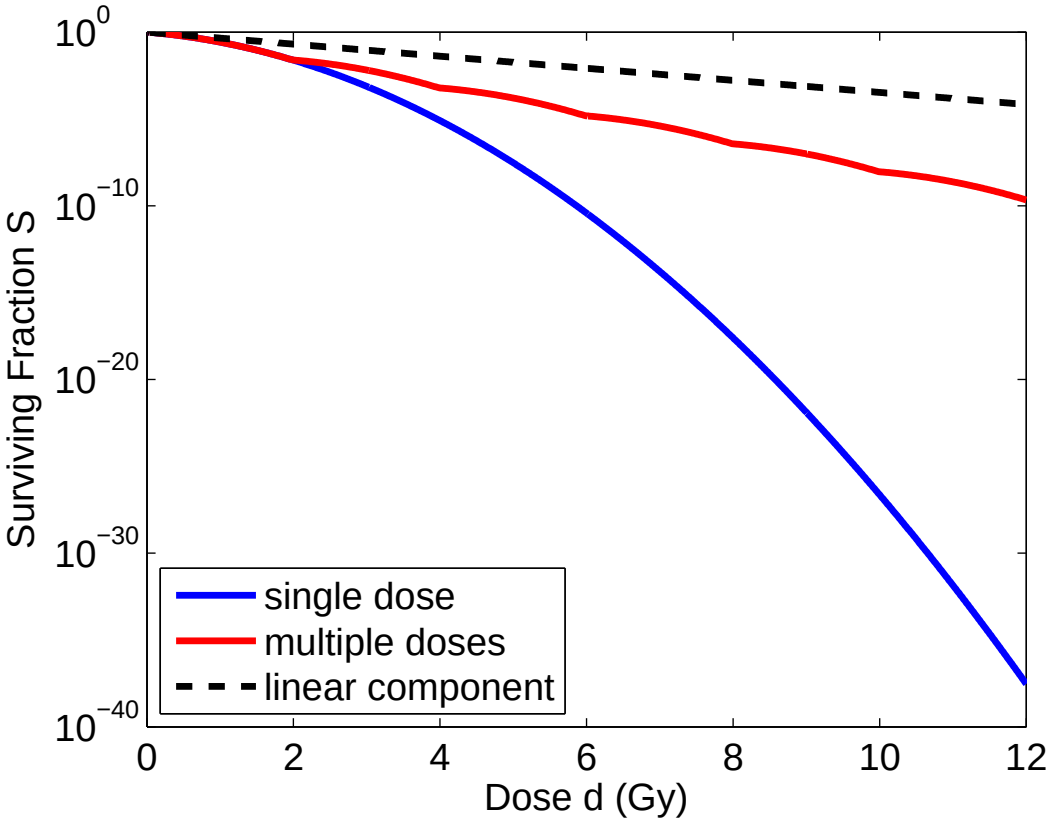

Figure 4-1: Illustration of the fractionation effect using the LQ model. The cell kill is exponential with both a linear and a quadratic term. Fractionating into multiple individual doses results in a much lower survival fraction compared to a single dose assuming the quadratic β term is significant.

with equality at the optimum.

Proof. See Appendix 4.8.1. □

Thus, a simplified version of the optimization problem without repopulation is

$$\underset{\{d_i \geq 0\}}{\text{maximize}} \quad \text{BED}_T \quad \text{s.t.} \quad \text{BED}_O = c. \tag{4.4}$$

We characterize the set of all optimal solutions to this problem in the following theorem, published in [52].

Theorem 4.3.2. *Let N be given. If $[\alpha/\beta]_O \geq \gamma[\alpha/\beta]_T$, an optimal solution is to deliver a single dose equal to*

$$d_j^* = \frac{[\alpha/\beta]_O}{2\gamma}\left[\sqrt{1+\frac{4c}{[\alpha/\beta]_O}}-1\right] \tag{4.5}$$

at an arbitrary time j and deliver $d_i = 0$ for all $i \neq j$. This corresponds to a hypo-fractionation regimen, i.e., a fractionation schedule that uses as few treatment days as possible. If $[\alpha/\beta]_O < \gamma[\alpha/\beta]_T$, the unique optimal solution consists of uniform doses given by

$$d_j^* = \frac{[\alpha/\beta]_O}{2\gamma}\left[\sqrt{1+\frac{4c}{N[\alpha/\beta]_O}}-1\right], \tag{4.6}$$

for $j = 1, 2, \ldots, N$. This corresponds to a hyper-fractionation regimen, i.e., a fractionation schedule that uses as many treatment days as possible.

Proof. A geometric proof is given in [52]. An alternate proof is provided in Appendix 4.8.2. □

The above theorem states that if $[\alpha/\beta]_O$ is small enough, i.e., the OAR is sensitive to large doses and $[\alpha/\beta]_O < \gamma[\alpha/\beta]_T$, it is optimal to deliver the same dose during the N days of treatment. Besides the distribution of doses during treatment for a fixed value of N, the above theorem also has an interpretation on the optimal number of treatment days, N^*. Note that taking N larger will only improve the objective BED_T and add extra degrees of freedom. If $[\alpha/\beta]_O \geq \gamma[\alpha/\beta]_T$, the theorem states that a single radiation

dose is optimal, i.e., $N^* = 1$. On the other hand, if $[\alpha/\beta]_O < \gamma[\alpha/\beta]_T$, the optimal solution consists of uniform doses with N as large as possible. This would correspond to choosing $N^* \to \infty$. For most disease sites, the condition $[\alpha/\beta]_O < \gamma[\alpha/\beta]_T$ is generally satisfied. Clearly, $N^* \to \infty$ is not realistic and is an artifact of modeling assumptions. Later in the chapter, we will show how modeling tumor repopulation results in a finite optimal number of treatment days.

4.4 Optimal fractionation for general tumor repopulation

In this section, we present the problem statement and a solution method that determines an optimal fractionation schedule for the case of general tumor growth.

4.4.1 Problem formulation

We are interested in minimizing the expected number of tumor cells at the end of treatment. The two aspects that determine the expected number of cells at any point in time are the sequence of doses that are delivered and the dynamics of the tumor growth in between doses. Let us denote by $x(t)$ the expected number of tumor cells at time t, for any t between 0 and $N-1$. We assume the sequence of N doses $d_0, d_1, \ldots, d_{N-1}$ are delivered at integer times, i.e., time is measured in days. For these integer times $i = 0, 1, \ldots, N-1$, the effect of radiation doses is described by the LQ model, resulting in

$$x(i^+) = x(i^-) \exp(-(\alpha_T d_i + \beta_T d_i^2)), \tag{4.7}$$

where i^- and i^+ are the times immediately before and after delivering the dose d_i. The dynamics of $x(t)$ modeling tumor growth for non-integer times in $[0, N-1]$ is described by the differential equation

$$\frac{1}{x(t)} \frac{\mathrm{d}x(t)}{\mathrm{d}t} = \phi(x(t)), \tag{4.8}$$

with the initial condition $x(0) = X_0$ for the initial number of cells. In the above equation, $\phi(x)$ represents an instantaneous tumor proliferation rate. By choosing an appropriate functional form of ϕ, we can describe a variety of tumor repopulation characteristics relevant for radiation therapy:

1. By choosing $\phi(x) = \rho$, we model exponential tumor growth with a constant proliferation rate ρ.

2. By choosing $\phi(x)$ to be a decreasing function of x, we are able to mimic the case of accelerated repopulation [91, 92]. In this case, the instantaneous tumor proliferation rate increases when, towards the end of treatment, the number of remaining tumor cells decreases.

In the remainder of this section, we first consider the optimal fractionation problem for a general proliferation rate $\phi(x)$. In Section 4.4.2, a DP approach is proposed to solve the problem. In Section 4.4.3, the property that the optimal doses are non-decreasing over time is established. In Sections 4.4.4 and 4.4.5, we consider the special cases of Gompertzian growth (as a model for accelerated repopulation) and exponential growth (as a model of constant repopulation), respectively.

We define some additional notation for ease of exposition. Since the range of possible values of $x(t)$ is large and the cell kill factor is exponential according to the LQ model, it is convenient to work with the logarithm of $x(t)$. Hence, we define $y(t) = \ln(x(t))/\alpha_T$. We also define $X_i^- = x(i^-)$ and $X_i^+ = x(i^+)$ to be the expected number of tumor cells remaining immediately before and after delivering the dose d_i, respectively. Similarly, the logarithmic counterparts are $Y_i^- = \ln(X_i^-)/\alpha_T$ and $Y_i^+ = \ln(X_i^+)/\alpha_T$. We will assume that the initial number of cells are $X_0 = X_0^-$, and $Y_0 = Y_0^-$ for the logarithmic version. Note that the equivalent of Equation (4.7) for $y(t)$ is

$$Y_i^+ = Y_i^- - \mathrm{BED}_T(d_i),$$

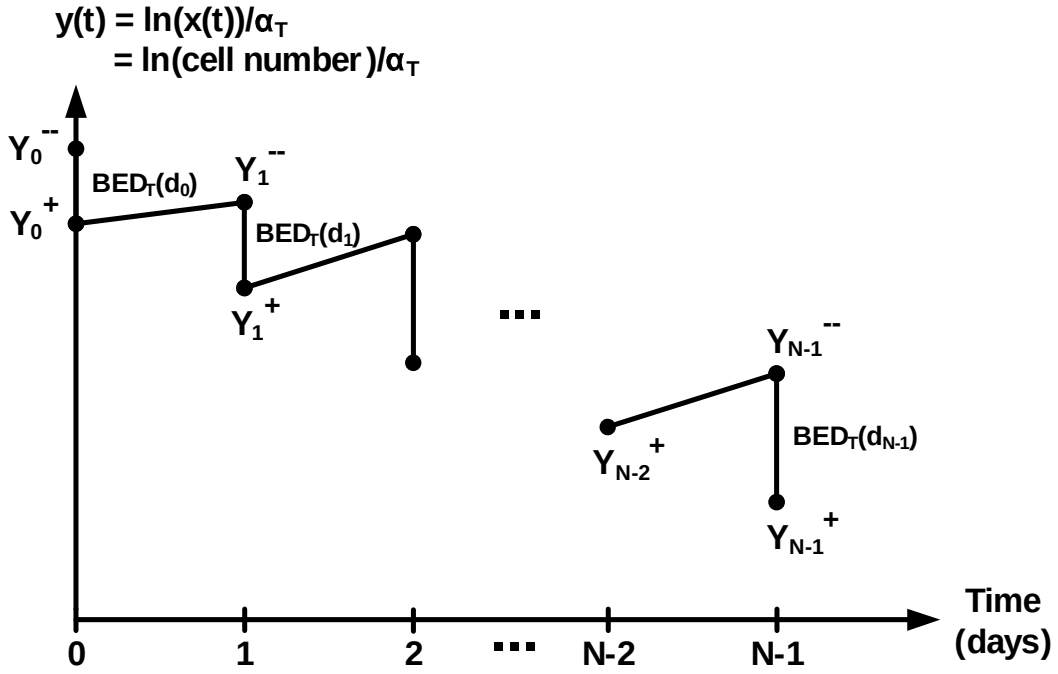

Figure 4-2: Schematic illustration of the expected number of tumor cells over the course of treatment. The effect of radiation dose d is a reduction in the log of the number of cells, proportional to $\text{BED}_T(d)$.

where $\text{BED}_T(d_i)$ is defined as before. We also define a growth function F that maps Y^+ to Y^- using the appropriate differential equation equivalent of (4.8). Thus, $Y_{i+1}^- = F(Y_i^+)$ for $i = 0, 1, \ldots, N-1$. Figure 4-2 provides an illustration of the behavior of the expected number of tumor cells over the course of treatment.

4.4.2 Dynamic programming approach

The optimization problem of interest is to minimize the expected number of tumor cells at the end of treatment, X_{N-1}^+, under the constraint that the BED in the OAR, BED_O, is less than or equal to some constant c. Equivalently, we choose to minimize Y_{N-1}^+. In order to get from the initial Y_0 to Y_{N-1}^+, one recursively alternates between applying a dose d and the growth function F. That is, Y_{N-1}^+ takes the form

$$Y_{N-1}^+ = F(\cdots F(F(Y_0 - \text{BED}_T(d_0)) - \text{BED}(d_1))\cdots) - \text{BED}(d_{N-1}). \qquad (4.9)$$

Such a recursive formulation lends itself naturally to a DP approach to solve the problem. We can solve the formulation by recursively computing an optimal dose backwards in time. Note that although non-linear programming methods can be used, there is no guarantee of the convexity of the objective (4.9), and the solution might provide only a local optimum. On the other hand, a global optimum is guaranteed if the DP approach is used.

We now formulate the problem in a DP framework. We define z_i to be the cumulative BED in the OAR resulting from delivering the doses $d_0, d_1, \ldots, d_{i-1}$. We wish to determine the dose d_i based on Y_{i-1}^+ and the cumulative BED in the OAR z_i. Here, Y_{i-1}^+ and z_i together represent the state of the system because they are the only relevant pieces of information needed to determine the dose d_i. Instead of additive costs, we choose to formulate the problem by including only a terminal cost. Specifically, we include the final expected (logarithmic) number of cells Y_{N-1}^+ in the terminal condition. In order to ensure that the BED_O constraint is satisfied, we also assign an infinite penalty to the terminal cost when the constraint is violated. The Bellman recursion to solve the problem is:

$$J_N(Y_{N-1}^+, z_N) = \begin{cases} Y_{N-1}^+, & \text{if } z_N \leq c, \\ \infty, & \text{otherwise,} \end{cases}$$

$$J_k(Y_{k-1}^+, z_k) = \min_{d_k \geq 0} \left[J_{k+1}(F(Y_{k-1}^+) - \text{BED}_T(d_k)) \right],$$

for $k = N-1, N-2, \ldots, 1$. The initial equation for time 0, given below, is slightly different because there is no prior tumor growth

$$J_0(Y_0^-, z_0) = \min_{d_0 \geq 0} \; J_1(Y_0^- - \text{BED}_T(d_0)).$$

For numerical implementation, the above state variables need to be discretized and the tabulated values stored. For evaluating the cost-to-go function J_k at any non-discretized values, an interpolation of appropriate discretized values can be used for accuracy.

4.4.3 Properties of the optimal fractionation scheme

We begin with two lemmas. The first one is simply a counterpart of Lemma 4.3.1 for the case where there is tumor repopulation.

Lemma 4.4.1. *Assume that $\phi(x) > 0$ for all $x > 0$. For the fractionation problem that includes tumor repopulation, the constraint on BED_O will be satisfied with equality.*

Proof. See Appendix 4.8.3. □

Lemma 4.4.2. *Assume that $\phi(x) > 0$ for all $x > 0$. Suppose that $i < j$ and that we apply the sequence of doses $d_{i+1}, \ldots, d_j$ starting with either Y_i^+ or $\widetilde{Y}_i^+$. If $Y_i^+ < \widetilde{Y}_i^+$, then $Y_j^+ < \widetilde{Y}_j^+$.*

Proof. See Appendix 4.8.4. □

The second lemma above provides a monotonicity property of the mapping of the expected number of cells from point in time to another, assuming that the same sequence of doses are applied. Next, we state the following theorem.

Theorem 4.4.3. *Let us fix N. Assume that the instantaneous tumor growth rate $\phi(x)$ is non-increasing as a function of the number of cells x, and that there is always some amount of repopulation, i.e., $\phi(x) > 0$ for all $x > 0$. If $[\alpha/\beta]_O \geq \gamma[\alpha/\beta]_T$, the optimal solution is to deliver a single dose as in Theorem 4.3.2. If $[\alpha/\beta]_O < \gamma[\alpha/\beta]_T$, then the optimal doses must increase over the course of treatment. That is, the optimal doses will satisfy $d_0^* \leq d_1^* \leq \cdots \leq d_{N-1}^*$.*

Proof. See Appendix 4.8.5. □

For the case where $[\alpha/\beta]_O \geq \gamma[\alpha/\beta]_T$, it is reasonable that the optimal solution is to use the most aggressive treatment of a single dose with the optimal $N^* = 1$ because this is the case even without repopulation. The interesting case is that when $[\alpha/\beta]_O < \gamma[\alpha/\beta]_T$, the doses must increase over time. Intuitively, due to the decreasing property of $\phi(x)$ as a function of x, the tumor grows at a faster rate when its size becomes smaller over the course of treatment; higher doses are then required to counter the increased proliferation.

4.4.4 Gompertzian tumor growth

In this subsection, we discuss the Gompertz tumor growth model and present a simplified DP approach with a reduced state space. The Gompertz equation a particular model of a decelerating tumor growth curve. The dynamics are described by a differential equation that has the instantaneous proliferation rate

$$\phi(x) = b \ln\left(\frac{X_\infty}{x}\right),$$

where X_∞ is the carrying capacity and b is a parameter that controls the rate of growth. (Here, the asymptotic limit X_∞ is more of a mathematical abstraction rather than a meaningful physical quantity; the death of a host would occur long before there are X_∞ tumor cells.) The resulting analytical solution $n(t)$ from solving the differential equation (4.8) with initial condition $n(0) = X_0$ is

$$\begin{aligned} n(t) &= X_\infty \exp\left[\ln\left(\frac{X_0}{X_\infty}\right)\exp(-bt)\right] \\ &= X_0^{\exp(-bt)} X_\infty^{1-\exp(-bt)}, \end{aligned} \tag{4.10}$$

Here, $n(t)$ is used to denote the expected number of tumor cells without radiation treatment; this is to avoid confusion with the already defined $x(t)$. The above equation models slower repopulation for larger tumor sizes and vice-versa (see Figure 4-3).

For the case of Gompertzian tumor growth, it turns out that one can significantly simplify the problem and solution approach. We will now derive an explicit expression for the expected number of tumor cells at the end of treatment. We claim that

$$Y_i^+ = \frac{1}{\alpha_T} \ln\left(n(i)\right) - \sum_{k=0}^{i} \exp[-b(i-k)]\mathrm{BED}_T(d_k), \tag{4.11}$$

for $i = 0, 1, \ldots, N-1$, where $n(t)$ represents the expected number of tumor cells without any radiation treatment. The above equation (4.11) holds for $i = 0$ because $n(0) = X_0$ and $Y_0^+ = \ln(X_0)/\alpha_T - \mathrm{BED}_T(d_0)$. For the inductive step, suppose the equation (4.11)

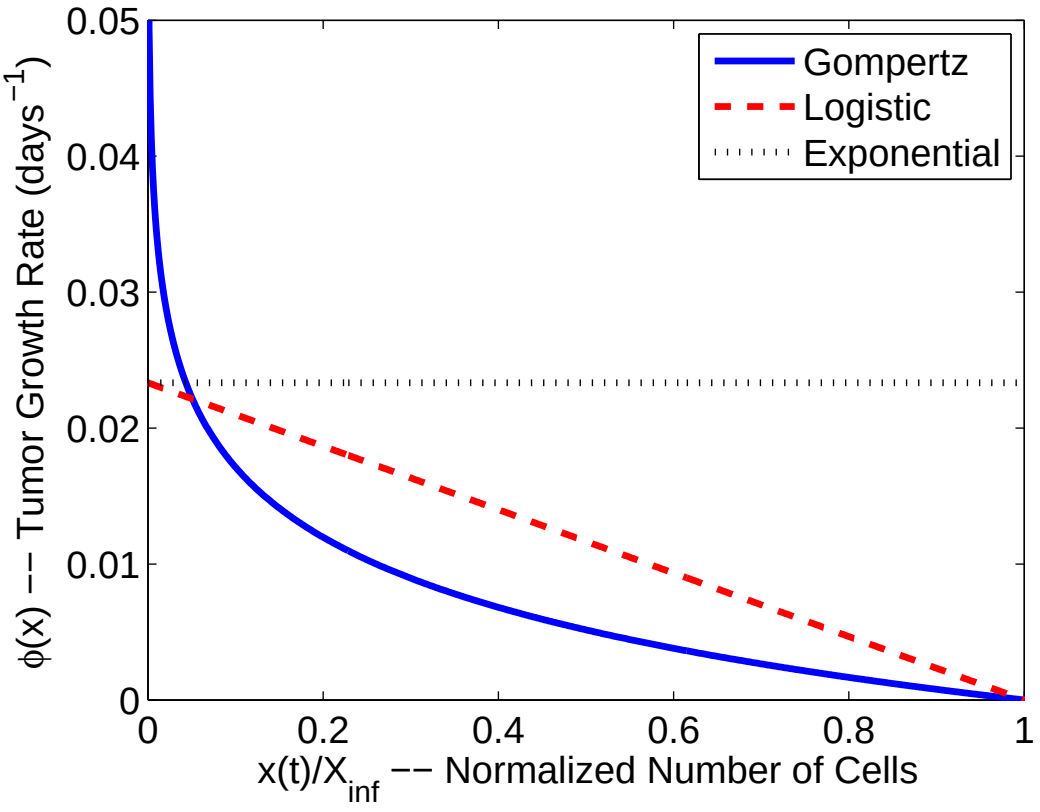

Figure 4-3: Various types of tumor growth curves. The Gompertz and logistic equations both model slower growth for larger number of cells. The exponential model assumes a constant growth rate.

holds true. From the Gompertz growth equation (4.10), assuming the time interval between fractions is one day (implying $t = 1$), we can write the function F mapping Y_i^+ to Y_{i+1}^- resulting from tumor growth as

$$Y_{i+1}^+ = F(Y_i^+) = \exp(-b)Y_i^+ + (1 - \exp(b))\frac{\ln(X_\infty)}{\alpha_T}.$$

Incorporating the growth and the radiation dose from d_{i+1}, we find

$$\begin{aligned} Y_{i+1}^+ &= F(Y_i^+) - \mathrm{BED}_T(d_{i+1}) \\ &= \frac{1}{\alpha_T}\ln\left(n(i)^{\exp(-b)}X_\infty^{(1-\exp(b))}\right) - \sum_{k=0}^{i+1}\exp[-b(i+1-k)]\mathrm{BED}_T(d_k) \\ &= \frac{1}{\alpha_T}\ln\left(n(i+1)\right) - \sum_{k=0}^{i+1}\exp[-b(i+1-k)]\mathrm{BED}_T(d_k), \end{aligned}$$

completing the inductive step. This results in the optimization problem

$$\begin{aligned} \underset{\{d_i \geq 0\}}{\text{minimize}} \quad & \frac{1}{\alpha_T}\ln\left(n(N-1)\right) - \sum_{k=0}^{N-1}\exp[-b(N-1-k)]\mathrm{BED}_T(d_k) \\ \text{s. t.} \quad & \mathrm{BED}_O \leq c, \end{aligned} \tag{4.12}$$

Notice the similarity between the problem without repopulation (4.4) and the above problem (4.12) that includes Gompertzian tumor growth. The only addition is the exponential weighting term in the objective and the additive term. Note that the additive term $\ln\left(n(N-1)\right)/\alpha_T$ has no impact on the optimization because it is independent of the dose fractions d_k. However, if we were also to optimize over the number of fractions, N, this term would come into play. Because the weighting term gives larger weight to later fractions, we can conjecture that the optimal fractionation scheme will result in larger fraction sizes towards the end of treatment.

From (4.12), we see that the expected number of tumor cells is not required as a state variable; we can thus simplify the DP equation. We also choose to include additive costs as opposed to a terminal cost as was done for the general case. The

updated algorithm is

$$J_N(z_N) = \begin{cases} 0, & \text{if } z_N = c, \\ \infty, & \text{otherwise,} \end{cases}$$

$$J_k(z_k) = \min_{d_k \geq 0} \Big[\exp[-b(N-1-k)]\text{BED}_T(d_k) + J_{k+1}(z_k + \text{BED}_O(d_k)) \Big], \qquad (4.13)$$

for $k = N-1, N-2, \ldots, 0$. For numerical implementation, we discretize the state variable z_k and solve a corresponding discrete problem. For evaluating the above J function for general values of z, linear interpolation was used.

4.4.5 Exponential tumor growth with constant repopulation rate

In this subsection, we discuss the exponential tumor growth model for which we provide the optimal fractionation scheme in closed form. As opposed to Gompertzian growth, the rate of growth does not change with tumor size (see Figure 4-3), and there is no upper limit (i.e., X_∞) on the number of tumor cells. The growth equation in this case is

$$n(t) = X_0 \exp(\rho t),$$

where X_0 is the initial number of cells, as before, and $\rho > 0$ is the proliferation rate. This corresponds to the case where $\phi(x)$ is constant and equal to ρ. We will show that for exponential growth, the solution can be described in closed form.

Assuming ρ represents a measure of growth per unit day (or fraction), the number of tumor cells is multiplied by a factor of $\exp(\rho)$ after every fraction. Since there are N dose fractions and $N-1$ days of repopulation in between treatment, the resulting survival fraction of cells S_T is

$$S_T = \exp\left(-\alpha_T \text{BED}_T + (N-1)\rho\right).$$

By taking the logarithm, we obtain the following optimization problem:

$$\underset{\{d_i \geq 0\}}{\text{maximize}} \quad \text{BED}_T - \frac{1}{\alpha_T}(N-1)\rho \quad \text{s.t.} \quad \text{BED}_O = c. \tag{4.14}$$

This is the same problem as the one for the case without repopulation, except for the additional $-\frac{1}{\alpha_T}(N-1)\rho$ term. For a fixed N, this additional term does not change when varying the set of doses $\{d_i\}$. Thus, the optimal doses under the case of constant exponential growth is exactly the same as in Theorem 4.3.2 for a fixed N.

To determine the optimal number of fractions N^*, one could compute the objective (4.14) by brute force for a range of reasonable values of N. However, for the exponential tumor growth case, one can characterize the optimal number of fractions in closed form. The result is consistent and similar to the work in [2, 32, 89] though it is interpreted differently here.

Theorem 4.4.4. *The optimal number of fractions N^* for exponential growth with constant repopulation rate ρ is obtained by following this procedure:*

1. *If $[\alpha/\beta]_O \geq \gamma[\alpha/\beta]_T$, then $N^* = 1$.*
2. *If $[\alpha/\beta]_O < \gamma[\alpha/\beta]_T$, then*
   (a) *Compute $N_c = A\left(\sqrt{\frac{(\rho+B)^2}{\rho(\rho+2B)}} - 1\right)$, where $A = \frac{2c_2}{[\alpha/\beta]_O}$, $B = \frac{\alpha_T[\alpha/\beta]_O}{2\gamma}\left(1 - \frac{[\alpha/\beta]_O}{\gamma[\alpha/\beta]_T}\right)$.*
   (b) *If $N_c < 1$, then $N^* = 1$. Otherwise, evaluate the objective at $\lfloor N_c \rfloor$ and $\lceil N_c \rceil$, and let the optimum N^* be the one that results in a larger objective value.*

Proof. See Appendix 4.8.6. □

This result also makes sense in the limiting cases when $\rho \to 0$ and $\rho \to \infty$. When approaching the case of no repopulation, i.e., $\rho \to 0$, we see that $N_c \to \infty$ and the optimum N approaches infinity. When $\rho \to \infty$, we see that $N_c \to 0$, meaning that the optimum N is a single dose when repopulation becomes very large. Recall that if $[\alpha/\beta]_O < \gamma[\alpha/\beta]_T$, the optimal N approaches infinity for the case without repopulation.

For the case of exponential repopulation with constant rate, the above result shows that the optimum N is finite. Indeed, even for general tumor growth characteristics, as long as there is repopulation, the optimal number of fractions is finite. The result is stated in the following theorem.

Theorem 4.4.5. *Suppose that there exists $r > 0$ such that $\phi(x) > r$ for all $x > 0$. Then, the optimal number of fractions N^* is finite.*

Proof. See Appendix 4.8.7. □

4.5 Numerical experiments

4.5.1 Faster tumor growth suggests shorter treatment duration

We use realistic choices of radiobiological parameters in order to simulate the effect of various rates of tumor growth on the optimal number of treatment days. Here, we assume exponential growth with a constant rate of repopulation. We use $[\alpha/\beta]_T = 10$ Gy, $[\alpha/\beta]_O = 3$ Gy, and $\alpha_T = 0.3$ Gy^{-1} for the tissue parameters; these are appropriate standard values [27]. We consider a standard fractionated treatment as reference, i.e., a dose of 60 Gy delivered to the tumor in 30 fractions of 2 Gy. For the above choice of α/β-ratios and $\gamma = 0.7$, this corresponds to an OAR BED of 61.6 Gy, which we use as the normal tissue BED constraint c. In order to choose appropriate values for the proliferation rate ρ, we relate it to the tumor doubling time τ_d. Since τ_d represents the time it takes for the tumor to double in size, we set $\exp(\rho t) = 2^{t/\tau_d}$, resulting in the following relation:

$$\rho = \frac{\ln(2)}{\tau_d}.$$

For human tumors, the doubling time can range from a few days to a few months, depending on the particular disease site. We show that for the parameters used above, the optimal number of treatment days is smaller for faster growing tumors (Figure 4-4).

The objective value plotted in Figure 4-4 is given by

$$\text{BED}_T - \frac{1}{\alpha_T}(N-1)\rho.$$

For the reference treatment ($N = 30$) and $\alpha = 0.3$, the decrease in the tumor BED due to the second term $(N-1)\rho/\alpha_T$ evaluates to about 1.3 Gy for a slowly proliferating tumor with doubling time $\tau_d = 50$. This is small compared to $\text{BED}_T = 72$. For a fast proliferating tumor with doubling time $\tau_d = 5$, the correction $(N-1)\rho/\alpha_T$ is about 13.4 Gy and becomes more important. Thus, smaller values of N are suggested for faster proliferating tumors.

4.5.2 Accelerated repopulation suggests increasing doses towards the end of treatment

One way to model accelerating repopulation is to use decelerating tumor growth curves (see Figure 4-3). We model this behavior by using the Gompertz tumor growth model and solve the fractionation problem by using the simplified DP equation (4.13). We illustrate optimal fractionation schemes for both slow and fast proliferating tumors. For a slow proliferating tumor, we choose the parameters $X_0 = 8.3\times10^6$, $X_\infty = 3\times10^{12}$, and $b = \exp(-6.8)$ so that the doubling time corresponding to the instantaneous growth rate $\phi(x)$ starts at 50 days in the beginning of treatment and decreases to 20 days at the end of treatment. For a fast proliferating tumor, we adjust the parameters accordingly so that the doubling time goes from 50 days to 5 days: $X_0 = 3.6 \times 10^{11}$, $X_\infty = 3 \times 10^{12}$, and $b = \exp(-5)$. As before, we use the parameters $[\alpha/\beta]_T = 10$ Gy, $[\alpha/\beta]_O = 3$ Gy, $\alpha_T = 0.3$ Gy^{-1}, $c = 61.6$ Gy, and $\gamma = 0.7$. As shown in Figure 4-5, for a fast proliferating tumor, the sequence of radiation doses increase from 1 Gy to 3 Gy, which is a significant difference from the standard treatment of 2 Gy per day for 30 days. For a slowly proliferating tumor, the doses closely resemble standard treatment and only increase slightly over the course of treatment. Note that the dose

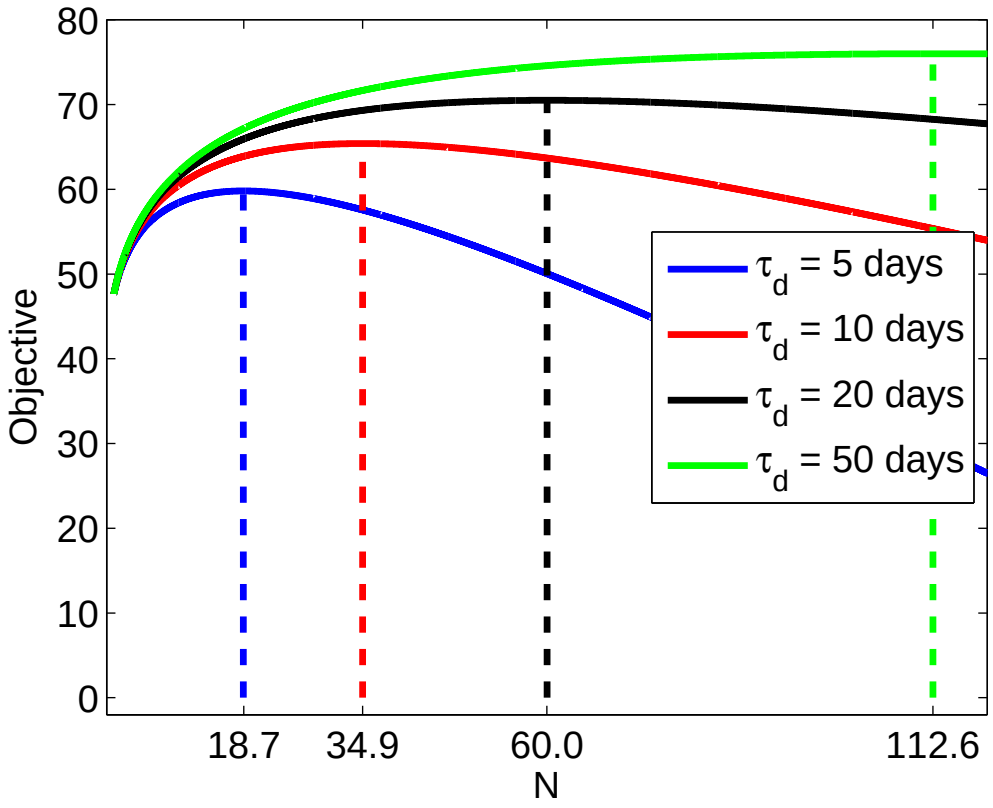

Figure 4-4: Optimal number of fractions assuming exponential tumor growth. The optimal number of treatment days is smaller for faster growing tumors. The expression in Theorem 4.4.4 was used to generate this plot. In order to obtain the actual optimum N, the objective must be evaluated at the floor and ceil of the continuous optimum N plotted above.

per day is almost exactly proportional to the plotted instantaneous proliferation rate $\phi(x)$. In summary, we find that the optimal fractionation scheme distributes the doses so that they are proportional to the instantaneous proliferation rate. For the reference treatment of 2 per day with $N = 30$, in the case of a fast proliferating tumor, the objective Y_{N-1}^{+} is 24.25. The objective Y_{N-1}^{+} for the optimal fractionation scheme in plot b) of Figure 4-5 is 23.64. This is only a change of 2.5% in Y_{N-1}^{+} and about 16.7% change in X_{N-1}^{+} in comparison to the reference treatment. It is not straightforward to make a meaningful statement about the improvement in tumor control simply based on these values. However, we can say that even a small improvement in tumor control for a specific disease site can make a significant impact because of the large of patients treated with radiation therapy every year.

4.5.3 Smaller α-β ratio of tumor results in larger changes in fraction size and more gain

We use a smaller value for the α-β ratio of tumor and re-run the calculations from the previous subsection. The parameters of the Gompertzian growth remain the same for the slow and fast proliferating tumor. As before, we use the parameters $[\alpha/\beta]_O = 3$ Gy, $\alpha_T = 0.3$ Gy^{-1}, $c = 61.6$ Gy, and $\gamma = 0.7$, with the only change being $[\alpha/\beta]_T = 5.7$ Gy. Note that the condition $[\alpha/\beta]_O = 3 < \gamma[\alpha/\beta]_T = 4$ is satisfied, meaning that delivering only a single dose of radiation is not optimal (see Theorem 4.4.3). As seen in Figure 4-6, we find that for a fast proliferating tumor, the sequence of radiation doses increase all the way to 5 Gy, which is an even more significant difference from the results in the previous section. Indeed, in this case, the objective Y_{N-1}^{+} is 16.00 for the reference treatment of 2 Gy per day, and is 14.01 for the optimal fractionation scheme in plot b) of Figure 4-6. This is a significant change of 12.4% in Y_{N-1}^{+} and about 44.5% change in X_{N-1}^{+} in comparison to the reference treatment. Due to the change in the optimal fractionation scheme, the rates of tumor growth have also changed. However, these tumor growth rate changes have not been significant: the tumor doubling time

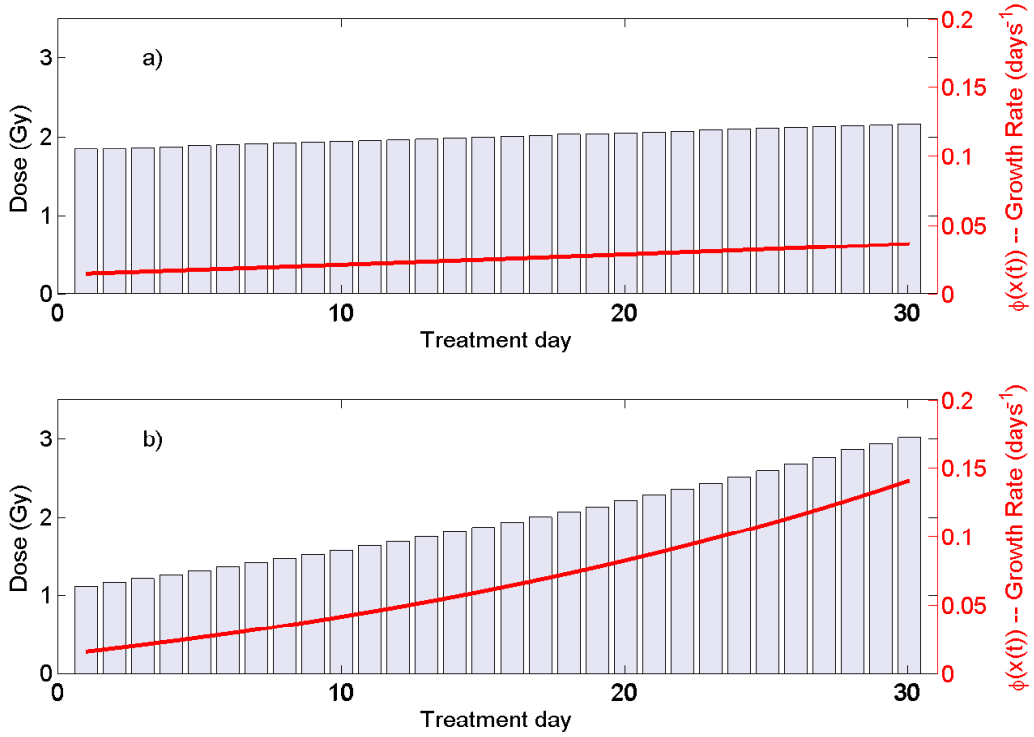

Figure 4-5: Optimal fractionation for accelerated repopulation. Plot a) is an example of a slow proliferating tumor, and plot b) is an example of a fast one. The doubling time for the proliferation rate $\phi(x)$ begins at $\tau_d = 50$ days and decreases to a) 20 and b) 5 days, respectively, at the end of treatment. Larger dose fractions are suggested later in the treatment to compensate for the increased tumor proliferation.

at the end of treatment is about 18 days for the slowly proliferating tumor and 4 days for the fast one. The exponential increase of the optimal fractions observed plot b) of Figure 4-6 is likely due to the assumed Gompertzian tumor growth characteristic. The take away message should not be that the dose increases have an exponential nature, but rather that the fractions are proportional to the instantaneous proliferation rate. Should it be that the proliferation rate increases linearly, the result would likely be linearly increasing dose fractions. We can infer that a smaller α-β ratio of the tumor suggests using larger changes in fraction size; this results in larger gains in the objective value and hence in overall tumor control. Low values of the α-β ratio have been observed for disease sites such as prostate cancer [51]. Of course, if the α-β ratio is very small, a single dose would be optimal (see Theorem 4.4.3).

4.6 Further remarks

4.6.1 Non-uniform irradiation of the OAR

Although we assumed throughout the chapter that a dose d results in a homogeneous dose γd to the OAR, in reality the OAR receives a non-uniform irradiation. In [78], the basic result stated in Theorem 4.3.2 is generalized to arbitrary inhomogeneous doses in the OAR. The arguments in [78] are also applicable to the case of repopulation as considered here. In this case, we can define an effective sparing factor γ_{eff} and an effective upper limit c_{eff} on the BED_O. The results differ for the case of parallel OAR and serial OAR. A parallel organ could remain functional even with damaged parts; a serial OAR on the other hand remains functional only when all of its parts remain functional. For the case of a parallel OAR (e.g., lung), assuming $\gamma_i d$ represents the dose in the ith voxel (or spatial point) in the OAR, the integral BED in the OAR is given by

$$\text{BED}_O = \sum_{k=0}^{N-1} \sum_i \gamma_i \, d_k \left(1 + \frac{\gamma_i \, d_k}{[\alpha/\beta]_O}\right).$$

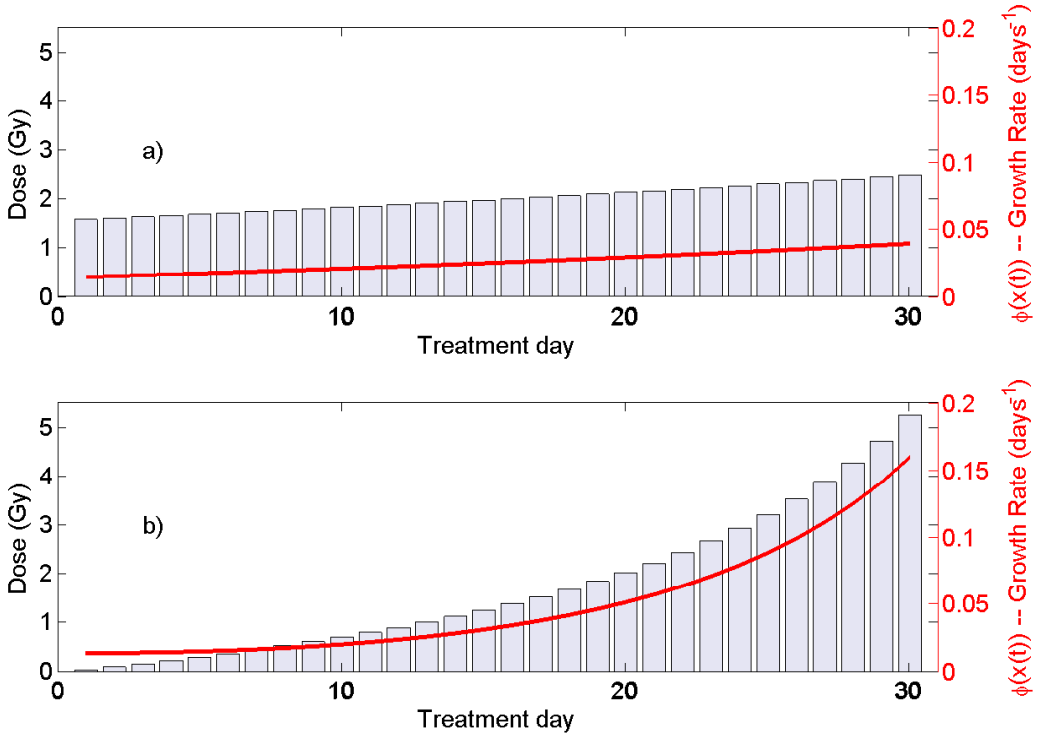

Figure 4-6: Optimal fractionation for accelerated repopulation in the case of $[\alpha/\beta]_T = 5.7$ Gy. Plot a) is an example of a slowly proliferating tumor, and plot b) is an example of a fast one. The doubling time for the proliferation rate $\phi(x)$ begins at $\tau_d = 50$ days and decreases to a) 18 and b) 4 days, respectively, at the end of treatment. Smaller $[\alpha/\beta]_T$ values result in larger changes in fraction size and more gain.

By algebraic manipulations, we obtain the same form for the normal tissue constraint as discussed in this chapter:

$$\sum_{k=0}^{N-1} \gamma_{\text{eff}}\, d_k \left(1 + \frac{\gamma_{\text{eff}}\, d_k}{[\alpha/\beta]_O}\right) = c_{\text{eff}},$$

where $\gamma_{\text{eff}} = \sum_i \gamma_i^2 / \sum_i \gamma_i$ and $c_{\text{eff}} = c\gamma_{\text{eff}} / \sum_i \gamma_i$. For the serial case (e.g., spinal cord), only the maximum dose to the OAR matters, resulting in $\gamma_{\text{eff}} = \max_i \gamma_i$ and $c_{\text{eff}} = c$. Further details can be found in [78].

4.6.2 Variable time intervals

The above methodology is applicable also for the case of variable time intervals (e.g., weekends, holidays). However, in our formulation we neglect the Lea-Catcheside factor, i.e., we assume that each radiation treatment is delivered in a short time period, and time between fractions is long. Without these assumptions, the survival fraction will have to take into account biological aspects such as incomplete sublethal damage. The LQ model used in our formulation does not take such factors into account. For optimal fractionation schemes resulting from incorporating incomplete sublethal damage repair, see [5].

4.6.3 Multiple OARs

When optimizing the spatial dose distribution, radiation treatments generally involves making tradeoffs in dose delivered to multiple OARs. In this work, we assume that the spatial dose distribution is fixed, and that the fractionation schedule is temporally optimized. Even with multiple OARs, a single OAR will be dose-limiting, which primarily determines the optimal fractionation schedule. Thus, this OAR can be used for the BED_O constraint discussed in this chapter.

4.7 Discussion and conclusions

There are multiple ways to model accelerated repopulation. One approach is to increase the tumor proliferation rate with already delivered dose or BED. In this chapter, we chose to model accelerated repopulation implicitly by using a decelerating tumor growth curve, e.g., Gompertzian growth, with a proliferation rate $\phi(x)$ that is dependent on the number of tumor cells. Due to radiation treatment, fewer cells remain towards the end of treatment resulting in faster tumor growth. We developed a DP framework to solve the optimal fractionation problem with repopulation for general tumor growth characteristics described by $\phi(x)$. More research is needed to determine $\phi(x)$ from clinical outcome data for a specific disease site. We derived the special structure of the problem when assuming Gompertzian tumor growth. This resulted in maximizing a discounted version of BED_T, which placed a higher weight for later treatment days due to increased tumor proliferation.

There are three main messages in this chapter. First, faster tumor growth suggests shorter overall treatment duration. Second, accelerated repopulation suggests larger dose fractions later in the treatment to compensate for the increased tumor proliferation. And, finally, the optimal fractionation scheme uses more aggressive changes in the dose fractions when the α-β ratio of the tumor is smaller; in this case, we can expect larger gains in tumor control.

The advantage of the methods presented in this chapter is that a change in the fractionation schedule can be readily implementable in a clinical setting, without technological barriers. However, the results presented in this chapter are for illustrative purposes and should not be taken as immediate recommendations for a change in clinical practice. We realize that actual tumor dynamics are more complex than presented in this chapter. Yet, we hope that this analysis can provide useful insights and a basis for further research.

4.8 Appendix: proofs

4.8.1 Proof of Lemma 4.3.1

Proof. Suppose an optimal solution is d_i^*, for $i = 0, 1, \ldots, N-1$, but the constraint in (4.3) is not active. That is, there exists $\delta > 0$ such that

$$\sum_{k=0}^{N-1} \gamma d_k^* \left(1 + \frac{\gamma d_k^*}{[\alpha/\beta]_O}\right) + \delta = c.$$

For every fraction i, let us increase d_i^* by the same positive constant ϵ. Choosing ϵ small enough so that $\sum_{k=0}^{N-1} \gamma\epsilon \left(1 + \frac{\gamma}{[\alpha/\beta]_O}(2d_k^* + \epsilon)\right) < \delta$, we see that

$$\begin{aligned}
\sum_{k=0}^{N-1} \gamma(d_k^* + \epsilon)\left(1 + \frac{\gamma(d_k^* + \epsilon)}{[\alpha/\beta]_O}\right) &= \sum_{k=0}^{N-1} \gamma d_k^* \left(1 + \frac{\gamma d_k^*}{[\alpha/\beta]_O}\right) + \sum_{k=0}^{N-1} \gamma\epsilon \left(1 + \frac{\gamma}{[\alpha/\beta]_O}(2d_k^* + \epsilon)\right) \\
&< \sum_{k=0}^{N-1} \gamma d_k^* \left(1 + \frac{\gamma d_k^*}{[\alpha/\beta]_O}\right) + \delta \\
&= c,
\end{aligned}$$

which means that the constraint in (4.3) is satisfied. Furthermore, choosing $d_i^* + \epsilon$, for $i = 0, 1, \ldots, N-1$, results in a strictly larger objective value than that of the supposed optimal solution. This is a contradiction because we have found a strictly better solution than the assumed optimal one. □

4.8.2 Proof of Theorem 4.3.2

Proof. Using the equality constraint in (4.4), we can equivalently write the objective BED_T as

$$\text{BED}_T = \left(1 - \frac{[\alpha/\beta]_O}{\gamma[\alpha/\beta]_T}\right) \sum_{k=0}^{N-1} d_k + \frac{[\alpha/\beta]_O}{\gamma[\alpha/\beta]_T} c.$$

Thus, if $[\alpha/\beta]_O \geq \gamma[\alpha/\beta]_T$, we would like to minimize $\sum_{k=0}^{N-1} d_k$ subject to a fixed BED_O. Otherwise, if $[\alpha/\beta]_O < \gamma[\alpha/\beta]_T$, we would like to maximize $\sum_{k=0}^{N-1} d_k$. First,

let us assume the former condition $[\alpha/\beta]_O \geq \gamma[\alpha/\beta]_T$ to be true. Suppose an optimal solution is to deliver a non-zero dose in more than one fraction, i.e., that there exists i and j with $i \neq j$ such that $d_i^* > 0$ and $d_j^* > 0$. We would like to show that, leaving d_k unchanged for $k \neq i, j$, a better solution is to set d_i equal to 0 and d_j equal to the dose that would satisfy the constraint in (4.4). Essentially, this would mean that there is no reason to "spread out" the dose among the fractions; it would be optimal to deliver all the dose in a single fraction. We now set $d_i = 0$ and $d_j = d_j^* + \delta$, where δ is positive constant appropriately chosen so that the constraint in (4.4) is satisfied. Writing out the constraint equation and carrying out algebra, we find

$$\begin{aligned}\sum_{k=0}^{N-1} \gamma d_k \left(1 + \frac{\gamma d_k}{[\alpha/\beta]_O}\right) &= \sum_{\substack{k\neq i \\ k\neq j}} \gamma d_k^* \left(1 + \frac{\gamma d_k^*}{[\alpha/\beta]_O}\right) + \gamma(d_j^* + \delta)\left(1 + \frac{\gamma(d_j^* + \delta)}{[\alpha/\beta]_O}\right) \\ &= c + f_1(d_i^*, d_j^*, \delta),\end{aligned}$$

where for the last equality we used the fact that the assumed optimal solution satisfies the constraint in (4.4). The function f_1 is defined as

$$f_1(d_i^*, d_j^*, \delta) = \gamma\delta\left(1 + \frac{\gamma\delta}{[\alpha/\beta]_O}\right) - \gamma d_i^*\left(1 + \frac{\gamma d_i^*}{[\alpha/\beta]_O}\right) + \frac{2\gamma^2\delta d_j^*}{[\alpha/\beta]_O}. \tag{4.15}$$

Thus, we can choose $\delta > 0$ that satisfies $f(d_i^*, d_j^*, \delta) = 0$ to ensure the constraint in (4.4). Since the third term in (4.15) is positive, such a choice of δ will result in $\delta < d_i^*$. However, this means that we have found a strictly better solution because

$$\sum_{k=0}^{N-1} d_k = \sum_{k\neq i} d_k^* + \delta < \sum_{k=0}^{N-1} d_k^*,$$

resulting in a contradiction of the optimality assumption. Therefore, for $[\alpha/\beta]_O \geq \gamma[\alpha/\beta]_T$, an optimal solution has exactly one non-zero dose. The closed-form solution, as given in (4.5), can be obtained by solving the quadratic equality constraint $\gamma d_j \left(1 + \frac{\gamma d_j}{[\alpha/\beta]_O}\right) = c$.

Now, assume that $[\alpha/\beta]_O < \gamma[\alpha/\beta]_T$, and suppose that there exists i and j with $i \neq j$ such that $d_i^* \neq d_j^*$, with both d_i^* and d_j^* non-zero. We would like to show that, leaving unchanged dose fractions at times other than i or j, a better solution is to deliver equal dose in fractions i and j, scaled appropriately so that the constraint in (4.4) is satisfied. Essentially, this would mean that the optimal solution "spreads out" the dose uniformly amongst all fractions. Hence, we set $d_i = d_j = \delta(d_i^* + d_j^*)/2$, with an appropriately chosen positive constant δ. Writing out the constraint equation and carrying out the algebra, we find

$$\begin{aligned}\sum_{k=0}^{N-1} \gamma d_k \left(1 + \frac{\gamma d_k}{[\alpha/\beta]_O}\right) &= \sum_{k\neq i,j} \gamma d_k^* \left(1 + \frac{\gamma d_k^*}{[\alpha/\beta]_O}\right) + 2\gamma\delta \frac{d_i^* + d_j^*}{2} \left(1 + \frac{\gamma\delta}{[\alpha/\beta]_O} \frac{d_i^* + d_j^*}{2}\right) \\ &= \sum_{k\neq i,j} \gamma d_k^* \left(1 + \frac{\gamma d_k^*}{[\alpha/\beta]_O}\right) + f_2(d_i^*, d_j^*, \delta), \end{aligned} \tag{4.16}$$

where

$$f_2(d_i^*, d_j^*, \delta) = \delta\gamma d_i^* \left(1 + \frac{\delta\gamma d_i^*}{[\alpha/\beta]_O}\right) + \delta\gamma d_j^* \left(1 + \frac{\delta\gamma d_j^*}{[\alpha/\beta]_O}\right) - \frac{(\gamma\delta)^2}{2[\alpha/\beta]_O}(d_i^* - d_j^*)^2.$$

Note that if we choose $\delta = 1$, Equation (4.16) would simplify to c minus the third term in the definition of the function f_2. Clearly, in order to ensure that the expression in (4.16) equals c and thus satisfies the BED_O equality constraint, $\delta > 1$ must be true. However, this means that we have found a strictly better solution because

$$\sum_{k=0}^{N-1} d_k = \sum_{\substack{k\neq i \\ k\neq j}} d_k^* + \delta(d_i^* + d_j^*) > \sum_{k=1}^{N} d_k^*,$$

resulting in a contradiction of the optimality assumption. Therefore, for $[\alpha/\beta]_O < \gamma[\alpha/\beta]_T$, the unique optimal solution consists of uniform doses. The closed-form solution, as given in (4.6), can be obtained by solving the quadratic equality constraint $\gamma N d_j \left(1 + \frac{\gamma d_j}{[\alpha/\beta]_O}\right) = c$. □

4.8.3 Proof of Lemma 4.4.1

Proof. We use a similar argument to the one given in Lemma 4.3.1. Let us suppose an optimal solution is d_i^*, for $i = 0, 1, \ldots, N-1$, under which the BED_O constraint is not active. Let $\{\widetilde{Y}_i^+\}$ be the result of delivering the optimal doses. Again, choose the positive constants δ and ϵ in the same way as in Lemma 4.3.1. Then, for every i, we are able to deliver $d_i = d_i^* + \epsilon$ while ensuring the BED_O constraint is satisfied. Let $\{Y_i^+\}$ now be the result of delivering the d_i, for $i = 0, 1, \ldots, N-1$. We will show by induction that $Y_i^+ < \widetilde{Y}_i^+$ for every i. For the base case, we have

$$Y_0^+ = Y_0 - \text{BED}_T(d_0) < \widetilde{Y}_0^+$$

because $d_0 > d_0^*$. Suppose for the inductive step that $Y_i^+ < \widetilde{Y}_i^+$. Then, we have

$$\begin{aligned} Y_{i+1}^+ &= F(Y_i^+) - \text{BED}_T(d_{i+1}) \\ &< F(\widetilde{Y}_i^+) - \text{BED}_T(d_{i+1}) \\ &= \widetilde{Y}_{i+1}^+, \end{aligned}$$

where the inequality holds because the growth function F is strictly increasing as a result of the $\phi(x) > 0$ assumption. The induction is complete, and we have shown that $Y_{N-1}^+ < \widetilde{Y}_{N-1}^+$. This is a contradiction of the optimality assumption. □

4.8.4 Proof of Lemma 4.4.2

Proof. Since $\phi(x) > 0$ for all x, the rate of change of the number of tumor cells is positive. Thus, assuming no delivered radiation, the number of cells is strictly increasing due to repopulation. Now, given $Y_i^+ < \widetilde{Y}_i^+$, it is clear that $Y_{i+1}^- < \widetilde{Y}_{i+1}^-$. And after applying radiation, we also have $Y_{i+1}^+ < \widetilde{Y}_{i+1}^+$. The lemma follows by induction. □

4.8.5 Proof of Theorem 4.4.3

Proof. Suppose that an optimal solution to the fractionation problem with repopulation is the sequence of doses $d_0^*, d_1^*, \ldots, d_{N-1}^*$, resulting in the sequence $\widetilde{Y}_0^+, \widetilde{Y}_1^+, \ldots, \widetilde{Y}_{N-1}^+$. We assume here that $d_i^* > 0$ and $d_j^* > 0$ for some i and j such that $i < j$. Consider another sequence $d_0, d_1, \ldots, d_{N-1}$ that satisfies $d_k = d_k^*$ for $k \neq i$ and $k \neq j$, which results in the sequence $Y_0^+, Y_1^+, \ldots, Y_{N-1}^+$. We will first show that if $Y_i^+ > \widetilde{Y}_i^+$ (or, equivalently, $d_i > d_i^*$), then $Y_j^+ \leq \widetilde{Y}_j^+ + \mathrm{BED}_T^* - \mathrm{BED}_T$, where BED_T^* and BED_T are the total BED in the tumor resulting from delivering $\{d_k^*\}$ and $\{d_k\}$, respectively. Before delivering the dose d_i, the same sequences of doses were applied; this means $Y_i^- = \widetilde{Y}_i^-$. Now, $Y_i^+ = Y_i^- - \mathrm{BED}_T(d_i)$ and $\widetilde{Y}_i^+ = \widetilde{Y}_i^- - \mathrm{BED}_T(d_i^*)$, implying that $Y_i^+ - \widetilde{Y}_i^+ = \mathrm{BED}_T(d_i^*) - \mathrm{BED}_T(d_i)$. Since $\phi(x)$ is non-increasing as a function of x, we have that

$$Y_j^- - \widetilde{Y}_j^- \leq \mathrm{BED}_T(d_i^*) - \mathrm{BED}_T(d_i). \tag{4.17}$$

Note that $\mathrm{BED}(d_i^*) > \mathrm{BED}(d_i)$ because of the initial condition $Y_i^+ > \widetilde{Y}_i^+$. Then, we have

$$\begin{aligned}
Y_j^+ &= Y_j^- - \mathrm{BED}_T(d_j) \\
&= Y_j^- - \mathrm{BED}_T(d_j) + \widetilde{Y}_j^+ - (\widetilde{Y}_j^- - \mathrm{BED}_T(d_j^*)) \\
&= \widetilde{Y}_j^+ + (Y_j^- - \widetilde{Y}_j^-) + \mathrm{BED}_T(d_j^*) - \mathrm{BED}_T(d_j) \\
&\leq \widetilde{Y}_j^+ + \mathrm{BED}_T(d_i^*) - \mathrm{BED}_T(d_i) + \mathrm{BED}_T(d_j^*) - \mathrm{BED}(d_j) \\
&= \widetilde{Y}_j^+ + \mathrm{BED}_T^* - \mathrm{BED}_T,
\end{aligned} \tag{4.18}$$

where the inequality is due to (4.17).

Suppose that $[\alpha/\beta]_O \geq \gamma[\alpha/\beta]_T$ and that there exists $i < j$ such that $d_i^* > 0$ and $d_j^* > 0$. We set $d_i = 0$ and $d_j = d_j^* + \delta$, where δ is a positive constant that enforces the BED equality constraint for the OAR. Then, we find, as done using exactly the same argument in the proof of Theorem 4.3.2, that $\mathrm{BED}_T^* < \mathrm{BED}_T$. Since $d_i = 0$ and $d_i^* > 0$ imply that $Y_i^+ > \widetilde{Y}_i^+$, we have from (4.18) that $Y_j^+ < \widetilde{Y}_j^+$. Using Lemma 4.4.2, we

conclude that $Y_{N-1}^{+} < \widetilde{Y}_{N-1}^{+}$, so that we have found a strictly better solution than the supposed optimal one. Thus, if $[\alpha/\beta]_O \geq \gamma[\alpha/\beta]_T$, the optimal solution is to deliver a single dose, as in Theorem 4.3.2.

Suppose $[\alpha/\beta]_O < \gamma[\alpha/\beta]_T$ and $\exists i < j$ such that $d_i^* > d_j^*$. Setting $d_i = d_j = \delta\left(\frac{d_i^*+d_j^*}{2}\right)$ so that δ ensures the BED constraint in the OAR. Again, we use the same argument in Theorem 4.3.2 and conclude that $\text{BED}_T^* < \text{BED}_T$. Since $d_i < d_i^*$, we have $Y_i^{+} > \widetilde{Y}_i^{+}$. From (4.18), we conclude $Y_j^{+} < \widetilde{Y}_j^{+}$. This means that $Y_{N-1}^{+} < \widetilde{Y}_{N-1}^{+}$ due to Lemma 4.4.2. Thus, we have found a strictly better solution than the supposed optimal one. For $[\alpha/\beta]_O < \gamma[\alpha/\beta]_T$ then, the optimal doses must increase over the course of treatment, i.e., $d_0^* \leq d_1^* \leq \ldots \leq d_{N-1}^*$. □

4.8.6 Proof of Theorem 4.4.4

Proof. We want to solve the optimization problem

$$\underset{N\in\mathbb{N}}{\text{maximize}} \quad \sum_{k=0}^{N-1} d_k^*\left(1+\frac{d_k^*}{[\alpha/\beta]_T}\right) - \frac{1}{\alpha_T}(N-1)\rho, \tag{4.19}$$

where d_k^* for $k = 0, 1, \ldots, N-1$ is an optimal solution to (4.4). If $[\alpha/\beta]_O \geq \gamma[\alpha/\beta]_T$, from Theorem 4.3.2, it is optimal to deliver a single dose on one day. Thus, the first term in (4.19) is independent of N, and maximizing the second term results in $N^* = 1$. For the case when $[\alpha/\beta]_O < \gamma[\alpha/\beta]_T$, we first show that the objective in (4.19) is strictly concave and eventually decreases as a function of N. Using the expression for d_j^* given in Theorem 4.3.2 and carrying out basic algebra, we find that the first term in (4.19) representing the BED in the tumor satisfies

$$\begin{aligned}\text{BED}_T &= \sum_{k=0}^{N-1} d_k^*\left(1+\frac{d_k^*}{[\alpha/\beta]_T}\right)\frac{B}{\alpha_T} \\ &= \sqrt{N^2+2AN} - \frac{B}{\alpha_T}N + E,\end{aligned}$$

where $A = \frac{2c_2}{[\alpha/\beta]_O}$, $B = \frac{\alpha_T[\alpha/\beta]_O}{2\gamma}\left(1 - \frac{[\alpha/\beta]_O}{\gamma[\alpha/\beta]_T}\right)$, and $E = \frac{[\alpha/\beta]_O c_2}{\gamma^2[\alpha/\beta]_T}$. We want to show that the objective (4.19) is concave in N for any $N \in [0, \infty)$. The domain $[0, \infty)$ is convex as desired. Now, we compute the first and second derivative with respect to N of this objective. After some algebra, we obtain the equations

$$\frac{\mathrm{d}}{\mathrm{d}N}\left[\mathrm{BED}_T - \frac{1}{\alpha_T}(N-1)\rho\right] = \frac{B}{\alpha_T}\left(\frac{N+A}{\sqrt{(N+A)^2 - A^2}} - 1\right) - \frac{\rho}{\alpha_T} \tag{4.20}$$

and

$$\frac{\mathrm{d}^2}{\mathrm{d}^2N}\left[\mathrm{BED}_T - \frac{1}{\alpha_T}(N-1)\rho\right] = -\frac{A^2B}{\alpha_T\left(N^2 + 2AN\right)^{3/2}}.$$

Note that $A > 0$, and since $[\alpha/\beta]_O < \gamma[\alpha/\beta]_T$, $B > 0$ is also true. Thus, the second derivative above is strictly negative for all $N \in [0, \infty)$; this implies that the objective is strictly concave. As N grows large, the first term in (4.20) approaches 0. Hence, the first derivative eventually becomes strictly negative due to the repopulation term, which means that the objective is a decreasing function for large enough N. Maximizing a strictly concave function that eventually decreases results in a unique optimum over the interval $[0, \infty)$. Now, we set the derivative (4.20) equal to 0 and solve for N. The result is

$$N_c = A\left(\sqrt{\frac{(\rho+B)^2}{\rho\,(\rho+2B)}} - 1\right).$$

Due to the concavity property of the objective, the additional constraint that N is a natural number means that the optimum N^* is either $\lfloor N_c \rfloor$ or $\lceil N_c \rceil$, whichever results in a larger objective value. The only exception is when $N_c < 1$, in which case $N^* = 1$ since N^* cannot be 0. □

4.8.7 Proof of Theorem 4.4.5

Proof. When $[\alpha/\beta]_O \geq \gamma[\alpha/\beta]_T$, we already know from Theorem 4.4.3 that $N^* = 1$ and thus the optimal number of fractions is finite. We now give the proof for the case when $[\alpha/\beta]_O < \gamma[\alpha/\beta]_T$. For a fixed N, we assume $d_0^*, d_1^*, \ldots, d_{N-1}^*$ is the sequence of

optimal dose fractions resulting from minimizing the logarithm version of the expected number of cells Y^*_{N-1} subject to the BED constraint in the OAR. From the equation $\mathrm{d}y/\mathrm{d}t = \phi(\exp(\alpha_T y(t)))/\alpha_T$, the assumption $\phi(x) > r$ implies $\mathrm{d}y/\mathrm{d}t > r'/\alpha_T$ for some other constant $r' > 0$. The function mapping Y^+ to Y^- as a result of repopulation satisfies

$$F(Y^+) > Y^+ + \frac{r'}{\alpha_T}.$$

Now, since F is applied $N-1$ times, we can bound below Y^+_{N-1}:

$$Y^+_{N-1} > -\mathrm{BED}^*_T + \frac{1}{\alpha_T}(N-1)r'$$

where BED^*_T is the BED in the tumor resulting from delivering the doses $d^*_0, d^*_1, \ldots, d^*_{N-1}$. From Theorem 4.3.2, we know that when $[\alpha/\beta]_O < \gamma[\alpha/\beta]_T$, uniformly distributed doses maximize BED_T subject to the constraint on BED_O. Let $\widetilde{\mathrm{BED}_T}$ represent the BED in the tumor resulting from delivering these uniformly distributed doses. Then, $\mathrm{BED}^*_T \leq \widetilde{\mathrm{BED}_T}$ and we have

$$Y^+_{N-1} > -\mathrm{BED}^*_T + \frac{1}{\alpha_T}(N-1)r' \geq -\widetilde{\mathrm{BED}_T} + \frac{1}{\alpha_T}(N-1)r'.$$

Using equation (4.20) from the proof of Theorem 4.4.4, we have

$$\frac{\mathrm{d}}{\mathrm{d}N}\left[-\widetilde{\mathrm{BED}_T} + \frac{1}{\alpha_T}(N-1)r'\right] = -\frac{B}{\alpha_T}\left(\frac{N+A}{\sqrt{(N+A)^2 - A^2}} - 1\right) + \frac{r'}{\alpha_T}.$$

Since the first derivative above eventually stays positive for large enough N, Y^+_{N-1} approaches infinity as $N \to \infty$. Thus, the optimal number of dose fractions N^* cannot be infinite. □

Chapter 5

Optimal fractionation for continuous dose rate treatment protocols

5.1 Introduction

We analyzed in the previous chapter the optimal fractionation scheme in the presence of tumor repopulation. However, the model used was reasonable only for conventional external beam radiation therapy, where there is plenty of time in between fractions. Incomplete repair of sublethal damage in cells becomes an important factor for treatment modalities such as brachytherapy, where a continuous dose is emitted from implanted seeds in the patient. In this chapter, we model this repair effect in addition to tumor repopulation and generalize the methods in the previous chapter to the case where a continuous dose rate $d(t)$ is delivered instead of individual dose fractions. It may be difficult for the reader to follow the arguments in this chapter without familiarity of the model, formulation, and results from Chapter 4.

As before, we would like to minimize the expected number of tumor cells at the end of treatment such that the BED in the OAR is constrained by an upper limit. The only

difference is that incomplete sublethal damage repair needs to be taken into account due to the continuous nature of the radiation dose. In this chapter, we derive an ordinary differential equation describing the behavior of the number of tumor cells at any point during treatment. This equation incorporates the effect of tumor growth, incomplete sublethal damage repair, and radiation dose. Although the same differential equation and a similar formulation is presented in [87], we hope that the derivation in this chapter is insightful and sheds new perspective. The model and formulation can be the basis for further research, e.g., determining the effect of accelerated tumor repopulation for modalities such as brachytherapy. In a related paper [5], the effect of exponential tumor repopulation and sublethal damage repair on optimal fractionation is analyzed for the case of discrete radiation dose fractions. However, our main focus in this chapter is on continuous dose rate treatment protocols and on general tumor growth characteristics.

In Section 5.2, we describe the model and formulation, including extensions of the tumor dynamics and BED model in the continuous case. In Section 5.3, we show that the presented continuous model is consistent with the discrete-time version in the previous chapter. In Section 5.4, we summarize and discuss possibilities for future research.

5.2 Model and formulation

In this section, we discuss the model and formulation for a continuous dose rate treatment protocol. First, we describe an LQ model that includes sublethal damage repair. Next, we develop a single differential equation that models the tumor dynamics. Then, we extend the BED model to the continuous case; we use this extended BED model to assert a constraint on the BED in the OAR. Finally, we summarize the problem formulation of minimizing the expected number of tumor cells at the end of treatment subject to an upper limit on the BED in the OAR.

5.2.1 LQ model with incomplete sublethal damage repair

We define T to be the total treatment time (analogous to the number of dose fractions N in the previous chapter). Assuming that the dose rate $d(t)$ is delivered over the time interval $[0, T]$, it is tempting to describe the cell survival fraction with the equation

$$S = \exp\left(-\int_0^T (\alpha d(t) + \beta d^2(t))\,\mathrm{d}t\right). \tag{5.1}$$

However, this equation does not make sense for radiation dose delivered over very small intervals of time. For example, suppose that a total dose d is uniformly delivered over an interval of length δ_1 or, alternatively, of length δ_2. If $0 < \delta_1 < \delta_2$, the above equation (5.1) would suggest that the survival fraction is smaller when dose is delivered over the interval of length δ_1. Assuming both δ_1 and δ_2 are very small intervals of time, this does not make intuitive sense. This apparent difficulty can be overcome by using a more general version of the LQ model that includes incomplete sublethal damage repair.

Incomplete repair can be incorporated into the LQ model by introducing the dose protraction factor G as done in [8, 67]. The surviving fraction including incomplete repair of sublethal damage is given by

$$S = \exp(-(\alpha D + G\beta D^2)), \tag{5.2}$$

where $D = \int_0^T d(t)\mathrm{d}t$ and

$$\begin{aligned} G &= \frac{2}{D^2}\int_0^T \int_0^T d(t)d(\tau)K(t,\tau)\,\mathrm{d}\tau\,\mathrm{d}t \\ &= \frac{2}{D^2}\int_0^T d(t)e(t)\,\mathrm{d}t, \end{aligned}$$

where

$$e(t) = \int_0^T d(\tau)K(t,\tau)\,\mathrm{d}\tau \tag{5.3}$$

and $K(t,\tau)$ is a suitable kernel function. We assume that the sublethal damage decays

exponentially, i.e., that the kernel $K(t,\tau)$ takes the form

$$K(t,\tau) = u(t-\tau)\exp(-(t-\tau)/\tau_r),$$

where $u(\cdot)$ is the unit step function and τ_r is the tissue repair time for sublethal damage.

Now, for very small values of the repair time τ_r, changes in the dose rate $d(t)$ over small instants of time can make a big difference in the survival fraction. Indeed, as $\tau_r \to 0$, it can be seen that the survival fraction is described by Equation (5.1). In our initial discussion, we provided an example of how dose variations over a small time interval can result in a large effect on the survival fraction. A large τ_r, on the other hand, results in little effect for these dose variations. Thus, based on the repair time parameter τ_r, this model allows the choice of the right tradeoff for the particular cell tissue under consideration.

5.2.2 Tumor dynamics

In this subsection, we derive a differential equation that describes the dynamics of the number of tumor cells $x(t)$ over the time interval $[0,T]$, where T is the total treatment time. It includes general tumor growth characteristics and incomplete sublethal damage repair due to continuous radiation dose administered. Assume that the dose rate $d(t)$ is delivered over the time interval $[0,T]$. Let $\phi(x(t))$ be the instantaneous tumor proliferation rate. Given $x(t)$, we will derive the resulting number of cells after a very small unit of time $\delta > 0$. This will lead us to the differential equation representation of the tumor dynamics.

Based on Equation (5.2), the survival fraction in the time interval $[t, t+\delta]$ will be

$$\exp\left(-\int_t^{t+\delta} (\alpha_T d(t) + 2\beta_T d(t) e(t))\,\mathrm{d}t\right) = \exp\left(-\alpha_T \int_t^{t+\delta} d(t)\left(1 + \frac{2e_T(t)}{[\alpha/\beta]_T}\right)\,\mathrm{d}t\right),$$

where $e_T(t)$ is defined using Equation (5.3) with the repair time for the tumor, τ_r^1. For small δ, the effect of tumor repopulation results in $x(t+\delta) \approx x(t) + \delta\phi(x(t))x(t)$.

Including the effect of radiation, we have that

$$\begin{aligned} x(t+\delta) &\approx \Big(x(t)+\delta\phi(x(t))x(t)\Big)\exp\left(-\alpha_T\int_t^{t+\delta} d(t)\left(1+\frac{2e_T(t)}{[\alpha/\beta]_T}\right)\,\mathrm{d}t\right) \\ &\approx \Big(x(t)+\delta\phi(x(t))x(t)\Big)\exp\left(-\delta\alpha_T\left(1+\frac{2e_T(t)}{[\alpha/\beta]_T}\right)\right) \\ &\approx \Big(x(t)+\delta\phi(x(t))x(t)\Big)\left(1-\delta\alpha_T d(t)\left(1+\frac{2e_T(t)}{[\alpha/\beta]_T}\right)\right), \end{aligned} \tag{5.4}$$

where in (5.4) we use a Taylor series approximation. Rearranging the above equation, we have that

$$\frac{1}{x(t)}\frac{x(t+\delta)-x(t)}{\delta} \approx \phi(x(t)) - \alpha_T d(t)\left(1+\frac{2e_T(t)}{[\alpha/\beta]_T}\right).$$

Thus, as δ approaches 0 in the limit, we arrive at the differential equation

$$\frac{1}{x(t)}\frac{\mathrm{d}x(t)}{\mathrm{d}t} = \phi(x(t)) - \alpha_T d(t)\left(1+\frac{2e_T(t)}{[\alpha/\beta]_T}\right). \tag{5.5}$$

The first term on the right-hand side of the above equation represents the increase in tumor growth due to repopulation, and the second term is the decrease due to radiation delivery. We can also write the above differential equation in terms of $y(t)$, which is related to the $x(t)$ through the definition $y(t) = \ln(x(t))/\alpha_T$:

$$\frac{\mathrm{d}y(t)}{\mathrm{d}t} = \frac{1}{\alpha_T}\phi(\exp(\alpha_T y(t))) - d(t)\left(1+\frac{2e_T(t)}{[\alpha/\beta]_T}\right).$$

The dynamics of tumor growth during therapy now is modeled. We would like to constrain BED in the OAR in the problem formulation. To do this, we proceed to derive the BED model including incomplete sublethal damage repair when using continuous radiation delivery.

5.2.3 BED model for continuous dose rate

We include the dose protraction factor G in the following derivation of the BED. We denote $\mathrm{BED}(d, t')$ to be the total BED resulting from delivering the dose rate $d(t)$ in the time interval $[0, t']$. Recall from Chapter 4 that the BED related to the survival fraction S through the equation $\mathrm{BED} = -\ln(S)/\alpha$. Using this relation, we find

$$\mathrm{BED}(d, t') = \int_0^{t'} d(t) \left(1 + \frac{2e(t)}{[\alpha/\beta]}\right) \mathrm{d}t.$$

Using the above relation, we define $\mathrm{BED}_O(d, t')$ as the BED in the OAR with parameter $[\alpha/\beta]_O$ and the sparing factor γ. We also define (for convenience in notation) the total BED in the OAR, BED_O from delivering the dose rate $d(t)$ over the time interval $[0, T]$:

$$\mathrm{BED}_O = \mathrm{BED}_O(d, T) = \int_0^{T} \gamma d(t) \left(1 + \frac{2\gamma e_O(t)}{[\alpha/\beta]_O}\right) \mathrm{d}t,$$

where $e_O(t)$ is defined using the equation (5.3) with the repair time for the OAR, τ_r^2. As done in Chapter 4, we assert the constraint $\mathrm{BED}_O \leq c$ in the optimization to ensure a given level of NTCP.

5.2.4 Problem formulation

We formulate the optimization problem as

$$\underset{d(t)\geq 0}{\text{minimize}} \quad X_{N-1}^{+} \quad \text{s.t.} \quad \mathrm{BED}_O \leq c,$$

where X_{N-1}^{+} is the expected number of tumor cells after radiation treatment and c is an appropriate constant. The dynamics of the tumor throughout the treatment are governed by the differential equation (5.5). Though we do not provide a solution method to solve this formulation, we discuss possible methods later in the chapter.

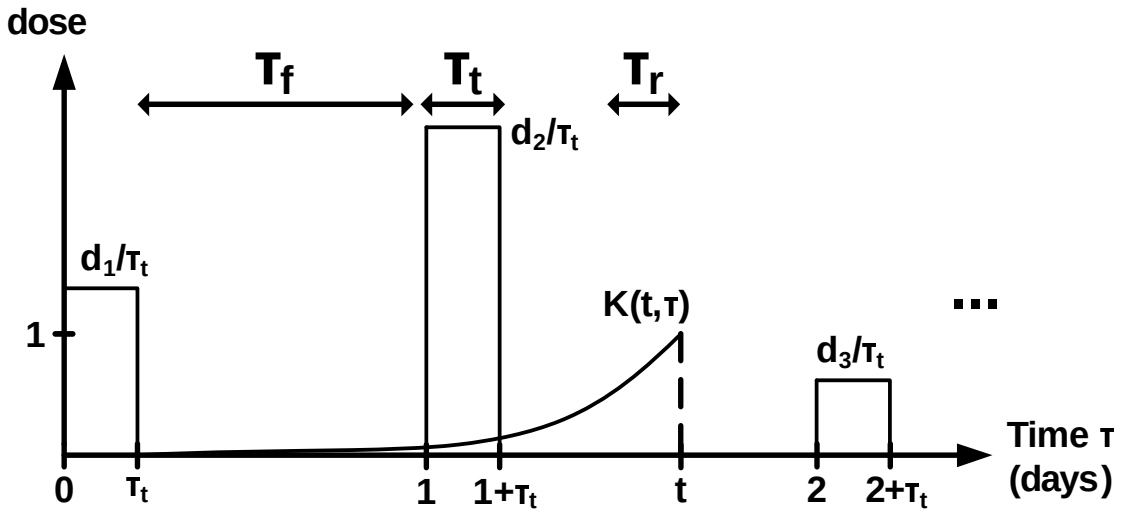

Figure 5-1: Illustration of the discrete-time setup using the continuous-time model. The repair time, treatment time, and time between fractions are τ_r,τ_t, and τ_f respectively.

5.3 Consistency with discrete-time model

In this section, we show that the continuous time model derived thus far is consistent with the discrete time version in Chapter 4. In particular, given that τ_t is the delivery time of a single dose fraction and τ_f is the time between dose fractions (Figure 5-1), we show that the discrete time model in Chapter 4 is a good approximation if $\tau_t \ll \tau_r \ll \tau_f$. That is, if the delivery time of one dose is fast enough in comparison to tissue repair times and if there is enough time between treatments for repair of sublethal damage, a discrete time model can be used.

We will first consider the case where a single dose of radiation is delivered. Suppose that a total dose of d_k is delivered uniformly over the interval $[k, k+\tau_t]$, i.e., $d(t)$ equals d_k/τ_t for $k \leq t \leq k+\tau_t$ and 0 otherwise. We would like to now compute the resulting

BED for this choice of $d(t)$. The function $e(t)$ is

$$\begin{aligned} e(t) &= \int_0^T d(\tau)u(t-\tau)\exp(-(t-\tau)/\tau_r)\,\mathrm{d}\tau \\ &= \int_k^t \frac{d_k}{\tau_t}\exp(-(t-\tau)/\tau_r)\,\mathrm{d}\tau \\ &\approx \int_k^t \frac{d_k}{\tau_t}\,\mathrm{d}\tau \\ &= \frac{d_k}{\tau_t}(t-k), \end{aligned}$$

where we modified the limits of integration due the definitions of $d(t)$ and $u(t)$ in the second equality, and we assumed $\tau_t \ll \tau_r$ to obtain the approximation in the third equation. Now we compute the BED:

$$\begin{aligned} \text{BED} &= \int_k^{k+\tau_t} d(t)\left(1+\frac{2e(t)}{[\alpha/\beta]}\right)\mathrm{d}t \\ &\approx \int_k^{k+\tau_t} \frac{d_k}{\tau_t}\left(1+\frac{2d_k/\tau_t\,(t-k)}{[\alpha/\beta]}\right)\mathrm{d}t \\ &= d_k\left(1+\frac{d_k}{[\alpha/\beta]}\right), \end{aligned}$$

which is exactly the expression for BED for a single dose in the discrete time case.

Now we generalize the expression for BED for multiple radiation doses. Suppose that N radiation doses $d_0, d_1, \ldots, d_{N-1}$ are delivered uniformly over time intervals of length τ_t. Let the separation between each of the doses be τ_f (Figure 5-1). We will assume $\tau_f \approx 1$ day; the analysis can be extended with the same arguments for any τ_f. Thus, the kth dose d_k is delivered in the time interval $[k, k+\tau_t]$, assuming time in units of days. We assume that the repair time τ_r is much smaller than the time between treatments τ_f, i.e. $\tau_r \ll \tau_f$. In this case, note that $\exp(-(t-\tau)/\tau_r) \approx 1$ when $k \le \tau \le k+\tau_t$ and $\exp(-(t-\tau)/\tau_r) \approx 0$ when $\tau \le k-1$, assuming $\tau_t \ll \tau_r$. We now

compute the total BED:

$$\begin{aligned}
\text{BED} &= \int_0^T d(t)\left(1+\frac{2e(t)}{[\alpha/\beta]}\right)\,\mathrm{d}t \\
&= \sum_{k=0}^{N-1}\int_k^{k+\tau_t} d(t)\left(1+\frac{2e(t)}{[\alpha/\beta]}\right)\,\mathrm{d}t \\
&\approx \sum_{k=0}^{N-1}\int_k^{k+\tau_t} d(t)\left(1+\frac{2\int_k^t d(\tau)\,\mathrm{d}\tau}{[\alpha/\beta]}\right)\,\mathrm{d}t \\
&= \sum_{k=0}^{N-1} d_k\left(1+\frac{d_k}{[\alpha/\beta]}\right), \qquad (5.6)
\end{aligned}$$

which is exactly the expression for BED in the discrete-time case.

Now, we would like to show that the continuous-time formulation is consistent with the discrete-time one. For the discrete-time case in Chapter 4, tumor growth was characterized by the differential equation

$$\frac{\mathrm{d}y(t)}{\mathrm{d}t} = \frac{1}{\alpha_T}\phi(\exp(\alpha_T y(t)))$$

and at an integer time k, the radiation dose resulted in

$$y(k^+) = y(k^-) - d_k\left(1+\frac{d_k}{[\alpha/\beta]_T}\right).$$

Let us again consider the single dose case in continuous-time. That is, let d_k be uniformly delivered over the interval $[k, k+\tau_t]$. Then,

$$y(t+\tau_t) \approx y(t) + \tau_t\frac{1}{\alpha_T}\phi(\exp(\alpha_T y(t))) - d_k\left(1+\frac{d_k}{[\alpha/\beta]_T}\right),$$

which for very small treatment time τ_t approaches the equation (5.3) for the discrete-time case. Furthermore, for $k+\tau_t \le t \le k+1$, the continuous-time differential equation consists only of the tumor repopulation term, and thus, matches the discrete-time version. Finally, the BED constraint in the OAR (5.6) is also the same as in the discrete

time formulation. We have thus shown that the tumor dynamics and the constraint in the continuous-time formulation is consistent with the discrete-time case.

5.4 Discussion, conclusions, and future outlook

We have extended the formulation from the previous chapter to the case of a continuous dose rate $d(t)$ treatment protocol. Due to the interactions between radiation dose in close instants of time, it was necessary to include incomplete sublethal damage repair into the LQ model. The dynamics governing the number of tumor cells at any instant of time was written as an ordinary differential equation. We showed that this continuous time model and formulation was consistent with the discrete-time one in the previous chapter. We do not claim that the model and formulation is novel because a similar setup is found in [87]. However, we hope that the derivations shed new perspective into the problem and it may serve as the basis for future work.

The solution method to solve the fractionation problem was not discussed in this chapter. One possibility is to use a dynamic programming approach similar to the one in the previous chapter. However, we need to consider a few additional issues. First, the continuous nature of the optimal control requires discretization in time. Using a fine discretization and Euler's approximation for example, the differential equation in this chapter can be converted to a state update equation similar to the one in the previous chapter. Second, due to inclusion of the incomplete sublethal damage repair, additional states $e_T(t)$ and $e_O(t)$ are required. Thus, the state of the system would be captured by $(e_T(t), y(t), e_O(t), z(t))$, where $z(t)$ is the cumulative BED in the OAR over the time interval $[0, t]$. Yet, an exact dynamic programming approach may not be computationally tractable. If, for example, each state variable is discretized into 100 units, we will have to evaluate 100 million states for each time instant. It may be necessary to resort to approximate dynamic programming methods in this case. Since we have a deterministic problem, an alternative approach could be to use general gradient-based non-linear programming methods. The dimension of the gradient would

be determined by how finely one discretizes over time. Of course, there are no convexity properties in this problem and only a local optimum is guaranteed with these methods. There is scope for future work in the choice of solution method for this fractionation problem.

The presented model and formulation could be used to analyze the implications of accelerated repopulation on optimal fractionation schemes for continuous dose rate treatment protocols such as brachytherapy. A recent paper has validated that accelerated repopulation exists in cervical cancer with relatively short onset time [29]. Given that conventional treatment for cervical cancer is a combination of external beam radiation therapy and low-dose rate brachytherapy [9], there is potential for further research investigating alternative fractionation schemes that can result in improved treatment for this disease site.

Chapter 6

Conclusions

In this thesis, we studied dynamic optimization of fractionation schedules for radiation therapy. In the first part, in Chapters 2 and 3, we considered varying the daily fraction size based on geometrical information from imaging of the patient anatomy. Along with characterizing properties of optimal policies, we found that adaptively varying the fraction size can be beneficial. We substantiated this conclusion with results from prostate patient datasets. For prostate cancer, the approaches are particularly beneficial because of the high sensitivity of the tumor to radiation. We also suggested daily selection of a treatment plan from a plan library in order to avoid daily QA procedures. Future work could couple the two problems and simultaneously optimize the dose intensities spatially and temporally.

In Chapters 4 and 5, we considered the effect of tumor repopulation on the optimal fractionation schedule. We were motivated primarily by the accelerated repopulation observed towards the end of radiation treatment, which is believed to play a role in treatment failure for some tumor sites. A dynamic programming framework was developed to determine the optimal fractionation scheme based on a model of cell kill due to radiation and tumor growth in between treatment days. We proved that the optimal dose fractions are increasing over time and suggested larger dose fractions later in the treatment to compensate for the increased tumor proliferation.

While much work has been done on the algorithmic aspects of adaptive fractionation, there is still a need to quantify the benefit for specific disease sites. The work in Chapter 3 found significant benefit for prostate cancer, particularly because of the high sensitivity of the tumor to radiation. We would also expect significant benefit for other tumors with high sensitivity. In Chapter 3, we also selected from a library of two treatments plans: one with a small margin and one with a large one. However, an interesting approach would be to generate the plan library itself by an optimization procedure. The question of interest would be: Given some knowledge of the uncertainty in motion, how can we generate two treatment plans? At first glance, this problem seems to have a combinatorial nature and thus difficult to solve. The advantage is that this type of selection from a plan library procedure and also adaptive fractionation does not have the drawback of daily QA procedures. For adaptive fractionation, the beam intensities simply need to be scaled up. For selection from a plan library, the treatment plans would be pre-approved prior to the start of treatment.

The two parts of this thesis, adaptive fractionation and optimal fractionation in the presence of tumor repopulation, were developed independently. But, an interesting consideration for future investigation could be to assume that the normal tissue sparing factor γ from Chapter 4 varies from day to day. This is similar to the adaptive fractionation work except that tumor repopulation is included. Including more realistic assumptions, such the repair effect from Chapter 5 and tumor re-oxygenation, into the analysis could also be useful.

In Chapter 4, we looked into the effect of tumor repopulation on how the dose should be varied temporally. A question of future interest is whether the dose should be varied both spatially and temporally assuming tumor repopulation or more generally a biological model. For example, it may be the case the a different dose distribution is optimal on each treatment day even when no organ motion is assumed and no imaging information is used. The work in [40] has looked into adapting spatio-temporally using biological-based imaging. Yet, it is still of interest to understand the biological modeling assumptions which lead to different treatment plans from day to day.

In the general area of optimal fractionation for cancer treatment, a vast amount of work has been done individually for radiation therapy and chemotherapy. Yet, far fewer studies have considered the potential of optimal scheduling of combined radiation and chemotherapy [22, 24, 31, 36, 43, 72, 90]. For certain cancers especially advanced and metastasized ones, chemotherapy (treatment through anti-cancer drugs) is more effective than radiation therapy. However, targeted tumor cells generally become more resistant over time, and increasing the drug dose cannot always be a viable option because it can cause systemic damage to the patient. There is significant potential for improving treatment by modeling and optimizing the complex interactions between anti-cancer drugs and radiation dose.

Biologically guided radiation therapy, where patient-specific treatment is achieved through both modeling and imaging advancements, provides an exciting possibility for the future. A survey and positive outlook towards clinical implementation is provided in [73]. With advancements in PET imaging techniques that can measure for example tumor proliferation rates during the course of therapy [3], the opportunity to adapt rather than use models becomes a possibility. In terms of the physical dose, technology and optimization techniques have enabled precise delivery to the tumor. Advances in technology have enabled new modalities such as volumetric arc therapy (VMAT), and there are challenges to overcome in the optimization of treatment planning. Still, it is fair to say that the potential for drastic changes and improvements in treatment planning exists more so when incorporating biological information. Understanding the biological processes at the molecular level together with advancements in imaging can enable effective treatment planning in the future.

Bibliography

[1] K. J. Almquist and H. T. Banks. A theoretical and computational method for determining optimal treatment schedules in fractionated radiation therapy. *Mathematical Biosciences*, 29:159–179, 1976.

[2] C. I. Armpilia, R. G. Dale, and B. Jones. Determination of the optimum dose per fraction in fractionated radiotherapy when there is delayed onset of tumour repopulation during treatment. *Br. J. Radiol.*, 77:765–767, 2004.

[3] J. R. Bading and A. F. Shields. Imaging of cell proliferation: Status and prospects. *J Nucl Med*, 49:64S80S, 2008.

[4] D. P. Bertsekas. *Dynamic Programming and Optimal Control*. Athena Scientific, 2007.

[5] A. Bertuzzi, C. Bruni, F. Papa, and C. Sinisgalli. Optimal solution for a cancer radiotherapy problem. *J. Math. Biol.*, 66:311–349, 2013.

[6] T. Bortfeld and H. Paganetti. The biologic relevance of daily dose variations in adaptive treatment planning. *Int. J. Radiat. Oncol. Biol. Phys.*, 65:899–906, 2006.

[7] D. J. Brenner. The linear-quadratic model is an appropriate methodology for determining iso-effective doses at large doses per fraction. *Semin Radiat Oncol.*, 18:234239, 2008.

[8] D. J. Brenner, E. J. Hall, Y. Huang, and R. K. Sachs. Optimizing the time course of brachytherapy and other accelerated radiotherapeutic protocols. *Int. J. Radiat. Oncol. Biol. Phys.*, 29:893–901, 1994.

[9] D. J. Brenner, Y. Huang, and E. J. Hall. Fractionated high dose-rate versus low dose-rate regimens for intracavity brachytherapy of the cervix: Equivalent regimens for combined brachytherapy and external irradiation. *Int. J. Radiat. Oncol. Biol. Phys.*, 21:1415–1423, 1991.

[10] J. H. Chang, D. L. Joon, S. T. Lee, S. J. Gong, N. J. Anderson, A. M. Scott, I. D. Davis, D. Clouston, D. Bolton, C. S. Hamilton, and V. Khoo. Intensity modulated radiation therapy dose painting for localized prostate cancer using 11c-choline positron emission tomography scans. *Int. J. Radiat. Oncol. Biol. Phys.*, 83:e691–e696, 2012.

[11] K. Chao, W. R. Bosch, S. Mutic, J. S. Lewis, F. Dehdashti, M. A. Mintun, J. F. Dempsey, C. A. Perez, J. A. Purdy, and M. J. Welch. A novel approach to overcome hypoxic tumor resistance: Cu-atsm-guided intensity-modulated radiation therapy. *Int. J. Radiat. Oncol. Biol. Phys.*, 49(4):1171–1182, 2001.

[12] M. Chao, Y. Xie, and L. Xing. Auto-propagation of contours for adaptive prostate radiation therapy. *Phys. Med. Biol.*, 53:4533–4542, 2008.

[13] M. Chen, W. Lu, Q. Chen, K. Ruchala, and G. Olivera. Adaptive fractionation therapy: II. Biological effective dose. *Phys. Med. Biol.*, 53:5513–5525, 2008.

[14] L. E. Court, L. Dong, A. K. Lee, R. Cheung, M. D. Bonnen, J. O'Daniel, H. Wang, R. Mohan, and D. Kuban. An automatic CT-guided adaptive radiation therapy technique by online modification of multileaf collimator leaf positions for prostate cancer. *Int. J. Radiat. Oncol. Biol. Phys.*, 62:154–163, 2005.

[15] R. G. Dale. The application of the linear-quadratic dose-effect equation to fractionated and protracted radiotherapy. *Br. J. Radiol.*, 58:515–528, 1985.

[16] A. de la Zerda, B. Armbruster, and L. Xing. Formulating adaptive radiation therapy (ART) treatment planning into a closed-loop control framework. *Phys. Med. Biol.*, 52:4137–4153, 2007.

[17] J. O. Deasy, A. I. Blanco, and V. H. Clark. Cerr: A computational environment for radiotherapy research. *Med. Phys.*, 30:979–985, 2003.

[18] G. Deng and M. C. Ferris. Neuro-dynamic programming for fractionated radiotherapy planning. *Springer Optimization and Its Applications*, 12:47–70, 2008.

[19] M. C. Ferris and M. M. Voelker. Fractionation in radiation treatment planning. *Math. Program.*, 101:387–413, 2004.

[20] J. F. Fowler. The linear-quadratic formula and progress in fractionated radiotherapy. *Br. J. Radiol.*, 62:679–694, 1989.

[21] J. F. Fowler and B. E. Stern. Dose-time relationships in radiotherapy and the validity of cell survival curve models. *Br. J. Radiol.*, 36:163–173, 1963.

[22] N. A. P. Franken, S. Hovingh, H. Rodermond, L. Staplers, W. Barendsen, and J. Crezee. Radiosensitization with chemotherapeutic agents and hyperthermia: Effects on linear-quadratic parameters of radiation cell survival curves. *Cancer Science and Therapy*, 2011.

[23] A. Ghate. Dynamic optimization in radiotherapy. *Tutorials in Operations Research*, pages 1–14, 2011.

[24] R. Glynne-Jones and D. Sebag-Montefiore. Chemoradiation schedules–what radiotherapy? *European Journal of Cancer*, 38(2):258–269, 2002.

[25] J. J. Gordon, E. Weiss, O. K. Abayomi, J. V. Siebers, and N. Dogan. The effect of uterine motion and uterine margins on target and normal tissue doses in intensity modulated radiation therapy of cervical cancer. *Phys. Med. Biol.*, 56:2887–2901, 2011.

[26] M. Guckenberger, J. Wilbert, A. Richter, K. Baier, and M. Flentje. Potential of adaptive radiotherapy to escalate the radiation dose in combined radiochemotherapy for locally advanced non-small cell lung cancer. *Int. J. Radiat. Oncol. Biol. Phys.*, 79:901–908, 2011.

[27] M. Guerrero and X. A. Li. Analysis of a large number of clinical studies for breast cancer radiotherapy: estimation of radiobiological parameters for treatment planning. *Phys. Med. Biol.*, 48:3307–3326, 2003.

[28] H. W. Hethcote and P. Waltman. Theoretical determination of optimal treatment schedules for radiation therapy. *Radiation Research*, 56:150–161, 1973.

[29] Z. Huang, N. A. Mayr, M. Gao, S. S. Lo, J. Z. Wang, G. Jia, and W. T. C. Yuh. Onset time of tumor repopulation for cervical cancer: First evidence from clinical data. *Int. J. Radiat. Oncol. Biol. Phys.*, 84:478–484, 2012.

[30] M. C. Joiner, B. Marples, P. Lambin, S. C. Short, and I. Turesson. Low-dose hypersensitivity: Current status and possible mechanisms. *Int. J. Radiat. Oncol. Biol. Phys.*, 49:379–389, 2001.

[31] B. Jones and R. G. Dale. The potential for mathematical modelling in the assessment of the radiation dose equivalent of cytotoxic chemotherapy given concomitantly with radiotherapy. *Br. J. Radiol.*, 78:939–944, 2005.

[32] B. Jones, L. T. Tan, and R. G. Dale. Derivation of the optimum dose per fraction from the linear quadratic model. *Br. J. Radiol.*, 68:894–902, 1995.

[33] P. Källman, A. Ågren, and A. Brahme. Tumour and normal tissue responses to fractionated non-uniform dose delivery. *Int. J. Radiat. Biol.*, 62:249–262, 1992.

[34] P. Källman, B. K. Lind, and A. Brahme. An algorithm for maximizing the probability of complication-free tumour control in radiation therapy. *Phys. Med. Biol.*, 37:871–890, 1992.

[35] S. Kamath, S. Sahni, J. Li, J. Palta, and S. Ranka. Leaf sequencing algorithms for segmented multileaf collimation. *Phys. Med. Biol.*, 48:307–324, 2003.

[36] D. P. Kelsen. Postoperative adjuvant chemoradiation therapy for patients with resected gastric cancer: Intergroup 116. *Journal of Clinical Oncology*, 18(21S):32S–34S, 2000.

[37] J. J. Kim and I. F. Tannock. Repopulation of cancer cells during therapy: An important cause of treatment failure. *Nature*, 5:516–525, 2005.

[38] M. Kim. *A Mathematical Framework for Spatiotemporal Optimality in Radiation Therapy*. PhD thesis, University of Washington, 2010.

[39] M. Kim, A. Ghate, and M. H. Phillips. A markov decision process approach to temporal modulation of dose fractions in radiation therapy planning. *Phys. Med. Biol.*, 54:4455–4476, 2009.

[40] M. Kim, A. Ghate, and M. H. Phillips. A stochastic control formalism for dynamic biologically conformal radiation therapy. *European Journal of Operational Research*, 219(3):541 – 556, 2012.

[41] K. M. Langen. Uncertainties and limitations in adaptive radiotherapy. In J. R. Palta and T. R. Mackie, editors, *Uncertainties in external beam radiation therapy*, pages 443–470. Medical Physics Publishing, 2011.

[42] M. Langer, S. S. Morrill, and R. Lane. A test of the claim that plan rankings are determined by relative complication and tumor-control probabilities. *Int. J. Radiat. Oncol. Biol. Phys.*, 41:451–457, 1998.

[43] T. S. Lawrence, W. A. Blackstock, and C. McGinn. The mechanism of action of radiosensitization of conventional chemotherapeutic agents. *Seminars in Radiation Oncology*, 13:13–21, 2003.

[44] U. Ledzewicz and H. Schättler. Application of control theory in modelling cancer chemotherapy. In *International Conference on Control, Automation, and Systems*, 2004.

[45] Y. Lei and Q. Wu. A hybrid strategy of offline adaptive planning and online image guidance for prostate cancer radiotherapy. *Phys. Med. Biol.*, 55:2221–2234, 2010.

[46] T. Li, D. Thongphiew, X. Zhu, W. R. Lee, Z. Vujaskovic, F.-F. Yin, and Q. J. Wu. Adaptive prostate igrt combining online re-optimization and re-positioning: a feasibility study. *Phys. Med. Biol.*, 56:1243–1258, 2011.

[47] X. A. Li. *Adaptive Radiation Therapy.* CRC Press, 2011.

[48] W. Lu, M. Chen, Q. Chen, K. Ruchala, and G. Olivera. Adaptive fractionation therapy: I. Basic concept and strategy. *Phys. Med. Biol.*, 53:5495–5511, 2008.

[49] J. T. Lyman. Complication probability as assessed from dose-volume histograms. *Radiat. Res. Suppl.*, 8:S13–9, 1985.

[50] H. McAneney and S. F. C. O'Rourke. Investigation of various growth mechanisms of solid tumour growth within the linear-quadratic model for radiotherapy. *Phys. Med. Biol.*, 52:1039–1054, 2007.

[51] R. Miralbell, S. A. Roberts, E. Zubizarreta, and J. H. Hendry. Dose-fractionation sensitivity of prostate cancer deduced from radiotherapy outcomes of 5,969 patients in seven international institutional datasets: $\alpha/\beta = 1.4\ (0.9 - 2.2)$ gy. *Int. J. Radiat. Oncol. Biol. Phys.*, 82:e17e24, 2012.

[52] M. Mizuta, S. Takao, H. Date, N. Kishimoto, K. L. Sutherland, R. Onimaru, and H. Shirato. A mathematical study to select fractionation regimen based on physical dose distribution and the linear-quadratic model. *Int. J. Radiat. Oncol. Biol. Phys.*, 84:829–33, 2012.

[53] R. Mohan, X. Zhang, H. Wang, Y. Kang, X. Wang, H. Liu, K. K. Ang, D. Kuban, and L. Dong. Use of deformed intensity distributions for on-line modification of image-guided IMRT to account for interfractional anatomic changes. *Int. J. Radiat. Oncol. Biol. Phys.*, 61:1258–1266, 2005.

[54] T. R. Munro and C. W. Gilbert. The relation between tumour lethal doses and the radiosensitivity of tumour cells. *Br. J. Radiol.*, 34:246–251, 1961.

[55] L. P. Muren, N. Jebsen, A. Gustafsson, and O. Dahl. Can doseresponse models predict reliable normal tissue complication probabilities in radical radiotherapy of urinary bladder cancer? the impact of alternative radiation tolerance models and parameters. *Int. J. Radiat. Oncol. Biol. Phys.*, 50(3):627–637, 2001.

[56] A. Niemierko. Reporting and analyzing dose distributions: A concept of equivalent uniform dose. *Med. Phys.*, 24:103–110, 1997.

[57] L. Norton and R. Simon. Tumor size, sensitivity to therapy, and design of treatment schedules. *Cancer Treat. Rep.*, 61:1307–1317, 1977.

[58] L. Norton and R. Simon. The norton-simon hypothesis revisited. *Cancer Treat. Rep.*, 70:163–169, 1986.

[59] J. J. Nuyttens, J. M. Robertson, D. Yan, and A. Martinez. The influence of small bowel motion on both a conventional three-field and intensity modulated radiation therapy (imrt) for rectal cancer. *Cancer/Radiothérapie*, 8:297–304, 2004.

[60] C. E. Pedreira and V. B. Vila. Optimal schedule for cancer chemotherapy. *Mathematical Programming*, 52:11–17, 1991.

[61] L. J. Peters. Accelerated fractionation using concomitant boost: A contribution of radiobiology to radiotherapy. *BJR Suppl.*, 24:200–203, 1992.

[62] M. Pinkawa, C. Attieh, M. D. Piroth, R. Holy, S. Nussen, J. Klotz, R. Hawickhorst, W. Schfer, and M. J. Eble. Dose-escalation using intensity-modulated

radiotherapy for prostate cancer evaluation of the dose distribution with and without 18f-choline pet-ct detected simultaneous integrated boost. *Radiotherapy and Oncology*, 93(2):213 – 219, 2009.

[63] G. Poludniowski, M. D. R. Thomas, P. M. Evans, and S. Webb. CT reconstruction from portal images acquired during volumetric-modulated arc therapy. *Phys. Med. Biol.*, 55:5635–5651, 2010.

[64] W. B. Powell. *Approximate Dynamic Programming: Solving the Curses of Dimensionality*. Wiley, 2011.

[65] J. Ramakrishnan, D. Craft, T. Bortfeld, and J. N. Tsitsiklis. A dynamic programming approach to adaptive fractionation. *Phys. Med. Biol.*, 57:1203–1216, 2012.

[66] H. Rehbinder, C. Forsgren, and J. Löf. Adaptive radiation therapy for compensation of errors in patient setup and treatment delivery. *Med. Phys.*, 31:3363–3371, 2004.

[67] S. Schell. *The linear quadratic damage model in radiation therapy planning: effect based optimization and automatic fractionation scheme adjustment*. PhD thesis, University of Heidelberg, 2008.

[68] N. Sharma, D. Neumann, and R. Macklis. The impact of functional imaging on radiation medicine. *Radiation Oncology*, 3:1–13, 2008.

[69] D. M. Shepard, M. C. Ferris, G. H. Olivera, and T. R. Mackie. Optimizing the delivery of radiation therapy to cancer patients. *SIAM Review*, pages 721–744, 1999.

[70] M. Y. Sir, M. A. Epelman, and S. M. Pollock. Stochastic programming for off-line adaptive radiotherapy. *Annals of Operations Research*, 179, 2010.

[71] P. Stavrev, D. Hristov, B. Warkentin, E. Sham, N. Stavreva, and B. G. Fallone. Inverse treatment planning by physically constrained minimization of a biological objective function. *Med. Phys.*, 30:2948–2958, 2003.

[72] D. J. Stewart. *Lung Cancer: Prevention, Management, and Emerging Therapies*. Humana Press, 2010.

[73] R. D. Stewart and X. A. Li. Bgrt: Biologically guided radiation therapy—the future is fast approaching! *Med. Phys.*, 34:3729–3751, 2007.

[74] M. Stuschke and H. D. Thames. Fractionation sensitivities and dose-control relations of head and neck carcinomas: analysis of the randomized hyperfractionation trials. *Radiother Oncol.*, 51:113–121, 1999.

[75] R. Svensson, P. Källman, and A. Brahme. An analytical solution for the dynamic control of multileaf collimators. *Phys. Med. Biol.*, 39:37–61, 1994.

[76] G. W. Swan. *Optimization of Human Cancer Radiotherapy*. Springer, 1981.

[77] G. W. Swan. *Applications of Optimal Control Theory in Biomedicine*. CRC Press, 1984.

[78] J. Unkelbach, D. Craft, E. Salari, J. Ramakrishnan, and T. Bortfeld. The dependence of optimal fractionation schemes on the spatial distribution. *Phys. Med. Biol.*, 58:159–167, 2013.

[79] J. R. Usher. Mathematical derivation of optimal uniform treatment schedules for the fractionated irradiation of human tumors. *Mathematical Biosciences*, 49:157–184, 1980.

[80] E. N. van Lin, J. J. Ftterer, S. W. Heijmink, L. P. van der Vight, A. L. Hoffmann, P. van Kollenburg, H. J. Huisman, T. W. Scheenen, J. A. Witjes, J. W. Leer, J. O. Barentsz, and A. G. Visser. Imrt boost dose planning on dominant intraprostatic

lesions: Gold marker-based three-dimensional fusion of ct with dynamic contrast-enhanced and 1h-spectroscopic mri. *Int. J. Radiat. Oncol. Biol. Phys.*, 65(1):291–303, 2006.

[81] J. Z. Wang and X. A. Li. Impact of tumor repopulation on radiotherapy planning. *Int. J. Radiat. Oncol. Biol. Phys.*, 61:220–227, 2005.

[82] X.-H. Wang, R. Mohan, A. Jackson, S. A. Leibel, Z. Fuks, and C. Ling. Optimization of intensity-modulated 3d conformal treatment plans based on biological indices. *Radiotherapy and Oncology*, 37(2):140 – 152, 1995.

[83] Y. Wang, J. A. Efstathiou, G. C. Sharp, H.-M. Lu, I. F. Ciernik, and A. V. Trofimov. Evaluation of the dosimetric impact of interfractional anatomical variations on prostate proton therapy using daily in-room ct images. *Med. Phys.*, 38:4623–4633, 2011.

[84] S. Webb. Adapting IMRT delivery fraction-by-fraction to cater for variable intrafraction motion. *Phys. Med. Biol.*, 53:1–21, 2008.

[85] S. Webb and T. Bortfeld. A new way of adapting IMRT delivery fraction-by-fraction to cater for variable intrafraction motion. *Phys. Med. Biol.*, 53:5177–5191, 2008.

[86] S. Webb and A. E. Nahum. A model for calculating tumour control probability in radiotherapy including the effects of inhomogeneous dose distributions of dose and clonogenic cell density. *Phys. Med. Biol.*, 38:653–666, 1993.

[87] L. M. Wein, J. E. Cohen, and J. T. Wu. Dynamic optimization of a linear-quadratic model with incomplete repair and volume-dependent sensitivity and repopulation. *Int. J. Radiat. Oncol. Biol. Phys.*, 47:1073–1083, 2000.

[88] T. E. Wheldon. *Mathematical Models in Cancer Research*. IOP Publishing Ltd, 1988.

[89] T. E. Wheldon, J. Kirk, and J. S. Orr. Optimal radiotherapy of tumour cells following exponential-quadratic survival curves and exponential repopulation kinetics. *Br. J. Radiol.*, 50:681–682, 1977.

[90] D. R. Wigg. *Applied Radiobiology and Bioeffect Planning*. Medical Physics Publishing, 2001.

[91] H. R. Withers. Treatment-induced accelerated human tumor growth. *Seminars in Radiation Oncology*, 3:135–143, 1993.

[92] H. R. Withers, J. M. G. Taylor, and B. Maciejewski. The hazard of accelerated tumor clonogen repopulation during radiotherapy. *Acta Oncologica*, 27:131–46, 1988.

[93] Q. J. Wu, D. Thongphiew, Z. Wang, B. Mathayomchan, V. Chankong, S. Yoo, W. R. Lee, and F.-F. Yin. On-line re-optimization of prostate IMRT plans for adaptive radiation therapy. *Phys. Med. Biol.*, 53:673–691, 2008.

[94] A. Y. Yakovlev, L. Pavlova, and L. G. Hanin. *Biomathematical Problems in Optimization of Cancer Radiotherapy*. CRC Press, 1994.

[95] D. Yan, D. Lockman, D. Brabbins, L. Tyburski, and A. Martinez. An off-line strategy for constructing a patient-specific planning target volume in adaptive treatment process for prostate cancer. *Int. J. Radiat. Oncol. Biol. Phys.*, 48:289–302, 2000.

[96] D. Yan, F. Vicini, J. Wong, and A. Martinez. Adaptive radiation therapy. *Phys. Med. Biol.*, 42:123–132, 1997.

[97] D. Yan, E. Ziaja, D. Jaffray, J. Wong, D. Brabbins, F. Vicini, and A. Martinez. The use of adaptive radiation therapy to reduce setup error: A prospective clinical study. *Int. J. Radiat. Oncol. Biol. Phys.*, 41:715–720, 1998.

[98] Y. Yang and L. Xing. Optimization of radiotherapy dose-time fractionation with consideration of tumor specific biology. *Med. Phys.*, 32:3666–3677, 2005.

[99] E. D. Yorke, G. J. Kutcher, A. Jackson, and C. C. Ling. Probability of radiation-induced complications in normal tissues with parallel architecture under conditions of uniform whole or partial organ irradiation. *Radiother. Oncol.*, 26:226–237, 1993.

[100] S. Zietz and C. Nicolini. Mathematical approaches to optimization of cancer chemotherapy. *Phys. Med. Biol.*, 52:4137–4153, 2007.